# Shelf Circulation in the Gulf of California

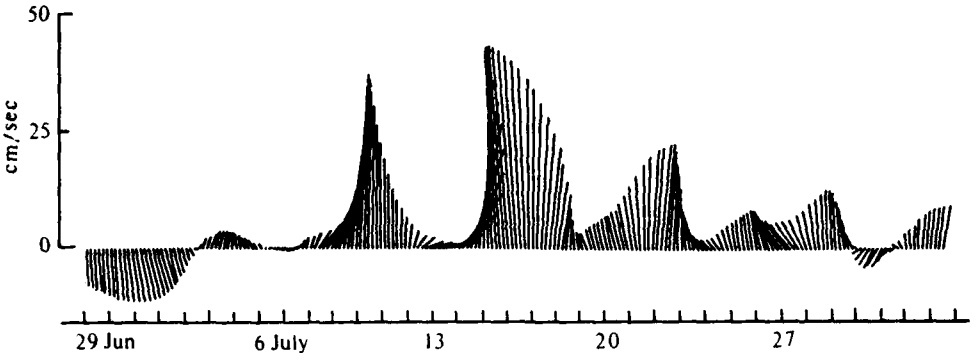




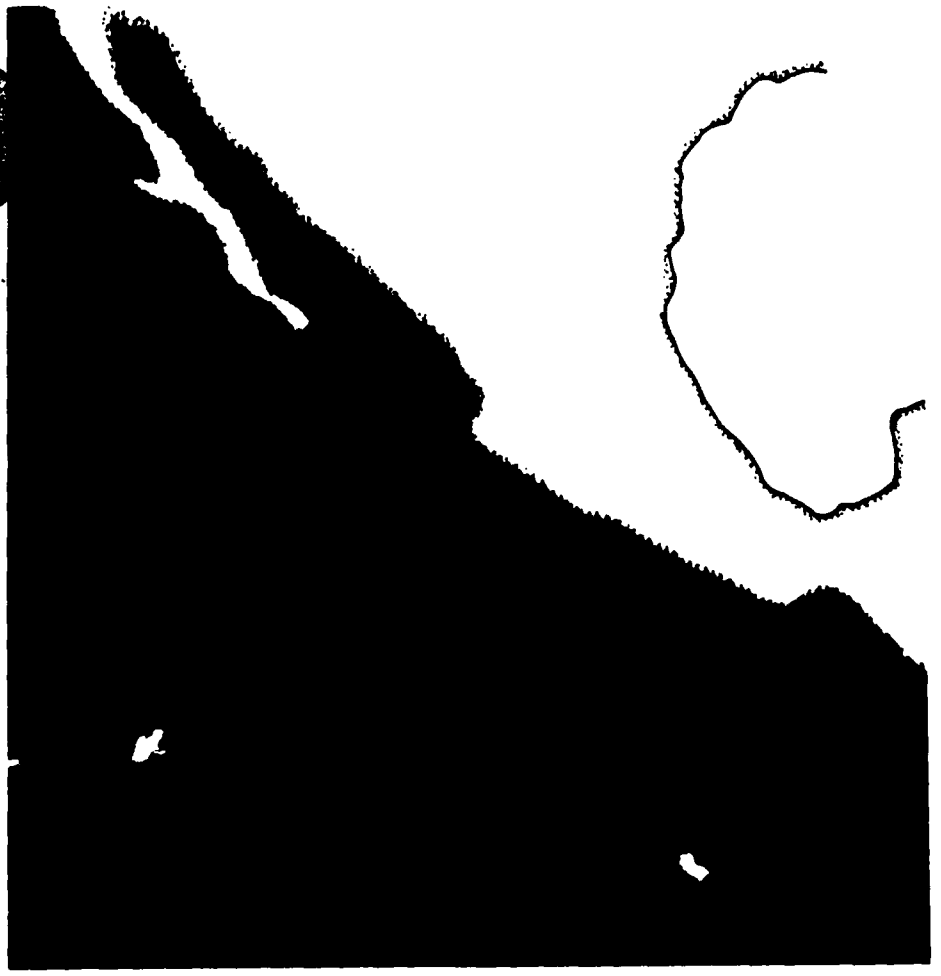

**Mark Andrew Merrifield**

**1989**

UNIVERSITY OF CALIFORNIA, SAN DIEGO

# Shelf Circulation in the Gulf of California

A dissertation submitted in partial satisfaction of the

requirements for the degree Doctor of Philosophy

in Oceanography

by

**Mark A. Merrifield**

Committee in charge:

Professor Clinton D. Winant, Co-chairman
Professor Robert T. Guza, Co-chairman
Professor Myrl C. Hendershott
Professor Joseph L. Reid
Professor Victor C. Anderson

1989

The dissertation of Mark A. Merrifield is approved,
and it is acceptable in quality and form
for publication on microfilm:

Co-chairman

Co-chairman

University of California, San Diego

1989

*To my family.*

Table of Contents

List of Figures and Tables

Chapter I



Chapter II

Chapter III

**Acknowledgements**

I was very fortunate to have had the opportunity to work with Professors Clint Winant and Bob Guza. Clint provided steady guidance, constant encouragement, and made numerous casual suggestions which continually turned into important results. Bob taught me most of what I know about data analysis, patiently listened to my rambling questions and turned them into coherent thoughts, and spent a considerable amount of time editing my manuscripts. The work on coastal-trapped waves was largely an extension of the work of Niels Christensen, who gave generously of his time and ideas and has my warmest thanks. I enjoyed sharing ideas about the gulf with good friends Cindy Paden, Nan Bray, Antoine Badan-Dangon, Myrl Hendershott, Clive Dorman, Bjorn Gjevik, and Juan Antonio Rodriguez-Sero.

I would like to thank my colleagues at the Center for Coastal Studies and at CICESE for their friendship and support, and for their expertise in collecting the observations used in this study. Special thanks go to Joan Semler and Mike Clark for their help in preparing my thesis. I was fortunate during my time at Scripps to have had two very close friends as office-mates. Uwe Send provided constant moral support, whether over morning coffee or a Friday margarita. Day-to-day contact with him will be sorely missed. Jerry Wanctick helped me maintain perspective on graduate school through his good humor and sage advice. There are many others at SIO whom I would like to thank, including Bill O'Reilly, Walt Waldorf, Julio Candela, Ron Flick, Diane Henderson, and Tom Herbers.

As in all phases of my life, I am always thankful for the help and support of my parents and family. I would like to make special mention of my grandfather, Arthur S. Merrifield, whose love of the ocean had a great impact on me. Most of all, I wish to thank my wife, Janet, for her love and patience. She and our daughter Sophie are the source of my greatest happiness.

This work was supported by the Office of Naval Research (contracts N00014-80-C-0440, N00014-85-C-0104, N00014-87-K-0005). Additional funding was provided by the Achievement Rewards for College Scientists foundation.

## VITA

| | |
|---|---|
| August 8, 1960 — | Born, Honolulu, Hawaii |
| 1978 — | A.B., Physics, University of California, Berkeley |
| 1982-1988 — | Research Assistant, Scripps Institution of Oceanography, University of California, San Diego |
| 1988 — | Doctor of Philosophy<br>University of California, San Diego |

## PUBLICATIONS

Merrifield, M. A., C. D. Winant, J. M. Robles, R. T. Guza, N. A. Bray, J. Garcia, A. Badan-Dangon, and N. Christensen, Jr., 1986, Observations of currents, temperature, pressure, and sea level in the Gulf of California 1982-1986. A Data Report. *SIO Ref. Series #86-11*, 153 pp.

Merrifield, M. A., A. Badan-Dangon, and C. D. Winant, 1987, Temporal behavior of lower atmospheric variables over the Gulf of California. 1983-1985. A Data Report. *SIO Ref. Series #87-6*, 192 pp.

Merrifield, M. A., and C. D. Winant, Shelf circulation in the Gulf of California: A description of the variability. Submitted to JGR, 1989.

## FIELDS OF STUDY

Major Field: Oceanography

Studies in Physical Oceanography and Fluid Mechanics
Professors Myrl Hendershott, Joe Reid, and Clinton Winant

Studies in Ocean Waves
Professors Robert Guza, Rick Salmon, and Rob Pinkel

Studies in Chemical Oceanography
Professor Joris Gieskes

Studies in Biological Oceanography
Professor Michael Mullin

Studies in Geological Oceanography
Professor Wolf Berger

Studies in Data Analysis and Numerical Methods
Professors Russ Davis, Robert Parker, and Richard Sommerville

Studies in Applied Mathematics
Professor Sinai Rand

ABSTRACT OF THE DISSERTATION

**Shelf Circulation in the Gulf of California**

by

**Mark A. Merrifield**

Doctor of Philosophy in Oceanography

University of California, San Diego, 1989

Professor Clinton D. Winant, Co-chairman
Professor Robert T. Guza, Co-chairman

The first long-term moored observations in the Gulf of California (1983-84) are used to describe the dynamically important spatial and temporal scales of the shelf circulation on opposite sides of the 150-km wide gulf, and to investigate the characteristics of coastal-trapped waves that propagate into the gulf along the mainland shelf. A description of the observations is contained in chapter 1. The main results of this section are:

1) Local wind forcing is not observed.

2) Flow on the two facing shelf regions is uncorrelated, although recirculation with basin flow is observed on both shelves. The net surface transport is correlated with the the cross-gulf pressure gradient.

3) A rise in subinertial sea level on the mainland shelf is accompanied by a drop in isotherm depths such that pressure fluctuations rapidly decay with depth.

4) Cross-shelf geostrophy is weakly apparent on both shelves. The acceleration of alongshelf currents is correlated with the alongshelf pressure gradient on the mainland shelf, indicating the presence of remotely forced waves. Only temperature observations show evidence of waves reaching the Baja California peninsula.

In chapter 2, an empirically derived propagating signal is compared with a coastal-trapped

wave model. The model is forced by a simple extrapolation of storm winds to the coast. The main results of this chapter are:

1) The observed temporal behavior of wave events is consistent with storm forcing of mode 1 coastal-trapped waves.

2) The observed and mode 1 density fields are similar in structure, although observed amplitudes are nearly three times larger than predicted. The observed offshore pressure field decays more rapidly with depth and has a shorter offshore decay scale than mode 1.

3) Alongshelf currents are barotropic during energetic wave events at the midshelf, in accordance with mode 1. Mode 1 cannot account for the observed cross-shelf structure in the alongshelf flow field.

4) Higher modes are not observed.

In chapter 3, complex empiric l orthogonal functions are assessed as a possible method for isolating propagating variability in the gulf data set. The results of this study indicate that CEOFs are inadequate for the detection of the wave signal due to the wide-banded frequency characteristics of the signal.

CHAPTER 1

# SHELF CIRCULATION IN THE GULF OF CALIFORNIA: A DESCRIPTION OF THE VARIABILITY

## 1. INTRODUCTION

Recent studies of shelf circulation have identified important dynamic processes of open coasts, e.g., cross-shelf geostrophy, upwelling, and coastal-trapped waves (see Brink, 1987 for a review). Circulation along sheltered coasts, as in a marginal sea, has received less attention. Marginal seas offer a particular advantage for shelf studies in that open ocean influences are diminished or more easily monitored. In turn, an understanding of shelf circulation in a marginal sea may give insight about the circulation of the basin as a whole since the shelves constitute a significant percentage of the total basin area. The Gulf of California is similar to a number of other marginal seas (Adriatic Sea, Red Sea, Persian Gulf) in that it is long and narrow (1000 km x 150 km), and open at the southern boundary. From 1983-1984, the gulf was the subject of a joint field experiment between Scripps Institution of Oceanography (SIO) and Centro de Investigación Científica y de Educación Superior de Ensenada (CICESE). The observations in the Guaymas Basin (Fig. 1), are the first long-term, moored measurements of currents, temperature, and bottom pressure, as well as winds, made in the Gulf of California. The objectives here are to present a basic description of these observations on seasonal, low frequency, and tidal time scales, to compare and constrast the two facing shelf regions, and to provide a qualitative assessment of the relative importance of local and remote forcing on gulf shelf circulation.

Of particular relevance to this study are the sub-tidal sea level events, with positive elevations of 10-30 cm and time scales of about 10 days, which propagate poleward along the Mexican coast into the Gulf of California (Christensen et al., 1983, Enfield and Allen, 1983). Enfield and Allen showed that these events are associated with tropical storms and hurricanes that occur during the summer-fall season off southern Mexico. Phase speeds indicate forced propagation in the region of storm activity slowing to free propagation in the gulf, where they are somehow dissipated, as they are not detected on the Pacific Ocean coast past the Baja California peninsula. Simple estimates of phase speed, length scale, and mass transport, based exclusively

on sea level observations, suggest that these events are hybrid form coastal-trapped waves, more similar to internal Kelvin than continental shelf waves. The present study provides information about the temperature and current fluctuations associated with these waves.

A brief review of circulation in the Gulf of California is given in section 2, and the experiment is described in section 3. In section 4, the basic observations (wind, temperature, pressure, and currents) are presented, with emphasis on identification of spatially coherent patterns. Rough momentum balances are given in section 5, a coastal-trapped wave event is described in section 6, and a summary follows in Section 7.

## 2. BACKGROUND

The Gulf of California, or Sea of Cortes, is located on the west coast of Mexico between the Baja California peninsula and the Mexican mainland (Figure 1). The gulf is divided into three distinct topographic regions. The northern region is shallow (typically < 200 m) and comprises roughly a third of the gulf's length. The southern province, in open communication with the Pacific Ocean to depths of 3000 m, is trough-shaped with a series of deep basins (1000-3000 m) flanked by a steep, rocky Baja California shelf and a wider mainland shelf. Numerous islands, capes, and inlets are found on either shelf. A third region of midriff islands, narrow passages, and shallow sills separate the northern and southern gulf.

Atmospheric forcing over the gulf is characterized by weak summer winds towards the northwest and stronger winter winds towards the southeast (Roden, 1964). Winds are polarized along the gulf axis by an uninterrupted mountain range along the Baja California peninsula (elevations higher than 700-1000 m) and to a lesser extent by the Sierra Madre Occidental (higher than 1500 m) further inland on the Mexican mainland. The peninsular mountains effectively isolate the gulf from the moderating influence of the Pacific Ocean resulting in a hot, arid climate more typical of the surrounding desert regions than the Pacific coastal zones. Conditions are somewhat more tropical during the summer when prevailing winds advect moist air in from the south. Tropical storms and hurricanes are active from May to October in the eastern north Pacific. These energetic disturbances, with wind speeds exceeding 100 knots, form at low latitudes and travel northwestward along the Mexican Pacific coast. The majority of storms turn westward before reaching the gulf, a lesser number turn toward the coast, while very few enter the gulf region directly (Roden, 1964). Only one storm crossed the southern mouth of the gulf during this experiment.

The circulation of surface waters in the southern gulf was first described by Thorade (1909), *using ship logs, as cyclonic with net surface transport in the direction of seasonal winds.* He also related colder mainland coast temperatures during winter to upwelling favorable winds. The cyclonic circulation pattern was also seen in late summer in hydrographic data (Roden and Groves, 1959) with low salinity water flowing northward on the mainland coast and high salinity water flowing southward along the peninsula at 50-m depth. A narrow jet of high salinity outflow was also seen along the Baja California coast at the gulf entrance during December (Roden, 1972) suggesting that the outflow may extend along the peninsula. Bray (1988), in a study of thermohaline circulation in the gulf, analyzed geostrophic currents at the same cross-gulf transect as our moored array. Her findings show cyclonic circulation in the Guaymas Basin during summer, weaker anti-cyclonic flow during spring and fall, and the vertical structure of the flow averaged across the gulf consisting of outflow between 50 m and 250 m, inflow between 250 m and 500 m, and a 50-m deep surface layer where transport is in the direction of seasonal surface winds.

The above description is representative of the basin scale flow. On shorter scales, circulation may be more complex. Brown (1965), in a series of drogue studies in the southern gulf, reported an irregular flow field changing with geographic location and depth. Eddy-like features have been observed in the Guaymas Basin with drogues (Emilsson and Alatorre, 1980) and in sea surface temperature (e.g., Badan-Dangon et al, 1985). Events which resemble the squirts observed off northern California (Kelly, 1985) have been detected north of Guaymas using drogues, current meters, and satellite images (M. Lavin, CICESE, unpublished data, 1988). Cold sea surface temperature plumes have been reported on both sides of the gulf and related to the onset of upwelling favorable winds (Badan-Dangon et al., 1985).

Tides in the gulf are mixed with considerable difference between the diurnal and semi-diurnal components. Filloux (1973), using observations of tidal elevation on the perimeter of the gulf, described the semi-diurnal tide as progressive towards the north with amplitudes in the central gulf of 0.1-0.3 m, increasing rapidly near the midriff islands to nearly 2 m at the head of the gulf. In contrast, the diurnal tide behaves like a standing wave with amplitudes ranging from 0.25 at the entrance to 0.5 m at the head of the gulf. The large semi-diurnal tidal range in the northern gulf is accompanied by strong tidal currents, particularly in the island passages where speeds of 3 m/s have been observed (Roden 1964). Hendershott and Speranza (1971) proposed that the strong currents in the north give rise to large tidal dissipation, manifested as a virtual amphidrome for the $M_2$ tide in the central gulf. The strong tidal flows also generate internal waves which contribute an estimated 10% to the dissipation of the semi-diurnal tide (Fu and Holt,

1984).

## 3. EXPERIMENT

The principal study site was a transect between Guaymas on the mainland coast and Santa Rosalia on the Baja California peninsula, in the guaymas Basin of the central gulf (Figure 1). The instruments were deployed in four phases, each approximately six months long (Figure 2). In the first phase (11/82-5/83), currents were measured on the Guaymas shelf to determine typical current speeds in this region prior to more extensive deployments. The second phase (5/83-11/83) was a pilot experiment designed to compare currents separated in the cross-gulf (Guaymas-Santa Rosalia) and along-gulf (Guaymas-Topolobampo) directions. Bottom pressure measurements were also made at these three shelf locations. The spatial scales of lower atmospheric variables, such as winds, pressure, and temperature, were sampled during July 1983 by extensive aircraft overflights in the northern half of the gulf (Candela et al., 1984). During the third phase (11/83-5/84), fixed PAMII (Portable Automated Mesonet) weather stations were deployed to measure winds, air temperature, and barometric pressure continuously for the remainder of the study (Merrifield et al., 1986). A second set of overflights was made during March 1984 (Candela et al., 1985). Moorings were maintained at Guaymas and Santa Rosalia to observe winter conditions on the two shelves. The main deployment (5/84-11/84) included a denser array across the Guaymas-Santa Rosalia transect with an additional mooring in the deep basin near the Guaymas slope, a mooring at Topolobampo, and pressure sensors at all three shelf locations as well as at San Francisquito Bay and Isla Tiburon, located north of the transect. In addition, sea level observations at Salina Cruz, Acapulco, Guaymas, Santa Rosalia, and Cabo San Lucas (Figure 1) were obtained from pre-existing tide gauges maintained by UNAM and CICESE. Mooring locations are shown in Figure 1; the depths and deployment times of each sensor are listed in Table 1.

Currents were usually measured (Table 1) with Vector Measuring Current Meters (VMCMs, Weller and Davis, 1980), but also with General Oceanics inclinometers (Barton et al., 1980). Records from a VMCM and inclinometer at 70-m and 75-m depth below the surface on the Guaymas shelf (M7) were in only fair agreement at low frequencies (correlation = 0.7) with the inclinometer yielding a noiser record. Temperature was measured at each current meter and pressure sensor package and, during the main deployment, with thermistor chains in 200-m depth on the Guaymas and Santa Rosalia shelves. Bottom pressure was measured by Paroscientific pressure sensors in a package designed and fabricated at SIO (Erdman, 1983). A complete

presentation of the moored observations and details of the data processing are given in Merrifield et al. (1986).

Low frequency or subinertial time series in this paper refer to series which have been convolved with a Groves 51-weight filter (Groves, 1955) and decimated to 6-hourly values. The Groves filter has a half-power point at approximately 0.3 cpd and is chosen for its ability to suppress leakage from strong tidal harmonics and its relative short length in the time domain, which minimizes data loss in time series with long gaps. In the following, a significant correlation between two time series excedes the 95% significance level. For the typical number of degrees of freedom (Davis, 1976), this corresponds to a correlation of at least 0.25.

## 4. DESCRIPTION OF OBSERVATIONS

*Winds*

Time series of low frequency winds at each of the PAMII weather stations (Figure 3) illustrate the dominant seasonal pattern of winds over the northern half of the gulf with winds toward the northwest during the summer and toward the southeast during the remainder of the year. Winds are strongest during winter with maximum speeds at Isla Tortuga (W5) of 15 m/s compared to 10 m/s during the summer. Principal axes of the low frequency winds are directed primarily along the gulf with local variations in orientation probably due to topographic steering (Figure 4). Standard deviations are typically 2-5 times larger in the along-gulf than cross-gulf wind component. The exception is at Isla Piojo (W2) where cross-gulf winds are as strong as along-gulf winds, likely due to lee waves over the Baja California mountains (C. E. Dorman, personal communication).

The spatial coherence of the low frequency wind field is examined with empirical orthogonal functions (EOFs). In this analysis, U and V wind components are combined into a vector time series and EOFs obtained from the complex covariance matrix (e.g., Kundu and Allen, 1977). This method is preferable to a scalar analysis because wind vectors sometimes rotate in time, with the U and V wind time series out of phase and hence yielding a low correlation at zero time lag. In contrast to a scalar analysis, the vector analysis combines coherent U and V winds into a single EOF mode. The first three spatial eigenvectors (Figure 4) are rotated so that the temporal expansion of each mode is aligned along its principal axis. Mode 1 winds describe 63.4% of the total observed low frequency variability, are aligned along the gulf axis, and are spatially coherent over the study region accounting for at least 50% of the variance at

each station. These winds are most energetic at the island stations W2 and W5, away from coastal boundaries. Mode 2 (19.5%) isolates the strong cross-gulf winds observed at W2. Modes 3 (11.3%) and 4 (4.4%, not shown) represent winds at Puerto Peñasco and Guaymas respectively that are probably associated with localized gales.

In later comparisons with moored observations, the dominant component of mode 1 wind is used to represent the along-gulf wind forcing. A representative amplitude of this forcing at the mooring transect, however, is not obvious (Figure 4) given that winds appear to be twice as strong at Isla Tortuga (W5) than at the coast (W4, W6). This also implies the presence of a cross-gulf wind curl which could have a significant effect on gulf circulation. One possible explanation for the varying wind speeds is the difference in station elevations at the transect. W5 was at the top of Isla Tortuga at approximately 150-m elevation, W4 was on a 100-m bluff at the coast, while W6 was on a 30-m high island less than 1 km from the coast. It is therefore unclear whether PAMII winds are representative of winds near the water surface. To investigate these issues, PAMII winds are compared with winds measured 30 m above the water surface during 14 overflights of the transect in March 1984. Overflight winds are averaged into 1-km sections along the cross-gulf track and EOFs obtained from the spatially-averaged covariance matrix. This analysis complements the wind station EOFs; whereas the PAMII data consists of 3 spatial measurements at the transect for over 300 days, the overflight data has 140 spatial measurements on 12 different days. The overflight and PAMII mode 1 spatial patterns (Figure 5) are normalized to unit value at Isla Tortuga (W5), leaving the temporal functions in physical units. The overflight pattern shows that winds are much more uniform across the gulf than implied by PAMII winds. The mode 1 temporal behavior of PAMII and overflight along-gulf winds are in good agreement indicating that, despite the poor temporal resolution of the overflights and the possibility of diurnal wind aliasing, the same variability is isolated in each EOF. In addition, the comparable amplitudes imply that PAMII winds at Isla Tortuga are similar to winds near the surface. The overflight winds indicate then that along-gulf wind amplitude can be considered uniform across the transect with negligible cross-gulf shears, and that this amplitude is best represented by the Isla Tortuga PAMII station rather than the coastal stations.

An important property of the along-gulf wind is its relationship to the surface pressure gradient. Geostrophic winds, computed from the difference in atmospheric pressure between Guaymas and Santa Rosalia, are in excellent agreement (correlation = 0.87) with PAMII mode 1 winds (Figure 6). Geostrophic winds are stronger than observed winds with a regression of 0.7 at Isla Tortuga, where mode 1 winds are at a maximum. This is consistent with observations made over water in the German Bight (Hasse and Wagner, 1971), where the regression between surface

and geostrophic winds was 0.6. The geostrophic wind can be simply obtained from pre-existing weather stations near Guaymas and Santa Rosalia and is used in later comparisons with moored observations in the absence of measured winds.

Diurnal winds dominate higher frequency wind fluctuations with peak speeds ranging from 3 to 5 m/s. These winds are oriented perpendicular to shore with winds measured at the coast 10-20% stronger than at the island stations. C. E. Dorman (personal communication) describes the diurnal circulation as a conventional sea breeze along the mainland coast and an upslope valley effect along the Baja California coast driven by the heating of mountain slopes. No significant difference, however, in the magnitude of diurnal winds at opposite sides of the gulf is observed.

*Temperature*

Near-surface temperatures in the Gulf of California exhibit a large seasonal range with especially high summer temperatures in comparison to Pacific waters at the same latitude across the Baja California peninsula (Robinson, 1973). The temperature range measured 10 m below the surface is about 18°C at Guaymas and 13°C at Santa Rosalia (Figure 7). The 1983 El Niño event (Robles and Marinone, 1987) is evident as Guaymas temperature is approximately 5°C warmer in the winter-spring of 1983 than in the same period of the following year. Although the averaged near-surface temperature over the period May 1983 to May 1984 is about the same (23°C) at Guaymas and Santa Rosalia, the range is larger at Guaymas with warmer summer and cooler winter temperatures. This same cross-gulf difference is also found in the island region north of the transect P7 - P10 (Figure 1). The larger temperature range on the mainland coast is consistent with seasonal upwelling (Thorade, 1909). Upgulf summer winds are up/downwelling favorable along the Baja California/mainland coast of the gulf resulting in the cooler temperatures at Santa Rosalia. The situation is reversed in winter when downgulf winds result in cooler temperatures on the mainland coast. The tendency then is for seasonal winds to moderate the seasonal solar heating of gulf water on the Baja California shelf while enhancing the extremes on the mainland shelf.

The occurrence of seasonal up/downwelling is also apparent in the contrasting vertical temperature profiles on opposite sides of the gulf (Figure 8). During the early summer, when thermistor chains were operating on both sides, temperatures below 100 m are slightly warmer at Santa Rosalia (1°C) while above this depth Guaymas temperatures are much warmer (5°C) with a well-developed thermocline region between 40-70-m depth (0.2°C/m). In constrast, the strongest gradient at Santa Rosalia (0.17°C/m) occurs in the upper 20 m. During the winter the vertical

structure has reversed across the gulf. At Guaymas, average temperatures for November 1984 resemble the summer upwelling profile at Santa Rosalia with the absence of a seasonal thermocline region. While the thermistor chain at Santa Rosalia was not operational during the winter, a CTD cast from November 1984 (PC6003 from Bray et al., 1986), near the shelf break, has a deeper thermocline region consistent with downwelling favorable winds for the Baja California shelf during this time of year.

Temperature fluctuations about the seasonal cycle are considerable at Guaymas during the summer, particularly at low frequencies (Figure 9). In contrast, temperature fluctuations at Santa Rosalia during the early summer are not as large. On both shelves, the largest fluctuations (Figure 10) occur at the depths of the highest mean vertical temperature gradient which, as noted above, is stronger and deeper in the water column at Guaymas in summer. When scaled by the mean temperature gradient at each depth, low frequency fluctuations are more uniform with depth on both shelves. Assuming that temperature fluctuations are primarily associated with the vertical displacement of isotherms, the weighted profile provides an approximate measure of typical isotherm displacements. At Santa Rosalia, these displacements increase from 5 m near the surface to 10 m below 80-m depth while values at Guaymas range from 10-15 m.

The spatial and temporal behavior of Guaymas low frequency temperature fluctuations, minus the seasonal cycle, are described with EOFs for the main 1984 deployment. Mode 1 (65% of the variance) describes temperature fluctuations which occur in phase over the entire shelf and are strongest in the thermocline region (Figure 11). There is a significant correlation (0.75) between the temporal behavior of mode 1 and Guaymas adjusted sea level, such that a rise in coastal sea level is associated with a sinking of isotherms over the shelf (Figure 11). A regression of sea level with the depth of the 21° isotherm at the Guaymas shelf break, which is generally below the surface mixed layer for most of the summer, shows that a 10-cm rise in sea level corresponds to a drop of approximately 20 m for this isotherm. The same is true for isotherms deeper in the water column. In addition, this relationship between sea level and temperature occurs in winter as well when temperature 70 m below the surface at the Guaymas midshelf (M7) and adjusted sea level are also correlated (0.62). Mode 2 (15.5%) has a spatial function with one zero crossing with depth such that fluctuations approximately above and below the thermocline (~30 m) are 180° out of phase (Figure 11). The temporal expansion for this mode is significantly correlated (0.65) with bottom pressure at the 100-m isobath (Figure 11). Visually, the similarity between the two time series is strongest during a pressure rise in July which will be seen in the following section to be the largest propagating event of the 1984 summer. This large event is also evident in mode 1 indicating that temperature fluctuations associated with propagating events are not

isolated by a single mode. The signal of the propagating events below 40-m depth in the first two modes sum constructively indicating that sub-thermocline isotherm displacements are emphasized during these events.

A similar EOF analysis is performed on residual low frequency temperature on the Santa Rosalia shelf (Figure 12) revealing a less coherent spatial structure than at Guaymas. Like Guaymas, low frequency temperature changes appear to be uniform across the shelf as fluctuations at the 100-m (M11) and 200-m (M10) moorings are similar at depth. Mode 1, however, describes only 53% of the total observed variability and has a zero crossing with the depth in contrast to mode 1 at Guaymas. The temporal behavior of mode 1 temperature is only weakly correlated (0.39) with adjusted sea level at Santa Rosalia (Figure 12).

On both shelves as well as in the basin, low frequency winds and temperature functions are not significantly correlated in any season. Instead, much of the temperature signal below the upper mixed layer is associated with propagating variability. This is somewhat surprising given the evidence for seasonal upwelling presented above and the reported upwelling events seen in satellite images (Badan-Dangon et al., 1985). One possibility is that the seasonal upwelling signal may be a result of upwelling primarily occurring about specific topographic features. Upwelling plumes along the mainland coast often occur north of the Guaymas moorings (Badan-Dangon et al., 1985), closer to the complicated topography of the island region. Upwelled water may then be mixed and advected to the transect array on longer time scales, creating the observed seasonal signal without a correlation between wind and temperature at low frequencies. The propagating signal in temperature is apparent in maximum correlations (Table 2), with Topolobampo leading Guaymas by 40 hours and Guaymas leading Santa Rosalia by 8.5 days. The nature of this long lag across the gulf is discussed below in the context of coastal-trapped waves (section 6).

Standard deviations of temperature fluctuations in the diurnal/inertial (0.92-1.08 cpd) and semi-diurnal (1.92-2.08 cpd) bands for Guaymas and Santa Rosalia during the summer 1984 deployment (Figure 13) show that, as for lower frequencies, the largest fluctuations occur at depths of strongest stratification on both shelves. When scaled by the mean temperature difference at each depth, displacements range from 2-8 m on each shelf with weak diurnal/inertial fluctuations at Guaymas (Figure 13). Semi-diurnal band EOFs at Guaymas reveal that much (83%) of the temperature signal is nearly in phase at all depths with a vertical structure similar to the rms profile shown in Figure 13. The temporal behavior of this mode has the same spring-neap modulation as the semi-diurnal band surface tide with sea level leading temperature by approximately 8 hours. These fluctuations are larger by a factor of 5 than the signal which could be produced by the barotropic tide moving the thermistor chain vertically by the mean

temperature gradient. Instead these fluctuations are likely due to internal tides. The observations described here are not adequate to determine the origin of this signal. Semi-diurnal fluctuations on the Santa Rosalia shelf, however, are incoherent with the surface tide and do not exhibit the same coherent vertical structure as at Guaymas. The same is true of tidal band fluctuations in the basin and on the mainland shelf at Topolobampo. It is unclear why this signal is only apparent at Guaymas. Diurnal fluctuations on both shelves are more stochastic and appear unrelated to the barotropic tide, diurnal winds, or daily heating and cooling.

*Bottom Pressure and Sea Level*

Sea level has a seasonal range of approximately 0.5 m in the gulf, reaching a maximum in July and a minimum in February. The same range is not observed in bottom pressure below 100 m suggesting that seasonal changes in sea level are associated with the heating of upper layer waters. To verify this, changes in sea surface height about a mean value is estimated from the 200-m thermistor chain and bottom pressure sensor (P5) at the Guaymas shelf break. Density changes in the gulf are roughly correlated with changes in temperature (Bray, 1988). CTD profiles near the Guaymas shelf provide a means of estimating density directly from temperature,

$$\rho(z) = 1.028 - 0.854 \times 10^{-4} T(z) - 0.355 \times 10^{-6} T(z)^2 \qquad (1)$$

with a standard error of $2.3 \times 10^{-5}$ g/cm$^3$. Pressure near the surface is then computed from the hydrostatic equation using bottom pressure and density from the thermistor chain,

$$P(z_o) = P(z_b) - g \int_{z_b}^{z_o} \rho(z) dz \qquad (2)$$

where $z_b = 200m$, and related to sea level,

$$\eta = (\rho(z_o) g)^{-1} \left[ P(z_o) - P_{atm} \right] . \qquad (3)$$

Over the duration of the thermistor chain deployment, the range in $\eta$ is approximately 0.2 m in both observed and computed sea level. In equations 2 and 3, $P(z_b)$ and $P_{atm}$ contribute only a

few cm to the seasonal range in $\eta$ confirming that density changes in the upper 200 m account for most of the observed seasonal sea level signal.

At subtidal frequencies, the poleward propagating events described by Christensen et al. (1983) and Enfield and Allen (1983) are evident in sea level and bottom pressure records along the mainland coast during this experiment (Figure 14). Atmospheric pressure fluctuations account for no more than 10% of sub-tidal sea level variability along the coast and cannot explain the propagating signal. Local winds are also uncorrelated with sea level and pressure in the gulf. Most of the events are present as far south as Salina Cruz (about 2000 km south of Topolobampo) and travel approximately non-dispersively into the Gulf of California. Sea level at Santa Rosalia does not show the event propagating down the Baja coast. Travel times and hurricane tracks suggest that events at Cabo San Lucas (CB) are not waves continuing down the Baja California peninsula but are instead forced by the hurricanes themselves as they skirt the southern tip of Baja California. Phase speeds are estimated from neighboring sea level and pressure sensors using lagged correlations and times between peak events (Table 3) with the events shown in Figure 14. The estimates are in good agreement with previous values obtained by Enfield and Allen, 1983.

On the mainland shelf, sub-tidal bottom pressure fluctuations decay rapidly offshore. Bottom pressure fluctuations at the Guaymas 200-m shelf break (P5), approximately 12 km from shore, are weak compared to coastal adjusted sea level particularly during the large propagating events of July 1984 (Figure 15). In contrast, pressure fluctuations at 100-m depth (P6) and adjusted sea level at Santa Rosalia are similar in magnitude. The Guaymas P5 bottom pressure, however, does not take into account the contribution of density on pressure, or internal pressure changes. Therefore, pressure just below the sea surface and at 100-m depth above the bottom pressure sensor P5 is computed from equation 2 ($z_o$ = 0 m and 100 m) using the 200-m thermistor chain at the Guaymas shelf. When compared at similar depths, pressure fluctuations are nearly identical across the shelf (Figure 15). The contribution of sea level changes to pressure is compensated by adjustments in the density field such that pressure fluctuations at 100 m are reduced to half the near surface amplitudes, and 200-m pressure is nearly constant. That the spatial scale of variation of bottom pressure is not the same as for sea surface elevation is evident in the first EOF (90% of total variance) of the the sub-tidal pressure field at Guaymas (Figure 16). The horizontal e-folding scale is on the order of 50 km, compared to the 30-km deformation radius given by Christensen et al. (1983), while the same decay occurs in 160 m in the vertical. On the Santa Rosalia shelf, density changes do not significantly contribute to fluctuations in the pressure field in the upper 100 m.

Although local winds are uncorrelated with sea level and pressure at all locations around the gulf, the wind response may be masked by the more energetic propagating variability. In order to account for this, near surface pressure at Isla Tiburon (P10) is estimated from adjusted sea level at Guaymas and along-gulf wind stress in a multiple regression. The Guaymas time series is lagged in time to obtain maximum correlation with sea level at Isla Tiburon and to approximate the portion of the signal associated with travelling waves. Wind stress is obtained from mode 1 winds described above using the relation given by Large and Pond (1981). Ideally if there is a residual relationship between wind and sea level, the multiple regression should return a significant coefficient for winds. The regression explains 81% of the variance at Isla Tiburon, but nearly 90% of the explained variance is attributed to lagged Guaymas adjusted sea level. The regression coefficient for along-gulf wind stress is small and not significantly different than zero. This result of no local wind forcing is similar for all pressure records around the gulf and for different lags of winds relative to pressure.

*Currents*

Representative subinertial currents on the Guaymas and Santa Rosalia shelves are compared in Figure 17 for the entire two-year experiment. Currents at Santa Rosalia were measured 10 m below the surface at the 90-m isobath while the Guaymas time series is a compilation of currents measured closest to the 100-m isobath (maximum separation = 3 km). The alongshelf directions are chosen as the principal axes for each time series which agree well with the orientation of local isobaths on each shelf. Currents are strongly polarized with 80-90% of the total variability directed in the alongshelf direction. Alongshelf currents are both stronger and more variable at Guaymas than at Santa Rosalia with peak speeds of 75 and 50 cm/s, and rms speeds of 15 and 10 cm/s repectively. Current spectra at Guaymas, Santa Rosalia, and the Guaymas Basin, are red with significant peaks at the tidal harmonics (Figure 18). Energy levels are higher in the summer than winter over all frequencies, although a direct comparison is only valid at Santa Rosalia given the different locations of Guaymas observations. Subinertial currents are most energetic at Guaymas in both seasons while higher frequency currents are more similar in energy content at the three locations. The difference in high frequency energy between Guaymas and Santa Rosalia during the winter is probably due to stronger currents in 1984 relative to 1983 rather than a difference between the two shelves.

Alongshelf currents at Santa Rosalia (Figure 17) appear to have a slight seasonal signal with a tendency for downgulf flows during summer and upgulf during winter. This is opposite to the direction of seasonal winds. To investigate seasonal patterns in the current field, mean

currents are computed separately for the summer (June- September), when winds are blowing to the north, and the remainder of the year, when winds are blowing southward. Currents during these two periods are considered to have a significant seasonal mean if the mean differs from zero by at least 3 standard errors, with the standard error of a sample mean defined as $(<v'^2>/N)^{0.5}$ where $v'$ is the standard deviation of the flow and $N$ is the number of independent samples (Davis, 1976). Along-gulf currents have significant mean flows in the basin at 50-m depth (order 10 cm/s) and on the Santa Rosalia shelf at 10-m and 30-m depth (5-8 cm/s) in both summer and winter, with 50-m basin currents flowing in the direction of seasonal winds and currents at Santa Rosalia directed against the wind. This occurrence of cyclonic summer and anti-cyclonic winter surface circulation in the Guaymas Basins was observed by Bray (1988) using hydrographic data. This pattern does not appear to extend onto the Guaymas shelf where mean flows are not significant. A causal relationship between seasonal winds and the sense of rotation of Guaymas Basin circulation is not known.

At low frequencies, currents vary considerably across the Guaymas-Santa Rosalia transect (Figure 19). On the Guaymas shelf, surface currents decay rapidly in amplitude towards the coast with rms speeds decreasing from 27 cm/s at the shelf break (M8) to 10 cm/s at midshelf (M6) and 2 cm/s at the inner-shelf (M4). Similarly the alongshelf polarization of currents increases towards the coast with the percentage of alongshelf to total rms current speed increasing from 74% at the shelf break to 86% near the coast. Correlations of alongshelf currents between the three moorings are significant but low (Table 4). Maximum correlations occur with alongshelf currents at the midshelf (M6) leading currents at the shelf break (M8) by 32 hours and inner shelf (M4) by 52 hours. The currents at these locations are most similar during several energetic events in late June and July, in part associated with propagating events described below. While the vertical structure of the current field is not well sampled, the alongshelf currents at M4 and in the upper 30 m at M6 are correlated at different depths (Table 4) and are similar in amplitude. In addition, alongshelf currents at 10 m and 70 m in 100-m total depth (M7), measured during winter and late summer of 1983, are also well correlated with comparable amplitudes indicating that alongshelf flow is reasonably barotropic over the shelf. In contrast, correlations of cross-shelf flows are typically not significant between the various sensors.

Current measurements in the basin (M9) are most energetic near the surface with rms speeds of 22 cm/s at 50-m depth compared to 7 cm/s at 300 m and 5 cm/s at 850 m. Currents at 50 m are directed primarily along the gulf and are not correlated with deeper flows. Currents at 300 m and 500 m are nearly identical with principal axes directed more in the across gulf direction, primarily due to one strong cross-gulf flow event in July. Weak currents at 850 m appear

unrelated to flows higher in the water column.

Currents on the steep Santa Rosalia shelf are more spatially uniform than at Guaymas (Figure 19) with rms speeds ranging from 10-15 cm/s. Currents seperated by 2 km across the shelf (M10 and M11) and 10 m below the surface are correlated (Table 4) in both the alongshelf (0.94) and cross-shelf (0.71) directions. The vertical structure of currents at M11 appears barotropic in Figure 19 particularly during the energetic flow in late July. The correlation is larger between flow at 10 m and 30 m, than flows between 10 m and 70 m, due in part to the change to upgulf surface flow in late fall which does not occur at 70-m depth. The weaker alongshelf flow observed in the summer/fall of 1983 (5-9 cm/s rms speeds) is even less uniform with depth as correlations between flow at 10 m and 65 m were not significant.

Santa Rosalia and Guaymas low frequency currents are uncorrelated in all seasons (Table 4), confirming the visual impression (Figures 17 and 19) that shelf flows on opposite sides of the gulf are unrelated. On the mainland coast, alongshelf currents at Topolobampo and Guaymas are correlated during both summer deployments with Topolobampo leading by about 29 hours, similar to the lags found in temperature and pressure correlations. Winter currents at Topolobampo were not available for comparison. Although currents are unrelated across the gulf, basin flow is correlated with alongshelf currents at both Santa Rosalia and Guaymas. Alongshelf currents in the basin at 50-m depth (M9 Figure 20) have longer time scales (4.8 days) than at 10-m depth on the Guaymas shelf (3.1 days). The significant negative correlation (-0.54) is most apparent in June and July during 4 periods of strong opposite flowing currents. Wind and current fluctuations appear related at this time although a causal relationship is unclear given that wind events are not particularly energetic and later periods of strong downgulf winds do not have an associated current response. These sporadic occurrences of opposing currents may indicate eddy-like flow features near the Guaymas shelf break. Although satellite images during these particular events are unavailable, the presence of eddies in this area is supported by satellite images showing entrainment patterns in sea surface temperature with scales on the order of 30 km (C. Paden, personal communication). The correlation between alongshelf currents at Santa Rosalia (10-m depth at M11) and at the basin is also negative (-0.61). The correlation on this side of the gulf is due primarily to opposing flows in July and early fall. The opposing flow is remarkably steady over the month of October and is related to the seasonal pattern described above.

Currents above the inertial frequency have typical rms speeds of 2-3 cm/s in this region of the gulf. Current spectra (Figure 18) show significant peaks at the diurnal and semi-diurnal bands at Santa Rosalia, while at Guaymas only the semi-diurnal band is signficant. Like low frequency currents, tidal flows are polarized in the alongshelf direction with more cross-shelf energy

further from the coast. Tidal band currents are not coherent at different sensor locations on either shelf or in the basin. Surprisingly, this is true at Guaymas where semi-diurnal temperature fluctuations suggest the presence of internal tides. Alongshore current at the Guaymas shelfbreak (10-m depth M8) is coherent (0.74) with the mode 1 semi-diurnal band temperature signal with currents lagging by roughly 2 hours.

## 5. MOMENTUM TERMS

*Cross-Shelf*

A number of recent field observations have verified that a near geostrophic balance exists at the coast between alongshelf current and cross-shelf pressure gradient,

$$v = (f\,\rho)^{-1} dP/dx \tag{4}$$

The first verifications using direct measurements of bottom pressure were made during the Nantucket Shoals Flux Experiment (NSFE, Brown et al., 1985) and the Coastal Ocean Dynamics Experiments (CODE, Brown et al., 1987, Winant et al., 1987). The CODE experiments were made along a straight coast in an upwelling regime characterized by strong local wind forcing, weak stratification, and nearly barotropic flows. NSFE was conducted on a wide shelf, 10 times the width of the Guaymas shelf, with moderate local wind forcing and high summer stratifications similar to those found in the gulf. In both of these studies, suitably averaged alongshelf current observations were in excellent agreement with the geostrophic current derived from the cross-shelf gradient in bottom pressure measurements. The depth-averaged, or barotropic transport, was compared to geostrophic current for the CODE observations, while cross-shelf averages at various depths were compared for the NSFE observations.

The geostrophic current at Guaymas is obtained from the pressure difference between adjusted coastal sea level and surface pressure at the shelf break (P5, see Figure 15). The pressure gradient is obtained in a similar manner on the Santa Rosalia shelf with surface pressure computed above the 100-m pressure sensor (P6) using temperature observations from the three current meters. This correction for internal pressure changes, however, is negligible at Santa Rosalia. In this construction of the pressure gradient, the geostrophic current is a measure of the transport near the surface. Observed current at Guaymas is taken as an average of the alongshelf currents at M8, M6 and M4, 10 m below the surface. Santa Rosalia current is from the 10-m

sensor at M11 in 100 m total water depth. Since pressure gradients are found to have a significant seasonal component that is associated with errors in computing density directly from temperature rather than with a physical signal, all time series involved in pressure gradient comparisons are band-passed (0.03-0.33 cpd). If the geostrophic balance is valid, the observed and geostrophic current at the sea surface should be well correlated with a regression near 1.0. Correlations between observed and geostrophic currents (Figure 21) on both sides of the gulf are signficant (0.47 at Guaymas, 0.41 at Santa Rosalia) with regression coefficients of 0.71 and 1.09 at Guaymas and Santa Rosalia respectively. Although the time series are only moderately correlated, many of the flow features at Guaymas, particularly during the large propagating event of July, are well represented by the geostrophic current. A comparison of the geostrophic current with the individual current records at Guaymas reveals that the highest correlation, 0.44, occurs at M8, decreasing to 0.37 at M6, with an insignifcant correlation at M4 indicating that geostrophic currents are not uniform across the shelf. An outer shelf geostrophic current maximum was also found in the NSFE observations. The correlation at Santa Rosalia does not change significantly if the depth-averaged flow is used in place of the single current record. When the geostrophic current is obtained from the pressure gradients measured along the bottom as in the aforementioned studies, correlations with observed alongshelf currents are no longer significant emphasizing the need to account for internal pressure effects in the present data set.

In a further test of geostrophy, the difference in adjusted sea level across the gulf between Guaymas and Santa Rosalia is examined. This cross-gulf pressure gradient is compared with the unweighted average of alongshelf currents at Santa Rosalia (M11), the basin mooring (M9), and Guaymas (M8). Including weaker nearshore flow at Guaymas does not significantly alter this average. The geostrophic current from the cross-gulf pressure gradient and average current from the three current records are well correlated (0.70) indicating that the net surface flow through a cross-gulf transect can be represented by a simple pressure gradient (Figure 22). This result gives insight into several aspects of gulf flow. First, most of the pressure gradient signal is due to pressure fluctuations at Guaymas with only weak fluctuations at Santa Rosalia (Figure 15a). The pressure signal at Guaymas has been shown to consist primarily of propagating variability along the mainland coast with very little local wind contribution. Hence most net subinertial transport at the surface past the Guaymas-Santa Rosalia transect occurs during propagating sea level events. Secondly, most of the net transport takes place at or near the Guaymas shelf. The portion of flow on the shelves correlated with the basin flow (see Figure 20) cancels out in the averaging with the remaining net flow comprised mainly of Guaymas current. The correlation of the cross-gulf pressure gradient with Guaymas current alone is (0.58). Much of the

current in the basin and at Santa Rosalia must be then associated with recirculating flow patterns not contributing to net surface transport. If the main surface transport is indeed associated with wave events at Guaymas, it may be inferred from the mode 1 characteristics of the density field at Guaymas that compensating flow for the net transport pictured in Figure 22 takes place deeper in the water column, as with an internal Kelvin wave. Deep currents near the Guaymas shelf were not available for confirmation. Fourth, the correlation is remarkably high given the limited sampling of the current field. This lends confidence to the assumption that the major patterns of along-gulf flow have been sampled, or alternatively, that any energetic flows not adequately sampled are associated with recirculating cells.

*Alongshelf*

The linear alongshelf momentum balance for subinertial flow is:

$$\frac{dv}{dt} + fu = \frac{-1}{\rho_o}\frac{dp}{dy} + \frac{\partial \tau^y}{\partial z} \tag{5}$$

where the principal sources of $\tau^y$ are surface wind stress and bottom friction. The relative magnitudes of terms in this equation vary over different shelf regions (Brink, 1987), however when local wind stress is strong, winds and alongshelf flow are generally related. Lentz and Winant (1986) found that the alongshelf momentum balance for depth-averaged subinertial flow varies across the southern California shelf. On the inner shelf, wind stress is balanced by bottom friction while in deeper water, in the absence of strong local winds, alongshelf currents are balanced by the alongshelf pressure gradient. A similar analytic result was obtained by Mitchum and Clarke (1986) who found that the inner shelf balance between surface wind stress and bottom friction extends offshore to total water depths of approximately 2.5 times the Ekman e-folding depth. A rigorous examination of the momentum balance in the gulf is not possible given the sparse mooring array. Instead, the relative importance of local winds and pressure gradients in forcing alongshelf flows is examined on both sides of the gulf.

A multivariate regression of the form

$$dv/dt = \beta_1\, dP/dy + \beta_2 \tau^y \tag{6}$$

is performed on each current record at the transect during the main deployment. The alongshelf pressure gradient on the mainland shelf is obtained from the difference between adjusted sea level at Guaymas and near surface pressure at Isla Tiburon (P10), and on the Baja California shelf

between adjusted sea level at Santa Rosalia and near-surface pressure at San Francisquito (P7). It is noted that point measurements of the flow are compared with pressure gradients over approximately 300 km distances. Bottom friction is not considered since current measurements are typically near the surface. In addition, $fu$ is not included given the noisy records and poor spatial coherence of cross-shelf currents over either shelf. In each regression, the two inputs are shifted in time to obtain maximum correlation with $dv/dt$. The hindcast skill equivalent to the percentage of $dv/dt$ variance explained in each regression, is significant on both shelves (Table 5), although less than 10% of the variance is accounted for at Santa Rosalia (M11). The regression is most successful in explaining currents at the Guaymas shelf break (M8) accounting for over 40% of the variance. On the Guaymas shelf, nearly all of the explained variance is due to the alongshelf pressure gradient with winds contributing a negligible percentage. The negative values of $\beta_1$ are consistent with equation 5. The pressure gradient lags $dv/dt$ at Guaymas as would be expected for a poleward propagating pressure signal as the pressure difference, taken between Guaymas and Isla Tiburon, is centered north of Guaymas. In contrast, the pressure gradient along the Baja California peninsula is not related to currents at Santa Rosalia. This does not necessarily imply that the pressure gradient in unimportant in driving flow along this shelf. The poor relationship may indicate that pressure gradients over shorter length scales than the 300 km sensor seperation are important between Santa Rosalia and San Francisquito. Winds are also unrelated to $dv/dt$ on the Santa Rosalia shelf and in the basin. The negligible effect of local wind is similar if $v$ is used instead of $dv/dt$ in equation 6. This is true on the Guaymas inner shelf where a relationship between wind stress and bottom friction (assumed proportional to $v$) was observed in the aforementioned studies. The lack of a wind response also occurs whether local winds (W4 or W6) are used instead of the spatially uniform EOF wind, or if different lags between wind and $dv/dt$ are used in the regression.

The reason for the weak correlation between winds and currents is examined by comparing wind magnitudes, stratification, and current wind response in the gulf with other shelf studies (Table 6). Currents in the first two studies in Table 6 were characterized as having a strong wind response, as indicated by typical correlations between alongshelf winds and currents near the surface at a midshelf location (Winant et al., 1987; Beardsley et al., 1985). Common to both studies was a combination of weak stratification and strong winds. A moderate wind response was reported in the next two studies. On the southern California shelf, winter winds were weak but the lack of stratification apparently allows a measureable wind response in the current record (Lentz and Winant, 1986). Conditions at NSFE were strongly stratified during the summer but winds were also fairly strong (Beardsley et al., 1985). The remaining studies are typified by a

weak wind response and in most cases characterized by high stratifications and weak winds. During the CUEA experiment on the Peruvian shelf (Brink et al., 1983), stratification was similar to CODE-2 but weak, fluctuating winds and the presence of coastal-trapped wave variability led to a low wind response. On the southern California shelf (Lentz and Winant, 1987), the relationship between winds and currents was inconclusive although a typical wind response was not observed, negative correlations occurred during summer. In the context of these studies, the absence of a measurable wind-driven subinertial circulation in the Gulf of California is not unusual given the weak winds and strong stratification found throughout most of the year.

## 6. A COASTAL-TRAPPED WAVE EVENT

The importance of remotely forced, propagating variability along the mainland shelf of the Gulf of California is evident in both lagged correlations of temperature, pressure, and current observations separated along the coast (section 4), and in the dynamic relationship between the alongshore pressure gradient and current accelerations at Guaymas (section 5). In this section, moored observations during the largest wave of the summer of 1984 are described, with the goal of establishing the qualitative structure and dynamic importance of these events. A more detailed comparison of observations with coastal-trapped wave theory will be presented in a later paper.

The event is actually a sequence of two 20-cm sea level elevations (Figure 14) in July 1984 associated with hurricanes Genevieve and Fausto which were active south of the gulf region (Gunther, 1985). As noted by Christensen et al. (1983), events often consist of 2-3 peaks in sea level, attributable to the grouped occurrence of storms (Gray, 1982). The poleward propagation of this event is evident in sea level and bottom pressure records along the mainland coast as far south as Salina Cruz. The event propagates non-dispersively from Topolobampo to Isla Tiburon with an amplitude of 20 cm and an alongshore scale on the order of the length of the gulf. The apparent damped amplitude at Topolobampo is due to the depth of the sensor (i.e., no adjustment for internal pressure, Figure 15). The event appears to continue into the northern gulf as is evident in the record at San Francisquito although now somewhat altered in temporal shape. Sea level at Santa Rosalia does not show the event propagating down the Baja California coast. A rise in sea level of 5 cm occurs at Santa Rosalia approximately 1 to 2 days after the leading edge of the event reaches Guaymas and lasts for the duration of the event. This occurs during an event of similar amplitude in 1983, and was also observed by Christensen et al. (1983, see their Figure 8) for a 1976 wave event. This may imply that larger events do span the width of the gulf.

The temperature and flow behavior at the Guaymas-Santa Rosalia transect during this wave event is illustrated in Figure 24. Alongshelf currents at Topolobampo (M1, 100-m isobath) are directed up the gulf with amplitudes of roughly 50 cm/s, and are barotropic. At Guaymas, the wave event occurs after a period of strongly fluctuating current, particularly at the shelf break (see M8 in Figure 20). Nevertheless currents at the mid (M6) and outer (M8) shelf have the same upgulf flow. There is a slight phase shift with the alongshore current at M6 leading M8 by roughly 10 hours. The strongest nearshore (M4) currents of the summer occur during the event but are directed downgulf counter to offshore currents and the geostrophic pressure gradient. One explanation may be some type of recirculation cell associated with the rough bathymetry at the coast. The M4 mooring was located just southward of a small cape and offshore island. Deeper shelf currents were not available although the barotropic alongshelf current structure observed at Topolobampo was also observed at Guaymas (M7 at the 100m isobath) during a simlar event in 1983. In the basin (M9), there is a current away from the mainland shelf at 300 m and 500 m when the event passes Guaymas although the double-peaked nature of the event seen on the Guaymas shelf is not evident in the basin. No changes in alongshelf current or temperature wave response is observed in the basin.

At Santa Rosalia (M11), the most energetic currents of the summer (50 cm/s) occur approximately 36 hours after the large event has passed the array at Guaymas. This current, directed downgulf, does not have the same temporal shape as the wave event nor is it apparent in the alongshelf pressure gradient between Santa Rosalia and San Francisquito. The same downgulf current response occurs, however, during an event of similar amplitude in the summer of 1983. The fact that the current is not associated with a pressure gradient between the island region and Santa Rosalia suggests that the current is not directly related to either the wave event or with a buildup of a sea level head as the wave enters the shallow northern gulf. One possibility is a cyclonic circulation cell setup in the basin by strong upgulf currents on the mainland shelf during the passage of energetic wave events (Niels Christensen, personal communication). Such a structure was observed spanning the width of the gulf near Topolobampo during a drogue study in August 1978 (Emilsson and Alatorre, 1980). An energetic event was present in the gulf approximately two weeks before the study was made. Downgulf currents at Santa Rosalia after the July 1984 event persist for approximately two weeks. The existence of such a closed flow pattern would constitute one of the major exchange mechanisms of waters across the gulf during the summer and warrants further investigation.

The temperature, or equivalently density, behavior observed on the mainland shelf is similar to a first mode internal Kelvin wave; isotherms across the shelf sink by approximately 60

m during the 20-cm rise in sea level. The displacements are not limited to the thermocline region but occur with similar amplitudes to at least 130 m. Temperature does not change noticeably in the upper mixed layer at 10-m depth. Alongshelf currents at Guaymas ($M6_{10\ m}$ and $M8_{10\ m}$) are correlated (-0.50) with mode 1 temperature at Guaymas, pictured in Figure 11a, over the entire deployment. This is the only signficant temperature-current correlation at the Guaymas-Santa Rosalia transect observed during this study. The negative correlation is consistent with the first mode internal Kelvin wave as a poleward alongshelf current corresponds to a deepening of isotherms over the shelf.

Pressure at Guaymas, as well as temperature (Table 3), is correlated with near bottom temperatures at Santa Rosalia with Guaymas leading Santa Rosalia temperature by approximately 8 days in both the 1983 and 1984 summer deployments (Figure 25). In 1983, the energetic events in August and September at Guaymas are clearly related to temperature fluctuations at Santa Rosalia. In 1984, the comparison is less clear although the large July event is apparent on both sides of the gulf. Temperature fluctuations at all depths at Santa Rosalia were stronger during the summer of 1984 than 1983 suggesting that the propagating signal is present but masked by other variability. A preliminary study of coastal-trapped wave phase speeds in the gulf, using the algorithm of Brink and Chapman, 1987, shows that mode 1 waves have a travel time of roughly 8 days between Guaymas and Santa Rosalia assuming the events travel around the head of the gulf without correction for coastline curvature or the blocking effect of the islands. If strong propagating events do in fact travel around the perimeter of the gulf to Santa Rosalia, their characteristics appear substantially altered with only weak sub-thermocline fluctuations apparent in our observations at this long lag time.

## 7. SUMMARY

Moored observations indicate that local winds are relatively unimportant as a direct forcing mechanism for subinertial shelf circulation in the Gulf of California. Along-gulf winds, which are to a large extent uniform over the northern gulf, are not correlated with fluctuations in the current, temperature, or pressure fields at low frequencies. The weak and variable winds and high stratification in the gulf are typical of regions of poor wind response.

On seasonal time scales, differences in temperature and vertical temperature profiles across the gulf reflect the occurrence of seasonal upwelling. Up/downwelling occurs in the summer on the Santa Rosalia/Guaymas shelf with the opposite situation occurring in winter. Seasonal-averaged mean currents are weak (< 10 cm/s). Near the surface, mean currents are in

the same direction as seasonal wind in the basin as reported by Bray (1988), and against the wind on the Santa Rosalia shelf. Mean currents at Guaymas are not significant.

Low-frequency current, temperature, and pressure fluctuations are stronger on the mainland than Baja California shelf and are not generally correlated across the gulf. Maximum lagged correlations on the mainland coast indicate poleward propagation of alongshelf current, temperature, and pressure signals. Current speeds are strongest at the shelf break at Guaymas with very weak nearshore flows. The pressure field at Guaymas displays an isostatic relationship between adjusted sea level and temperature fluctuations such that bottom pressure at 200-m depth is nearly constant. Adjusted sea level and temperature fluctuations in the upper water column are weakly correlated on the Santa Rosalia shelf. Alongshelf currents at Guaymas and Santa Rosalia are correlated with the cross-shelf pressure gradient with the correlation at Guaymas strongest for currents near the shelf break. Baroclinic pressure must be taken into account when determining geostrophic currents from pressure at different depths. In the alongshelf momentum balance, the time derivative of alongshelf currents and pressure gradients along the coast are correlated at Guaymas indicating that a signifcant percentage of the current variabilty along the mainland coast is associated with nonlocal forcing. Correlations between currents and pressure gradients are again highest for currents at the shelf break. This relationship between currents and alongshelf *pressure gradients* was not observed at Santa Rosalia where propagating variability is not observed in sea level and bottom pressure records.

Tidal and inertial currents are weak (order 5 cm/s) in this region of the gulf. Semidiurnal temperature fluctuations on the Guaymas shelf have a zero mode vertical structure and are coherent with sea level displaying in amplitude with the spring-neap cycle. Alongshelf currents are weakly coherent with this signal. These fluctuations are believed to represent internal tides although they are only observed on the Guaymas shelf.

Storm-generated coastal waves have phase speeds on the order of 200-300 km/day as reported by Enfield and Allen (1983). Along the mainland shelf during the passage of a 20-cm event, the alongshelf current on the mid shelf is roughly 50 cm/s and is barotropic in structure. Currents near the surface are strongest at the shelf break and decay rapidly towards the coast with slight phase differences across the shelf. The density field responds like a first mode internal baroclinic wave with a 20-cm rise in sea level associated with a 40-m depression of isopycnals throughout much of the water column. The same current and temperature signals are not found at Santa Rosalia during coastal-trapped wave events. Alongshelf currents are energetic after large events but are not associated with observed alongshelf pressure gradients. Sub-thermocline temperatures at Santa Rosalia and Guaymas are correlated with Guaymas leading Santa Rosalia by

7-9 days which is consistent with the computed travel time of these waves around the head of the gulf.

Our conclusion is that shelf circulation on either side of the gulf is largely independent of each other. Basin flow is related to flow patterns on both the Guaymas and Santa Rosalia shelves. Guaymas and the basin share energetic counter flows near the shelf break with order 1 week time scales, while longer period flows at seasonal time scales run counter at Santa Rosalia and the basin. The mainland shelf appears to derive much of its energy from disturbances which propagate in from the Pacific ocean. This is certainly true during large storm generated events, but also appears to be the case for weaker variability judging from the good comparison between currents and alongshelf pressure gradients. During large storm-generated events, a response is detected on the Baja shelf although it is different in character than on the mainland shelf. The cross-gulf net geostrophic current is correlated with a simple average of along-gulf currents between Guaymas and Santa Rosalia. Most of this net transport occurs on the Guaymas shelf during propagating events.

It is unclear to what extent shelf circulation on the mainland coast of the Gulf of California is influenced by remote wind forcing other than summer storm events. Shelf measurements along the eastern Pacific coast at Washington (Battisti and Hickey, 1984), Oregon (Cutchin and Smith, 1973) , California (Chapman, 1987), and Peru (Smith, 1978) all document the importance of remotely forced variability. Enfield and Allen (1983) also detected slower poleward propagation over shorter length scales in winter when tropical storms were not active. Shelf circulation in the Gulf of California may be unique from other marginal seas of similar proportions in that it has a rather long coastal-trapped wave fetch along the Mexican Pacific coast from which to draw energy. One might imagine a very different current climate if for example the gulf were open to the north and closed to direct poleward propagation. The role of winds south of the central gulf needs to be considered in future studies of shelf circulation in this region.

Acknowledgments

We gratefully acknowledge the many people at the Centro de Investigación Científica y de Educación Superior de Ensenada and the Scripps Institution of Oceanography, and the crews of the RV/*New Horizon* and *El Puma* who contributed to the success of the moored array component of the Pichicuco cruises. Special thanks to R. T. Guza, N. A. Bray, C. A. Paden, N. Christensen, Jr., and A. Badan-Dangon for many valuable discussions of the gulf observations. Earlier versions of the manuscript were greatly improved by the suggestions of U. Send and J. M. Becker. This study was supported by the Office of Naval Research (contracts N00014-80-C-

0440, N00014-85-C-0104, N00014-87-K-0005) and by the National Science Foundation (grant NSF-OCE83-10639).

## REFERENCES

Badan-Dangon, A., C. J. Koblinsky, and T. Baumgartner, Spring and summer in the Gulf of California: Observations of surface thermal patterns, *Oceanol. Acta, 8*, 13-22, 1985.

Barton, E. D., J. M. Robles, A. Amador, and C. Morales, A year of current and temperature observations off Baja California North. Data report, CICESE, Mexico, 162 pp., 1980.

Battisti, D. S., and B. M. Hickey, Application of remote wind-forced trapped wave theory to the Oregon and Washington coast, *J. Phys. Oceanogr., 14*, 887-903, 1984.

Beardsley, R. C., D. C. Chapman, K. H. Brink, S. R. Ramp, and R. Schlitz, The Nantucket shoals flux experiment (NSFE79), Part 1: A basic description of the current and temperature variability, *J. Phys. Oceanogr., 15*, 714-748, 1985.

Bray, N. A., Thermohaline circulation in the Gulf of California, *J. Geophys. Res., 93*(C5), 4993-5020, 1988.

Bray, N. A., M. C. Hendershott, J. M. Robles, and A. C. Carrasco, Pichicuco 6: Gulf of California CTD data report, *SIO Ref. 86-4*, 254 pp., 1986.

Brink, K. H., Coastal ocean physical processes, *Rev. of Geophys., 25*, NO. 2, 204-216, 1987.

Brink, K. H., and D. C. Chapman, Programs for computing properties of coastal-trapped waves and wind-driven motions over the continental shelf and slope, *Woods Hole Oceano. Inst. Tech. Rept. 85-17*, 99 pp., April 1985.

Brink, K. H., D. Halpern, and R. L. Smith, Circulation in the Peruvian upwelling system near 15°S, *J. Geophys. Res., 85*, 4036-4048, 1980.

Brown, D. M., Results of current measurements with drogues, 1963-1964., *SIO Ref. 65-3*, 42 pp., 1965.

Brown, W. S., J. D. Irish, and C. D. Winant, A description of subtidal pressure field observations on the Northern California continental shelf during the Coastal Ocean Dynamics Experiment, *J. Geophys. Res., 92*, 1605-1635, 1987.

Brown, W. S., N. R. Pettigrew, and J. D. Irish, The Nantucket Shoals Flux Experiment (NSFE79), Part II: the structure and variability of across-shelf pressure gradients, *J. Phys. Oceanogr., 15*, 749-771, 1985.

Candela, J., A. Badan-Dangon, and C. D. Winant, Spatial distribution of lower atmospheric physical variables over the Gulf of California. A data report. Volume 1. Summer 1983., *SIO Ref. 84-33*, 211 pp., 1984.

Candela, J., A. Badan-Dangon, and C. D. Winant, Spatial distribution of lower atmospheric physical variables over the Gulf of California. A data report. Volume 2. Winter 1984., *SIO*

*Ref. 85-11*, 303 pp., 1985.

Chapman, D. C., Application of wind-forced, long coastal-trapped wave theory along the California coast, *J. Geophy. Res., 92*, 1798-1816, 1987.

Christensen, N. Jr., R. de la Paz, and G. Gutierrez, A study of sub-inertial waves off the west coast of Mexico, *Deep-Sea Res., 30*, 835-850, 1983.

Cutchin, D. L., and R. L. Smith, Continental shelf waves: Low frequency variations in sea level and currents over the Oregon continental shelf, *J. Phys. Oceanogr., 3*, 73-82, 1973.

Davis, R. E., Predictability of sea surface temperature and sea level pressure anomalies over the North Pacific Ocean, *J. Phys. Oceanogr., 6*, 249-266, 1976.

Emilsson, I., and M. A. Alatorre, Investigaciones recientes sobre la circulacion en al parte exterior del Golfo de California, *Contribucion No. 210 del Centro de Ciencias del Mar y Limnologia*, UNAM, Mexico, 35 pp., 1980.

Enfield, D. B., and J. S. Allen, The generation and propagation of sea level variability along the Pacific coast of Mexico, *J. Phys. Oceanogr., 13*, 1012-1033, 1983.

Erdman, M. R., Observations of bottom pressure on the continental shelf. PhD thesis, SIO-UCSD, San Diego, 96 pp., 1983.

Filloux, J. H., Tidal patterns and energy balance in the Gulf of California, *Nature*, 243, 217-221, 1973.

Fu, L.-L., and B. Holt, Internal waves in the Gulf of California: observations from a spaceborne radar, *J. Geophys. Res., 89* (C2), 2053-2060, 1984.

Gray, W. M., Hurricanes: their formation, structure, and likely role in the tropical circulation. In: D. B. Shaw (Editors), *Meteorology over the tropical oceans*, 155-218, 1978.

Groves, G. W., Numerical filters for discrimination against tidal periodicities, *Trans. Amer. Geo. Union, 36:6*, 1073- 1084, 1955.

Gunther, E. B., and R. L. Cross, Annual Summary: Eastern North Pacific tropical cyclones of 1984, *Monthly Weather Review, 113*, 1393-1410, 1985.

Hasse, L., and K. Wagner, On the relationship between geostrophic and surface wind at sea, *Monthly Weather Review, 99*(4), 255-260, 1971.

Hendershott, M. C., and A. Speranza, Co-oscillating tides in long, narrow bays; the Taylor problem revisited, *Deep-Sea Res., 18*, 959-980, 1971.

Kelly, K. A., The influence of winds and topography on the surface temperature patterns over the northern California slope, *J. Geophys. Res., 90*(11) 783-798, 1985.

Kundu, P. K., and J. S. Allen, Some three-dimensional characteristics of low-frequency current fluctuations near the Oregon coast, *J. Phys. Oceanogr., 6*, 181-199.

Large, W. G., and S. Pond, Open ocean momentum flux measurements in moderate to strong winds, *J. Phys. Oceanogr., 11*, 324-336, 1981.

Lentz, S. J. and C. D. Winant, Subinertial currents on the southern California shelf, *J. Phys. Oceanogr., 16*, 1737-1750, 1986.

Merrifield, M. A., A. Badon-Dangon, and C. D. Winant, Temporal behavior of lower atmospheric variables over the Gulf of California. 1983-1985. A data report., *SIO Ref. 87-6*, 192 pp., 1987.

Merrifield, M. A., C. D. Winant, J. M. Robles, R. T. Guza, N. A. Bray, J. Garcia, A. Badan-Dangon, and N. Christensen, Jr., Observations of currents, temperature, pressure, and sea level in the Gulf of California 1982-1986. A data report., *SIO Ref. 86-11*, 153 pp., 1986.

Mitchum, G. T., and A. J. Clarke, The frictional nearshore response to forcing by synoptic scale winds, *J. Phys. Oceanogr., 16*, 934-946, 1986.

Robinson, M. K., Atlas of monthly mean sea surface and subsurface temperatures in the Gulf of California, Mexico, *San Diego Soc. Nat. Hist., Mem., 5*, 97 pp., 1973.

Robles, J. M., and S. G. Marinone, Seasonal and interannual thermohaline variability on the Guaymas Basin in the Gulf of California, *Cont. Shelf Res., 7*. 715-733, 1987.

Roden, G. I., Oceanographic and meteorological aspects of the Gulf of California, *Pac. Sci., 12*(1), 21-45, 1958.

Roden, G. I., Oceanographic aspects of the Gulf of California, In: T. H. van Andel and G. G. Shor Jr. (Editors), *Marine Geology of the Gulf of California: A symposium*, Amer. Assoc. Pet. Geol., Mem., 3, 30-58, 1964.

Roden, G. I., Thermohaline structure and baroclinic flow across the Gulf of California entrance and the Revillagigedo Islands region, *J. Phys. Oceanogr., 2*(2), 177-183, 1972.

Roden, G. I., and G. W. Groves, Recent oceanographic investigations in the Gulf of California, *Mar. Res. J., 18*(1), 10-35, 1959.

Smith, R. L., Poleward propagating perturbations in currents and sea levels along the Peru coast, *J. Geophys. Res., 83*, 6083-6092, 1978.

Stock, G. G., Modeling of tides and tidal dissipation in the Gulf of California, PhD thesis, SIO-UCSD, San Diego, 102 pp., 1976.

Thorade, H., Uber die Kalifornische Meeresstromung, *Hydrogr. Marit. Meteorol. Ann., 37*, 17-34, 63-76, 1909.

Weller, R. A., Observations of horizontal velocity in the upper ocean made with a new vector measuring current meter, PhD thesis, SIO-UCSD, San Diego, 169 pp., 1978.

Winant, C. D., R. C. Beardsley, and R. E. Davis, Moored wind, temperature and current

observations made during CODE-1 and CODE-2 over the northern California Shelf, *J. Geophys. Res.*, *92*, 1569-1604, 1987.

Winant, C. D., and A. W. Bratkovich, Temperature and currents on the Southern California shelf: A description of the variability, *J. Phys. Oceanogr.*, *11*, 71-86, 1981.

TABLE 1. Deployment record for instrumentation from 1982-1984.

| | Site | Water Depth (m) | Instrument Depth/Elevation(+) (m) | Deployment Length (days) |
|---|---|---|---|---|
| Deployment 1: 11/82-5/83 | M7 | 100 | 10, 70[1] | 164 |
| Deployment 2: 5/83-11/83 | M1 | 100 | 10[2], 70[1] | 153 |
| | M5 | 35 | 10[2] | 130 |
| | M7 | 100 | 10[2], 70[1], 75 | 186 |
| | M11 | 86 | 10, 65[1] | 190 |
| | P1 | 100 | 100 | 169 |
| | P2 | 35 | 35 | 187 |
| | P6 | 86 | 86 | 188 |
| Deployment 3: 11/83-5/84 | M7 | 100 | 10[2], 70[1] | 190 |
| | M11 | 90 | 10, 65[1] | 190 |
| | W1 | - | +20 | 443 |
| | W2 | - | +50 | 350 |
| | W3 | - | +0 | 125 |
| | W4 | - | +150 | 424 |
| | W5 | - | +100 | 446 |
| | W6 | - | +10 | 322 |
| Deployment 4: 5/84-11/84 | M1 | 100 | 10, 70 | 107 |
| | M4 | 15 | 5, 12 | 191 |
| | M6 | 50 | 10, 20, 30[2] | 188 |
| | M8 | 200 | 10 | 188 |
| | M8 t-chain | 200 | 10, 20, 30, 40, 50, 60, 70, 85, 100, 115, 130, 145, 160, 175 | 188 |
| | M9 | 1000 | 50, 100[2], 300[1], 500[1], 850[1] | 179 |
| | M10 | 200 | 10 | 120 |
| | M10 t-chain | 200 | 10, 20, 30, 40, 50, 60, 70, 85, 100 115, 130, 145, 160, 175 | 58 |
| | M11 | 90 | 10, 30, 70 | 188 |
| | P1 | 100 | 100 | 187 |
| | P4 | 100 | 100 | 381 |
| | P5 | 200 | 200 | 188 |
| | P6 | 90 | 90 | 187 |
| | P7 | 7 | 7 | 194 |
| | P10 | 7 | 7 | 191 |

[1] - inclinometer
[2] - temperature only
+ - above sea level

TABLE 2. Correlations for low frequency temperature records during the summer/fall deployments of 1983 and 1984. Instrument location is represented by mooring number followed by depth of sensor beneath the surface. Maximum correlations, if different than zero-lag correlation, and time lag for maximum correlation are also listed. A positive lag means that temperature at the first sensor leads the second.

| Instrument Location | Correlation | Maximum Correlation | Lag (days) |
|---|---|---|---|
| 1983 | | | |
| Topolobampo-Guaymas | | | |
| $M1_{10}$ - $M7_{10}$ | 0.78* | | 0.0 |
| $M1_{70}$ - $M7_{75}$ | 0.52* | 0.62* | 1.38 |
| $M1_{100}$ - $M7_{75}$ | 0.54* | 0.73* | 1.63 |
| Topolobampo-Santa Rosalia | | | |
| $M1_{10}$ - $M11_{10}$ | 0.66* | | 0.0 |
| $M1_{70}$ - $M11_{65}$ | 0.04 | 0.67* | 8.42 |
| $M1_{100}$ - $M11_{86}$ | -0.02 | 0.69* | 9.29 |
| Guaymas-Santa Rosalia | | | |
| $M7_{10}$ - $M11_{10}$ | 0.50* | 0.56* | 7.13 |
| $M7_{75}$ - $M11_{65}$ | 0.14 | 0.62* | 7.50 |
| $M7_{75}$ - $M11_{86}$ | 0.08 | 0.71* | 7.33 |
| 1984 | | | |
| Topolobampo-Guaymas | | | |
| $M1_{10}$ - $M8_{10}$ | 0.16 | | 0.0 |
| $M1_{70}$ - $M8_{70}$ | 0.45* | 0.64* | 1.79 |
| $M1_{100}$ - $M7_{100}$ | 0.47* | 0.67* | 1.58 |
| $M1_{100}$ - $M8_{100}$ | 0.45* | 0.64* | 1.79 |
| Topolobampo-Santa Rosalia | | | |
| $M1_{70}$ - $M11_{70}$ | 0.07 | 0.39* | 9.42 |
| $M1_{100}$ - $M11_{90}$ | 0.03 | 0.46* | 9.21 |
| Guaymas-Basin | | | |
| $M8_{50}$ - $M9_{50}$ | -0.16 | | 0.0 |
| $M8_{100}$ - $M9_{100}$ | -0.21 | | 0.0 |
| Guaymas-Santa Rosalia | | | |
| $M8_{10}$ - $M11_{10}$ | -0.08 | | 0.0 |
| $M8_{30}$ - $M11_{30}$ | -0.21 | | 0.0 |
| $M8_{70}$ - $M11_{70}$ | -0.03 | 0.55* | 8.96 |
| $M7_{100}$ - $M11_{90}$ | 0.03 | 0.55* | 8.46 |
| Basin-Santa Rosalia | | | |
| $M9_{50}$ - $M11_{30}$ | 0.09 | | 0.0 |
| $M9_{100}$ - $M11_{100}$ | 0.36 | | 0.0 |

* above 95% significance level

TABLE 3. Phase speeds of propagating pressure signals from lagged correlations and time lags between peak events for May-September 1983 and 1984. Values obtained by Enfield and Allen (1983) for the 1971 summer are included for comparison.

| | 1983 | | 1984 | | 1971 | |
|---|---|---|---|---|---|---|
| | Lag Correlation | Peak Events | Lag Correlation | Peak Events | Cross Spectra | Peak Events |
| AC-TO | 316 | 344 | 283 | 313 | 250 | 316 |
| TO-GY | 204 | 212 | 252 | 224 | 225 | 229 |
| GY-IT | | | 260 | 252 | | |

AC = Acapulco
TO = Topolobampo
GY = Guaymas
IT = Isla Tiburon

TABLE 4. Correlations, as in TABLE 2, for alongshelf currents during the 4 instrument deployments.

| | Location | Instrument Correlation | Maximum Correlation | Lag (days) |
|---|---|---|---|---|
| 11/82-5/83 | | | | |
| GY | $M7_{10m}$ - $M7_{70m}$ | 0.82* | | 0.0 |
| 5/83-11/83 | | | | |
| GY-TO | $M1_{70m}$ - $M7_{70m}$ | 0.49* | 0.60* | 1.1 |
| GY-SR | $M7_{70m}$ - $M11_{65m}$ | -0.28 | | 0.0 |
| 11/83-5/84 | | | | |
| GY-SR | $M7_{70m}$ - $M11_{10m}$ | 0.07 | | 0.0 |
| 5/84-11/84 | | | | |
| GY | $M4_{5m}$ - $M6_{20m}$ | -0.14 | 0.51* | -2.2 |
| | $M8_{10m}$ - $M4_{5m}$ | 0.14 | 0.24* | 1.0 |
| | $M4_{4m}$ - $M9_{50m}$ | -0.26* | | 0.0 |
| | $M6_{20m}$ - $M8_{10m}$ | 0.35* | 0.52* | 1.3 |
| SR | $M11_{11}$ - $M11_{30m}$ | 0.86* | | 0.0 |
| | $M11_{10m}$ - $M11_{70m}$ | 0.34* | | 0.0 |
| | $M11_{30m}$ - $M11_{70m}$ | 0.55* | | 0.0 |
| | $M10_{10m}$ - $M11_{10m}$ | 0.94* | | 0.0 |
| TO | $M1_{10m}$ - $M1_{70m}$ | 0.78* | | 0.0 |
| BA | $M9_{300m}$ - $M9_{500m}$ | 0.90* | | 0.0 |
| | $M9_{300m}$ - $M9_{850m}$ | 0.41* | | 0.0 |
| TO-GY | $M1_{10m}$ - $M8_{10m}$ | -0.08 | 0.30* | 1.9 |
| GY-BA | $M6_{20m}$ - $M9_{50m}$ | -0.15 | -0.46* | 3.3 |
| | $M8_{10m}$ - $M9_{50m}$ | -0.48* | -0.53* | 1.0 |
| BA-SR | $M9_{50m}$ - $M11_{10m}$ | -0.54* | -0.65* | 2.7 |
| | $M9_{50m}$ - $M11_{30m}$ | -0.55* | 2.1 | |

* - above 95% significance
TO - Topolobampo
GY - Guaymas
BA - Guaymas Basin
SR - Santa Rosalia

TABLE 5. Multivariate analysis of the alongshelf pressure gradient (dP/dy) and along-gulf wind stress regressed on dV/dt at various moorings from equation 6. Hindcast skill is the amount of variance explained in the regression, % variance represents the variance explained by each input.

| | | $dP/dy$ | | | $\tau^y$ | | |
|---|---|---|---|---|---|---|---|
| (x100) | Hindcast Skill | $\beta_1$ | Lag (hours) | % Variance | $\beta_2$ | Lag (hours) | % Variance |
| **dV/dt** | | | | | | | |
| $M4_5$ | 11.2* | -0.05 ± 0.06 | 0 | 11.3 | 0.02 ± 0.03 | 0 | 1.0 |
| $M6_{20}$ | 14.9* | -0.27 ± 0.27 | -37 | 15.5 | -0.04 ± 0.15 | 0 | 0.1 |
| $M8_{10}$ | 41.6* | -0.82 ± 0.61 | -15 | 33.0 | 0.51 ± 0.33 | 0 | 3.7 |
| $M9_{50}$ | 9.1 | 0.11 ± 0.09 | 0 | 4.4 | 0.06 ± 0.06 | 0 | 4.9 |
| $M11_{10}$ | 7.7* | -0.09 ± 0.05 | 32 | 4.3 | 0.06 ± 0.06 | 0 | 3.5 |
| $M11_{30}$ | 2.7* | -0.05 ± 0.03 | 33 | 2.6 | 0.01 ± 0.05 | 0 | 0.1 |
| $M11_{70}$ | 6.5 | 0.00 ± 0.03 | 33 | 2.3 | -0.06 ± 0.05 | 0 | 5.3 |

* above 95% significance level

TABLE 6. Comparison of stratification, wind stress, and wind-current correlations measured during different field studies.

| Experiment | Brunt-Vaisala Frequency N (cpd) | $\langle\tau^y\rangle$ Mean Alongshelf Wind (PA) | $\tau^{y\prime}$ St.Dev. of Alongshelf Wind (PA) | $(v,\tau^y)$ Correlation Between Near-surface, Midshelf Alongshelf Current and Wind |
|---|---|---|---|---|
| CODE-2 | 100 | -0.12 | 0.12 | 0.7 - 0.8 |
| NSFE79 (summer) | 30 | 0.01 | 0.27 | 0.63 |
| So. California (winter) | 50 | - | 0.01 | 0.41 - 0.69 |
| NSFE79 (summer) | 280 | 0.01 | 0.05 | 0.36 |
| Gulf of Calif. (winter) | 140-170 | -0.01 | 0.02 | 0.2 |
| Peru | 100 | 0.06 | 0.01 | 0.18 |
| Gulf of Calif. (summer) | 190-240 | 0.01 | 0.01 | 0.02 |
| So.California (summer) | 250 | - | 0.01 | -0.46 |

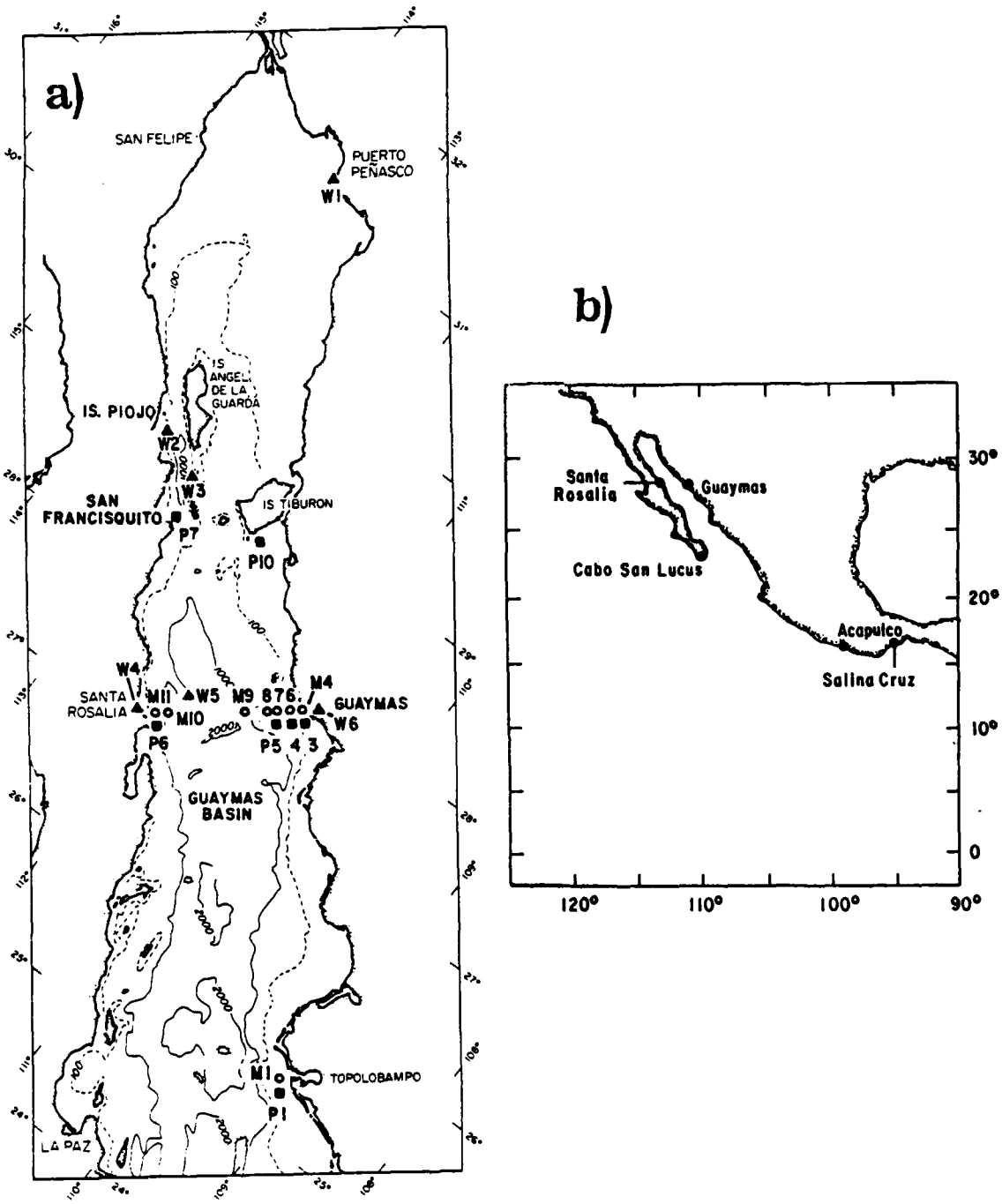


Figure 1.

(a) The Gulf of California showing mooring (M), bottom pressure (P), and PAMII meteorological station (W) locations; (b) Locations of sea level observations.

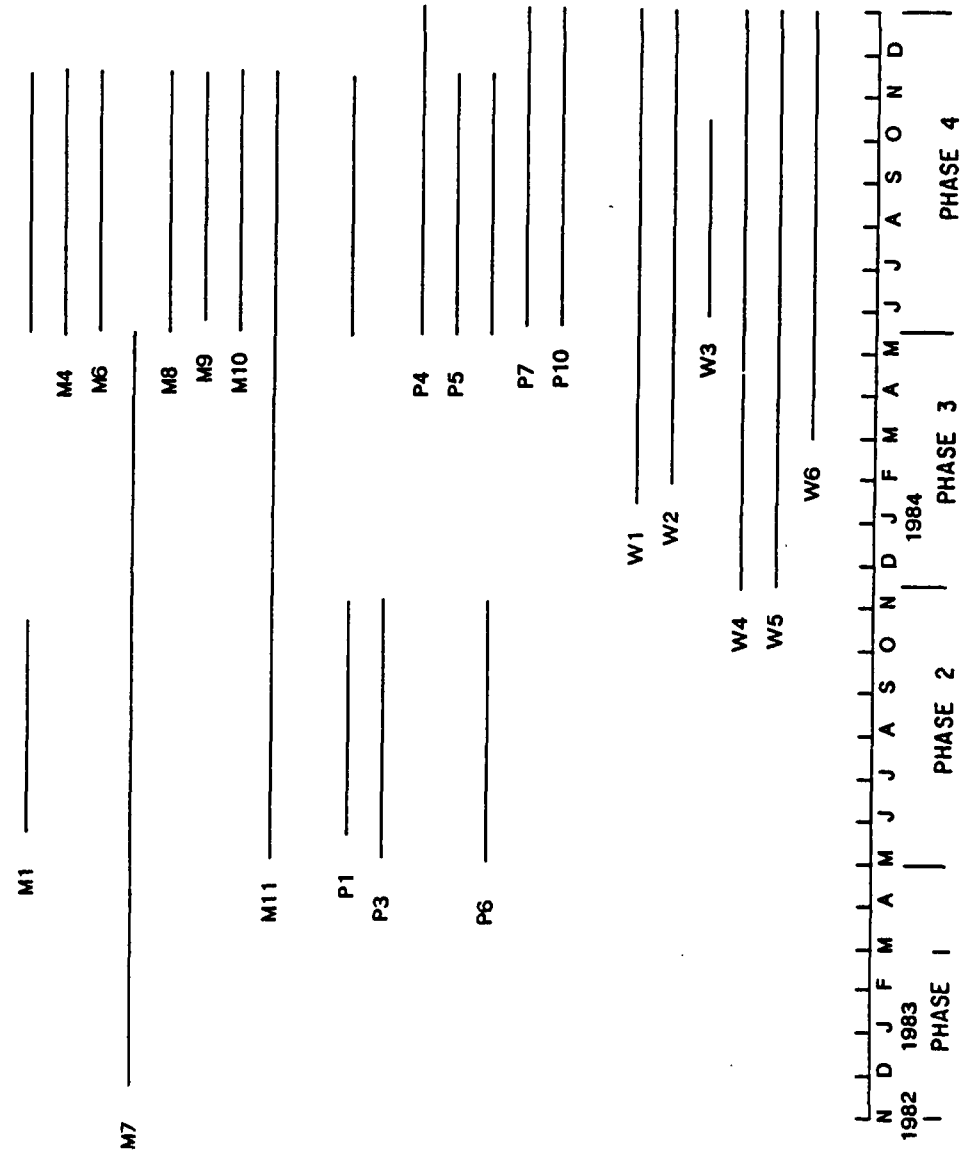


Figure 2. Deployment periods of instrument moorings (M), bottom pressure sensors (P), and PAMII meteorological stations (W).

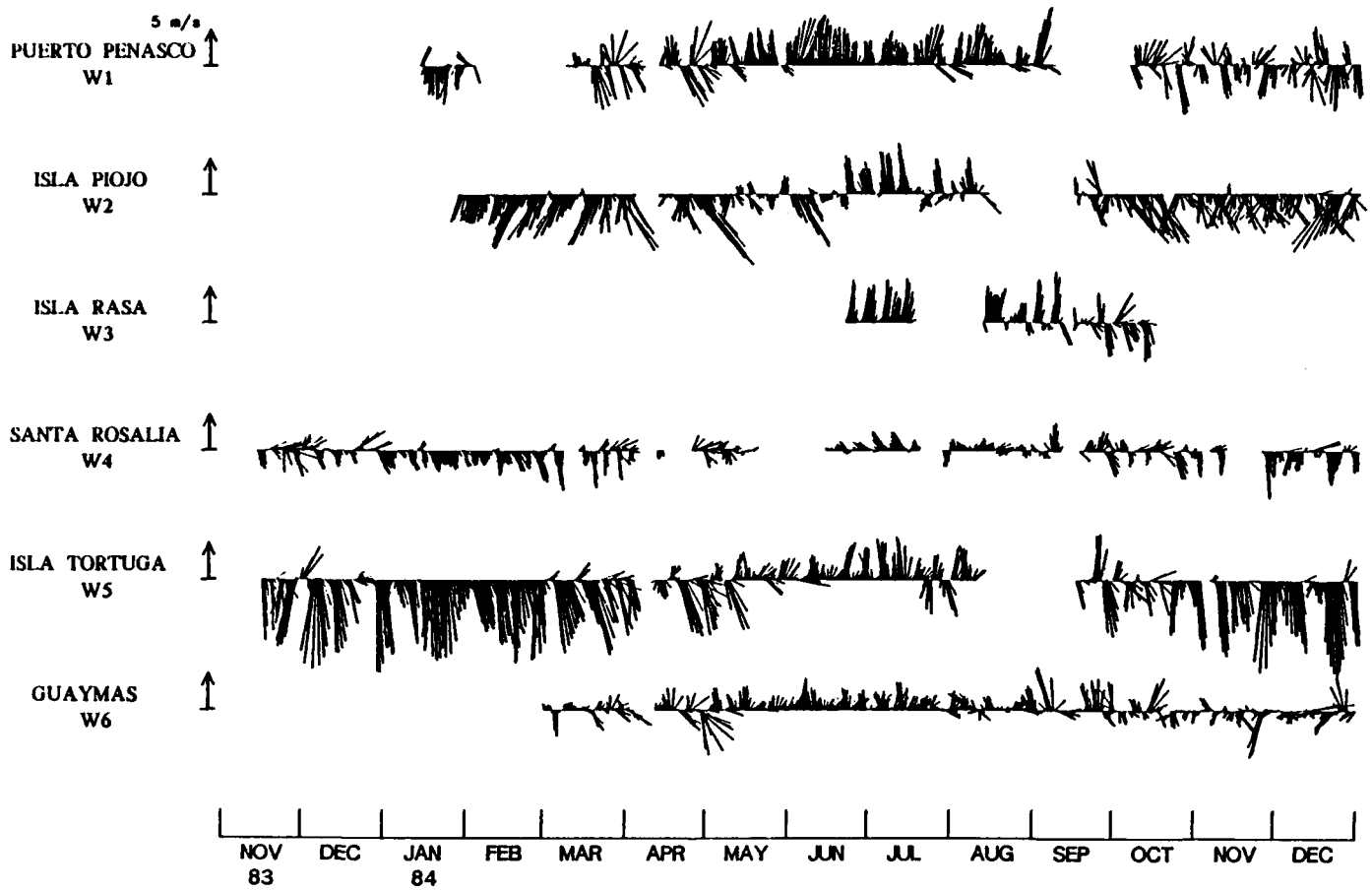


Figure 3. Low frequency vector time series of PAMII wind observations showing the seasonal wind pattern over the Gulf of California. Vectors pointing up the page represent winds blowing up the Gulf axis (330°).

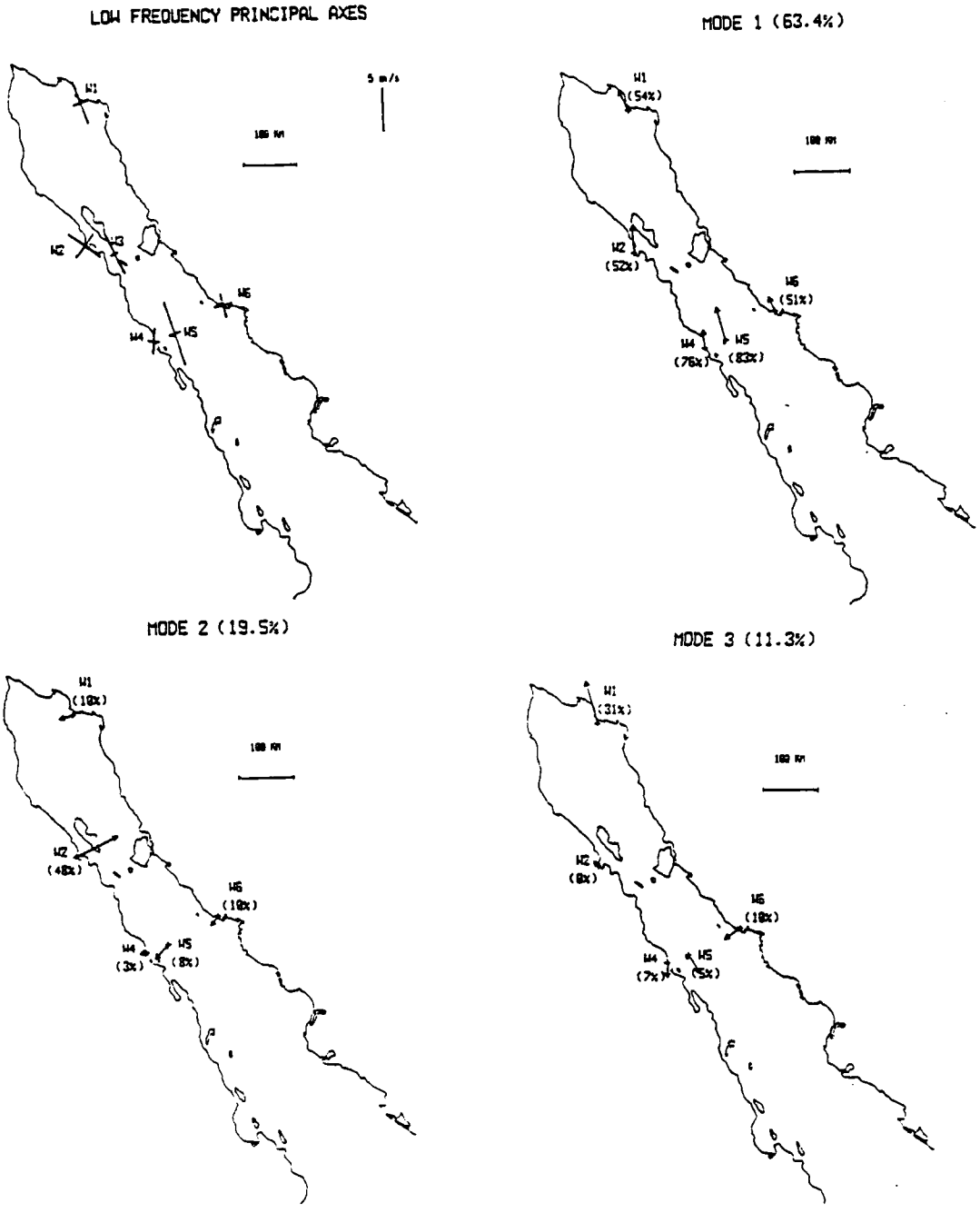


Figure 4.

Principal axes for low frequency wind fluctuations and the three lowest spatial EOF modes of the low frequency vector wind observations during the time period March 1984-February 1985. Station W3 is not included in the EOF analysis. Vector amplitudes are in arbitrary units. Values next to arrows represent the percentage of variance explained in each mode at that particular station. Vectors are rotated by a constant value for each mode to coincide with the principal axis for the temporal expansion of that mode.

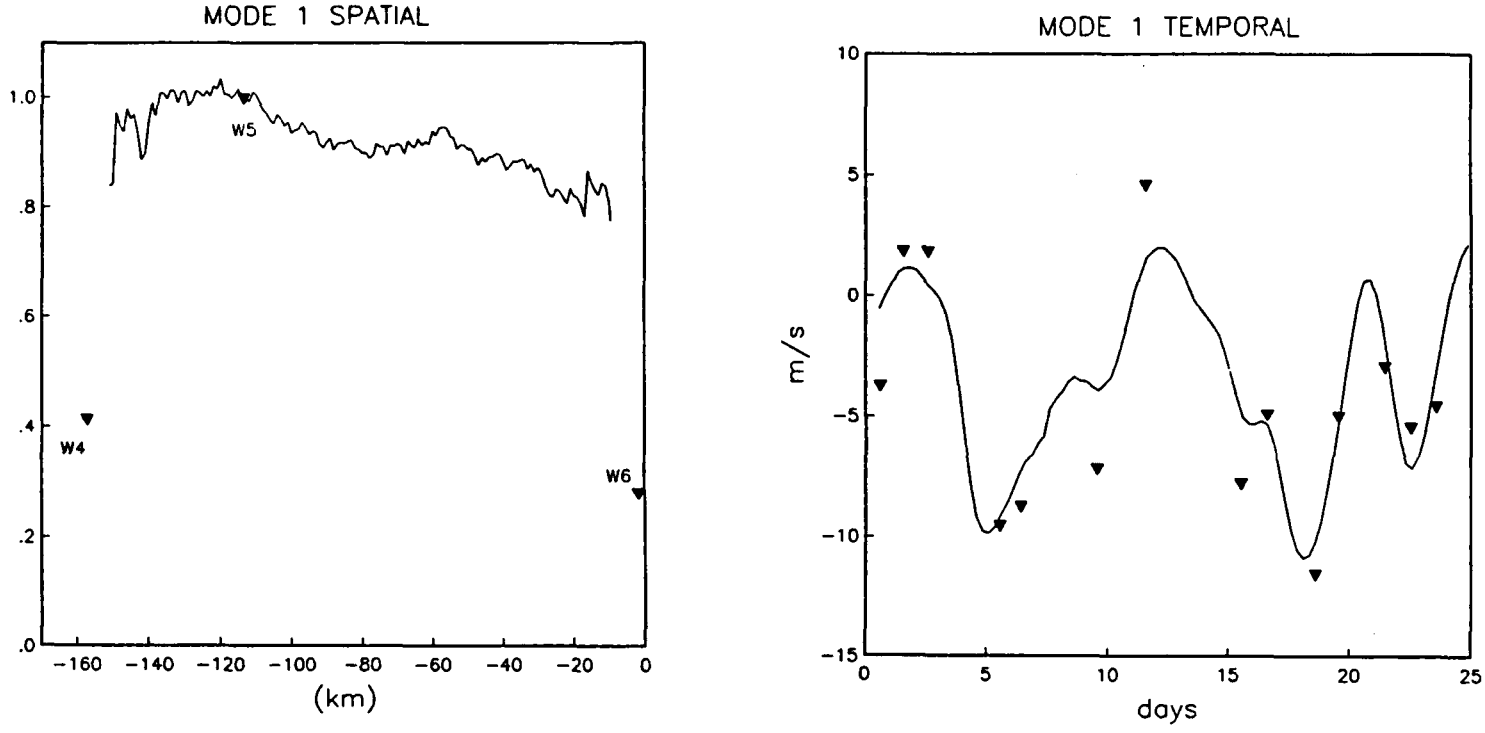


Figure 5. A comparison of the spatial and temporal behavior of along-gulf winds from separate mode 1 EOFs obtained from the PAMII (solid line) and overflight (triangles) observations at the Guaymas-Santa Rosalia transect during March 1984. The spatial amplitudes have been normalized to unit value at Isla Tortuga (W5). Temporal amplitudes are in physical units.

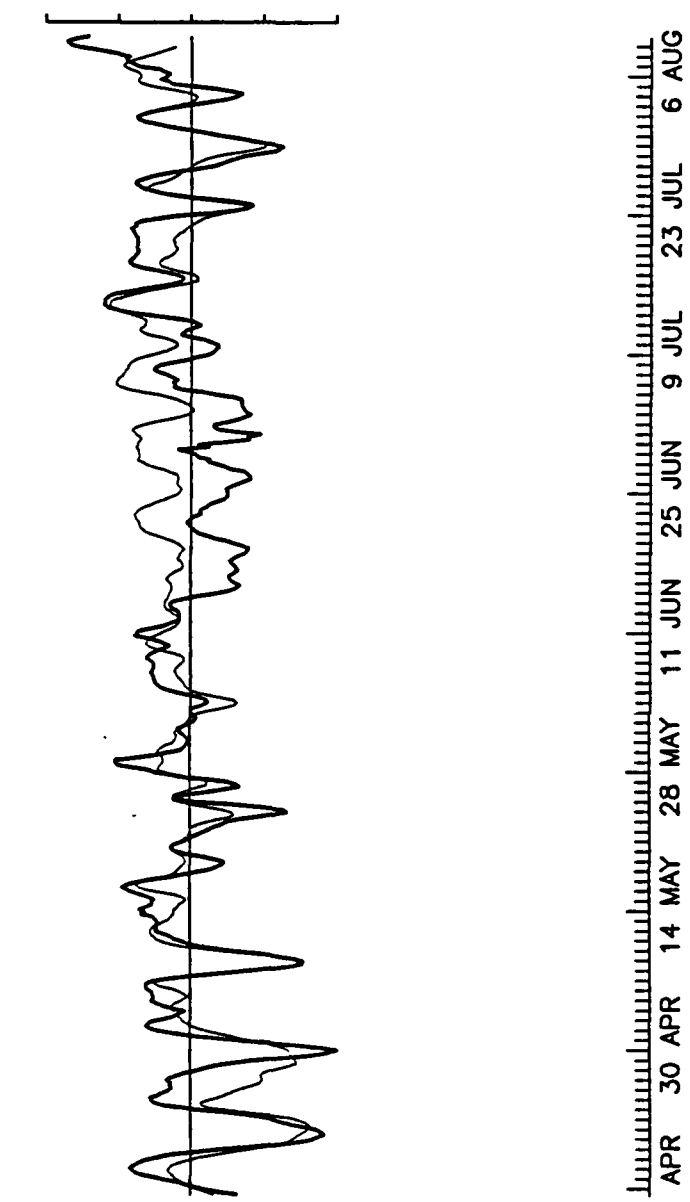


Figure 6. Along-gulf wind at W5 (thin) compared with the geostrophic wind obtained from the surface atmospheric pressure gradient between W4 and W6.

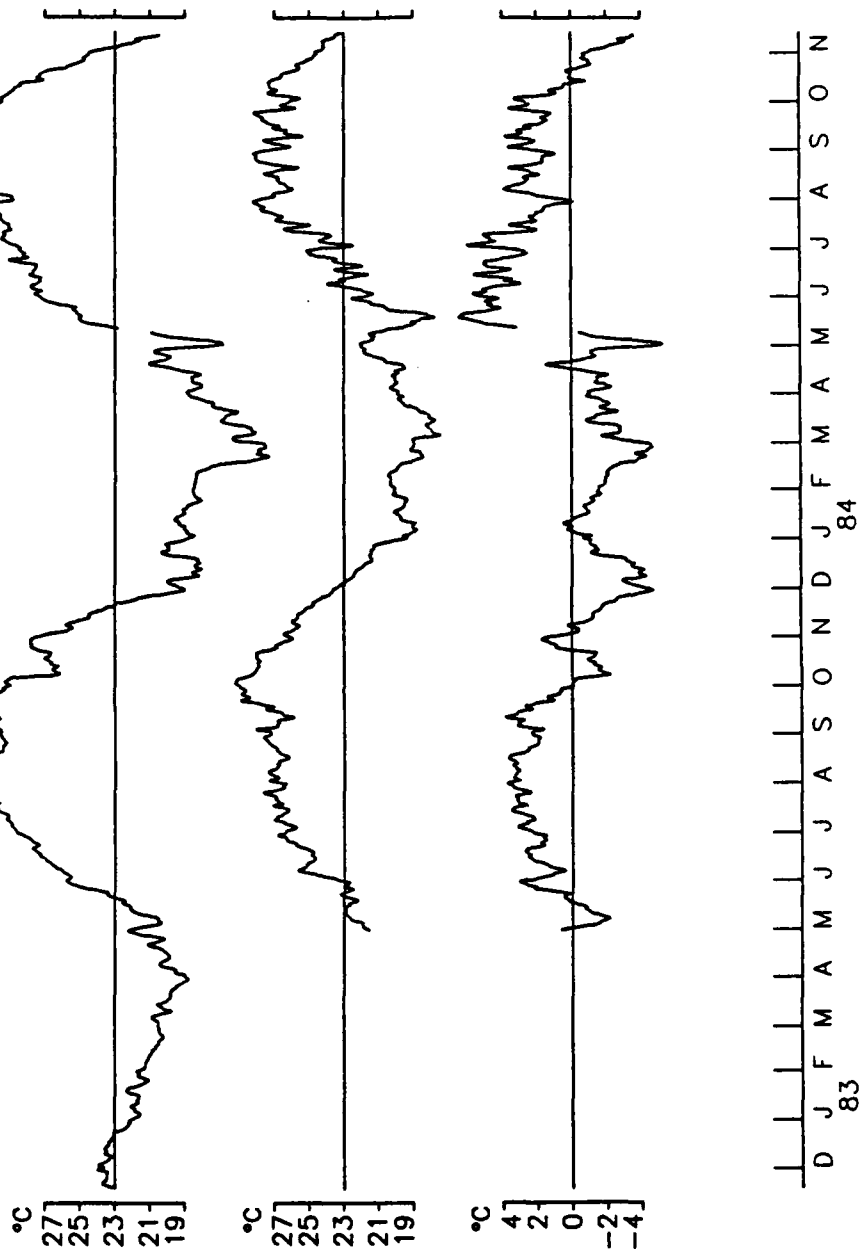


Figure 7. Subinertial temperature measured 10 m below the surface at mid-shelf locations on the Guaymas and Santa Rosalia shelves and the difference between the two series.

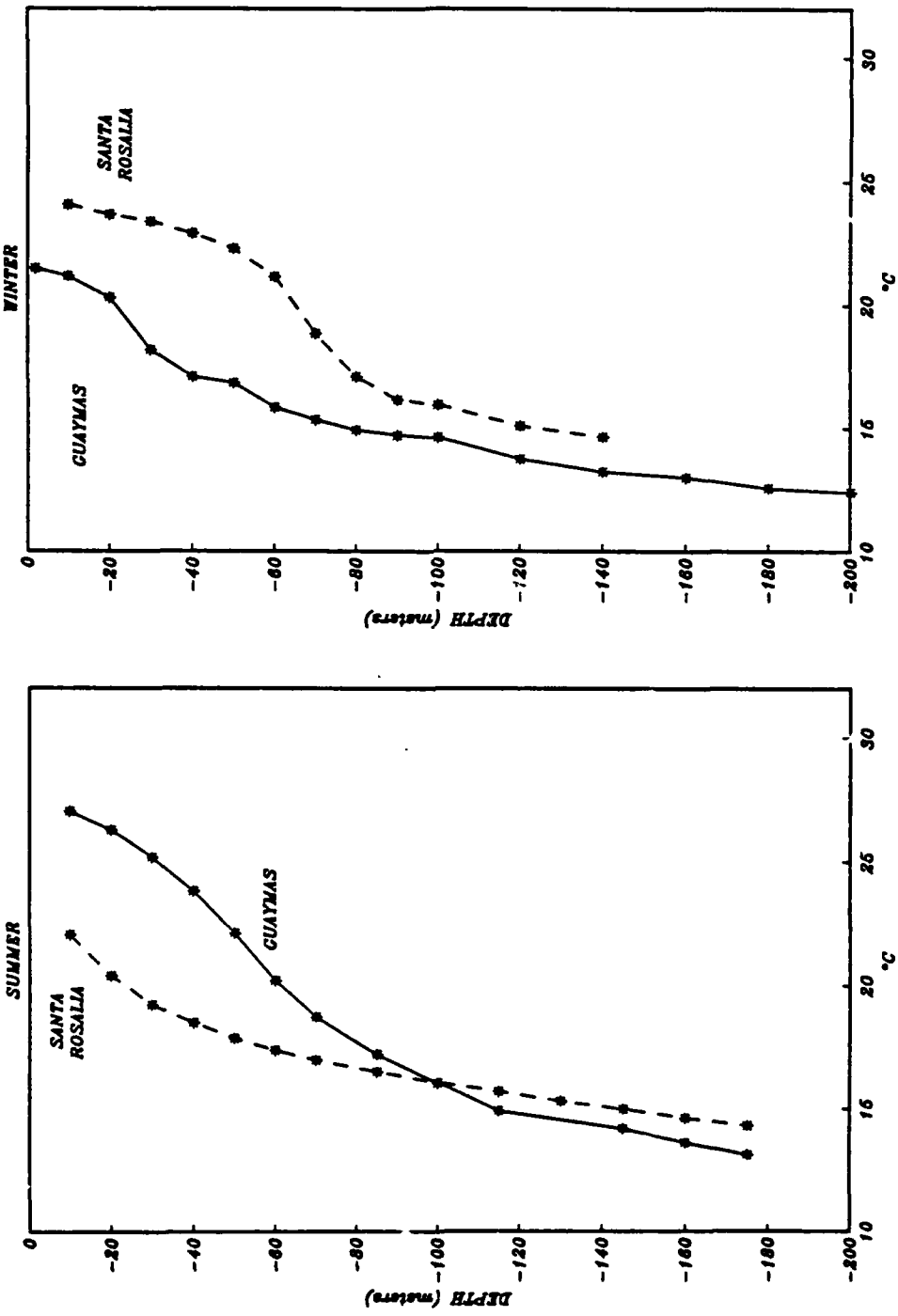


Figure 8. Vertical temperature profiles at Guaymas (solid) and Santa Rosalia (dashed) for summer and winter. Summer values are average temperatures from the 200-m thermistor chains at M8 and M10. Averages are formed during the common time period May 11-July 8, 1984. The winter profile at Guaymas is the average temperature at M8 during November 1984, the profile at Santa Rosalia is from a CTD cast made near M10 on November 14, 1984.

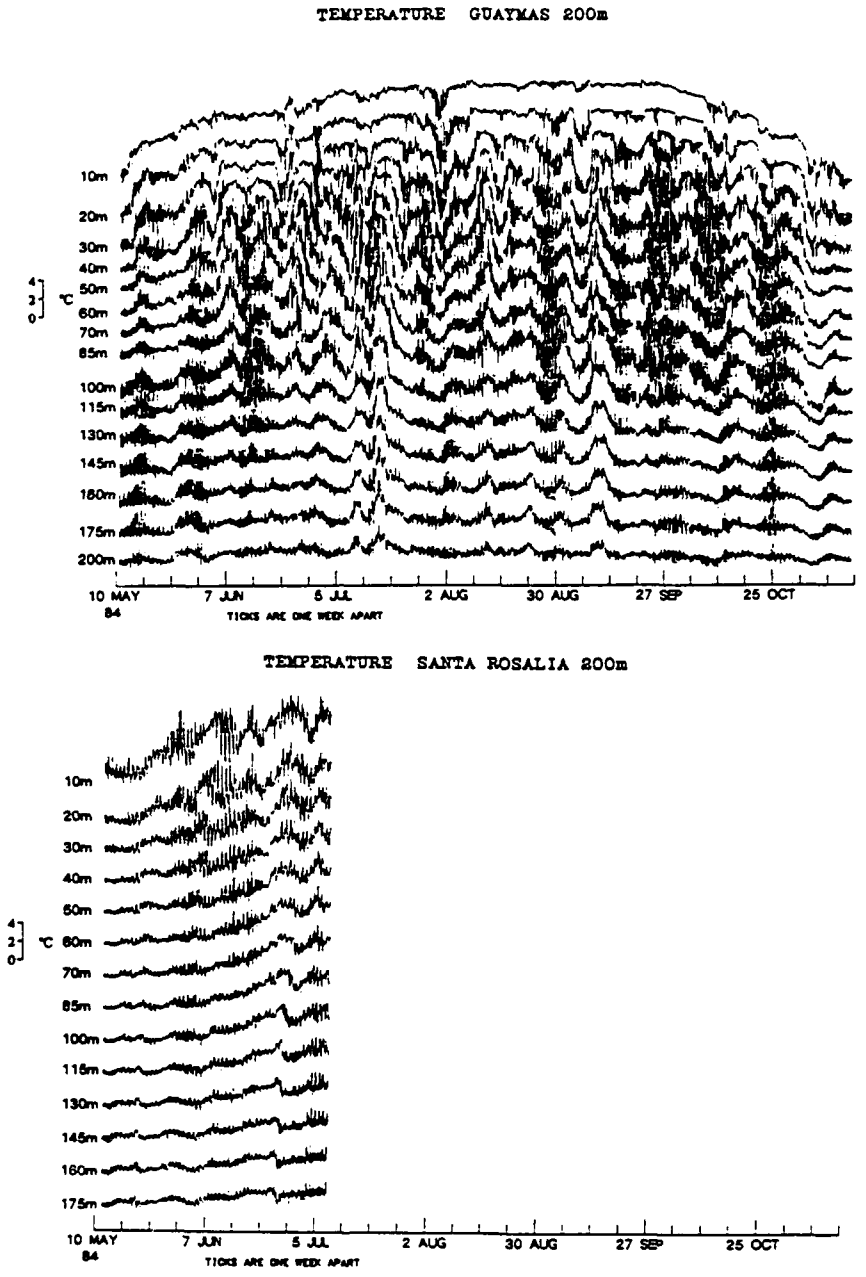


Figure 9.

Hourly-averaged temperature versus depth at the 200-m thermistor chains at Guaymas (M8) and Santa Rosalia (M10). Temperature series are equally spaced in the vertical. Mean temperature at each depth is pictured in Figure 8. Mean temperatures at M8 do not change significantly when averaged over the entire deployment.

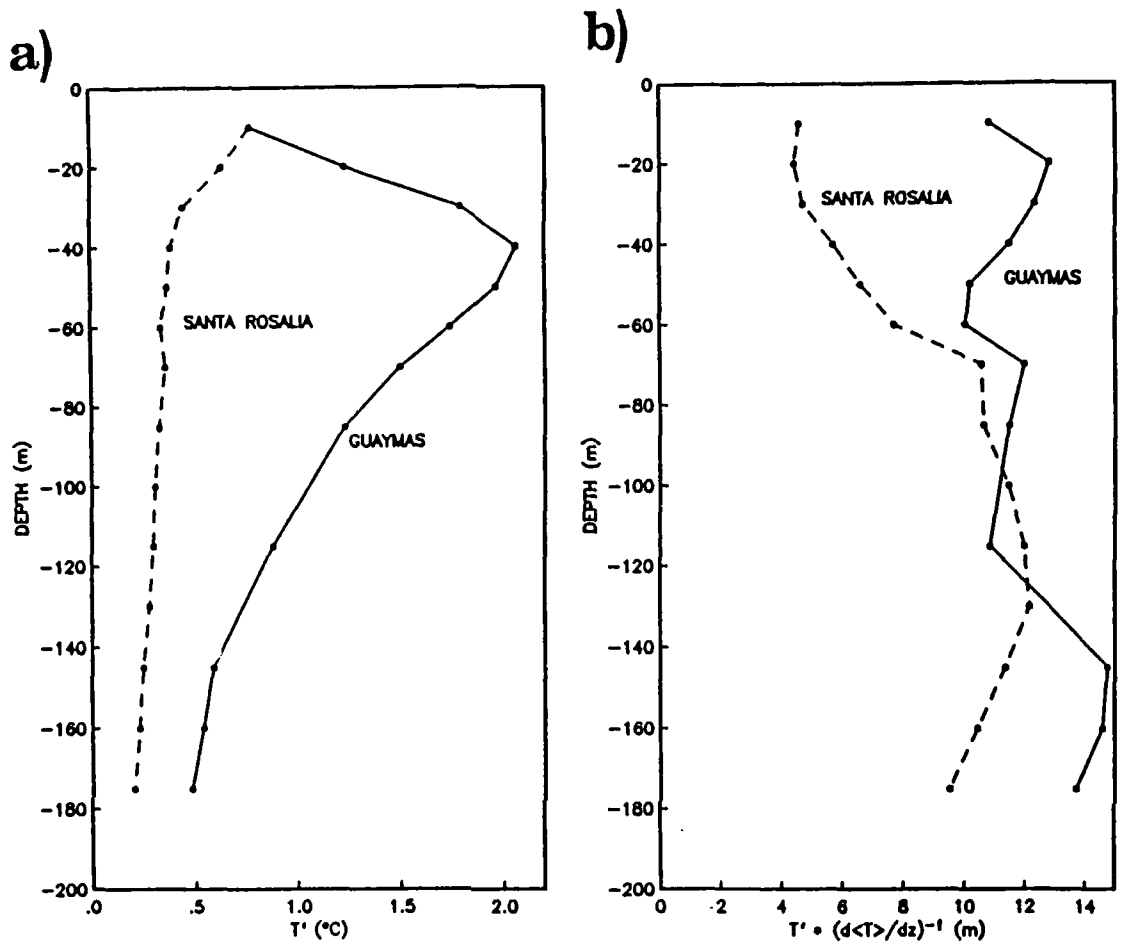


Figure 10.

(a) Standard deviations of low frequency temperature fluctuations versus depth at the Santa Rosalia (dash) and Guaymas (solid) 200-m thermistor chains for the time periods pictured in Figure 8. (b) The same profiles scaled by the average vertical temperature gradient computed at each depth .

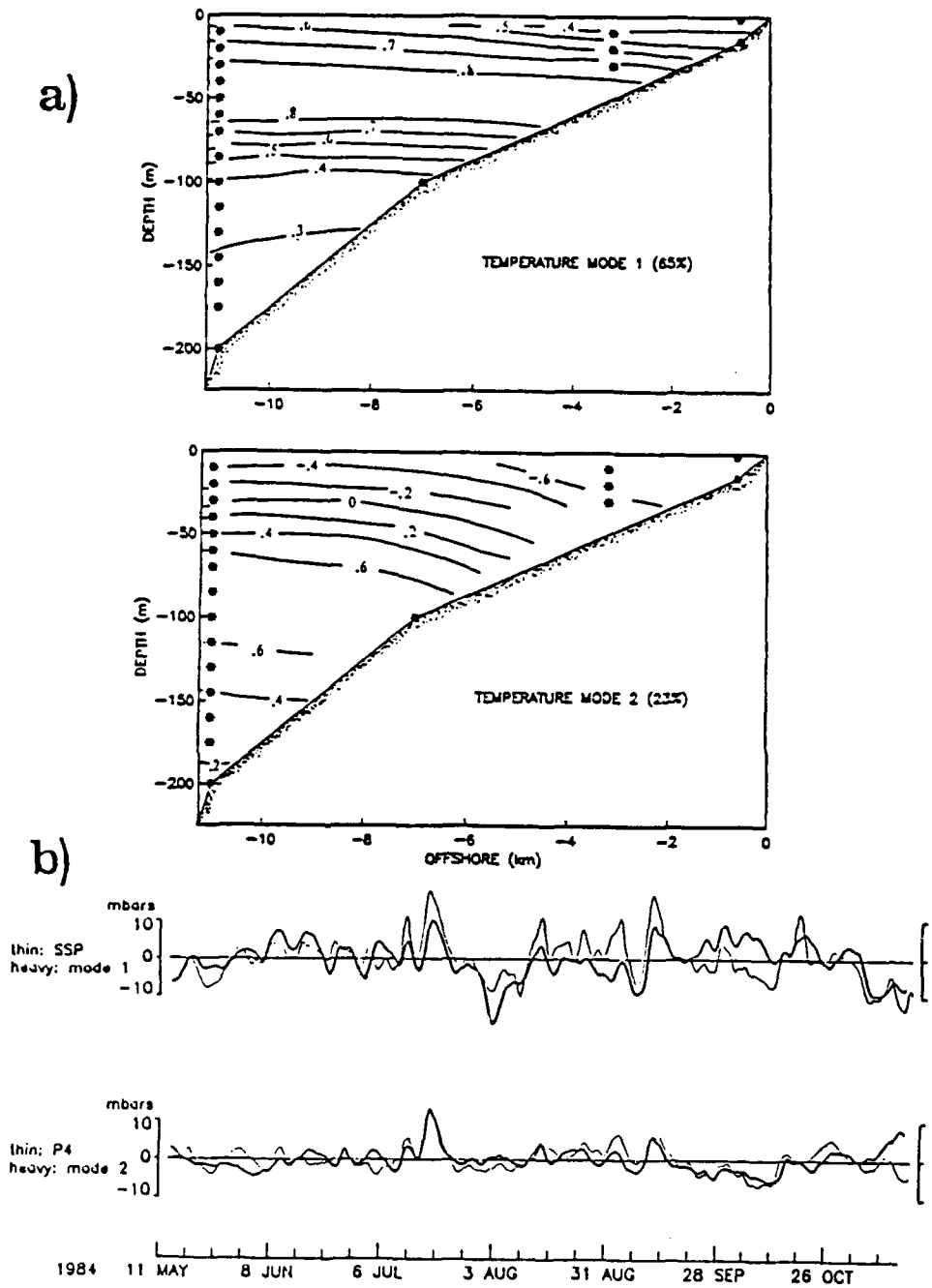


Figure 11.

(a) The two lowest spatial EOF modes of low frequency temperature at the Guaymas shelf during the summer/fall 1984 deployment. Values are proportional to the amount of variance explained. An annual harmonic was removed from each time series before forming the unweighted covariance matrix for this analysis. Asterisks indicate sensor positions. (b) A comparison of the mode 1 temporal expansion and Guaymas adjusted sea level, and the mode 2 temporal expansion and 100-m bottom pressure (P4). Units of temporal expansions are arbitrary.

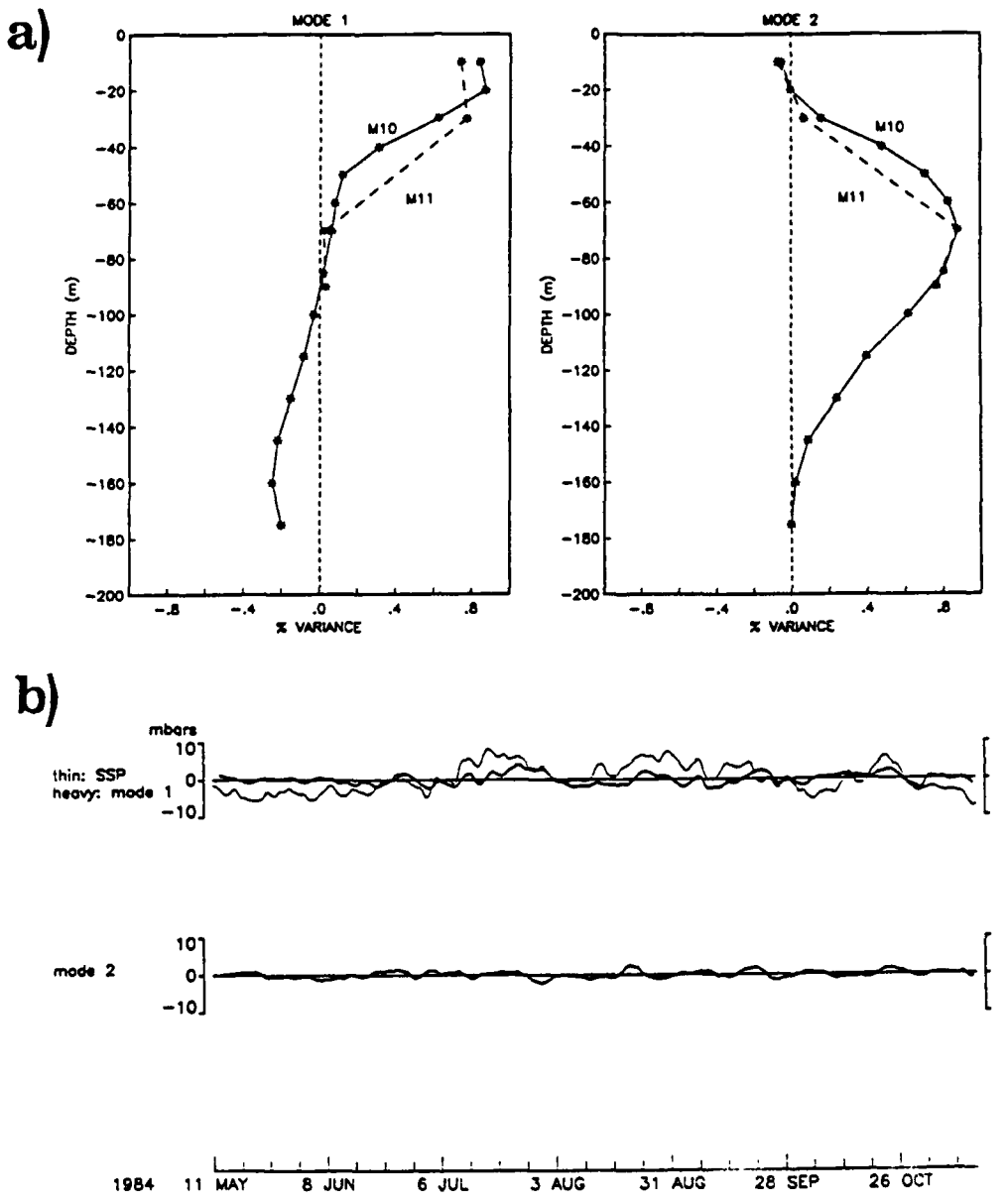


Figure 12.

The two lowest spatial EOF modes of low frequency temperature at the Santa Rosalia shelf during May-July 1984 for the thermistor chain at M10 (solid) and the VMCM mooring at M11 (dash). Asterisks indicate sensor locations. Values are proportional to the amount of variance explained at each sensor. (b) A comparison of the mode 1 temporal expansion and Santa Rosalia adjusted sea level, and the mode 2 temporal expansion. Temporal expansions are in arbitrary units.

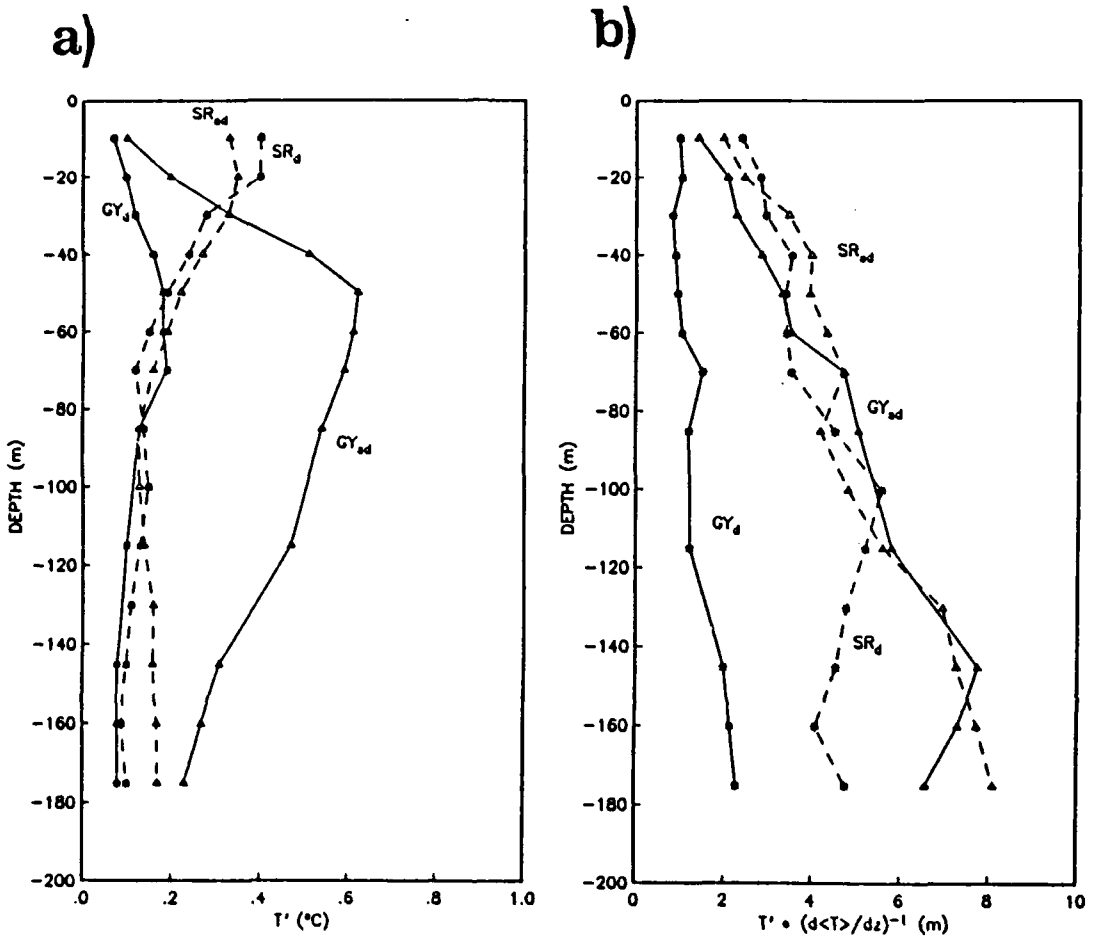


Figure 13.

Standard deviations of diurnal (asterisks) and semi-diunal (triangle) band temperature fluctuations versus depth at the Santa Rosalia (dash) and Guaymas (solid) 200-m thermistor chains for the time periods pictured in Figure 8. The diurnal band is defined as 0.92-1.08 cpd and the semi-diurnal as 1.92-2.08 cpd. (b) The same profiles scaled by the average vertical temperature gradient at each depth.

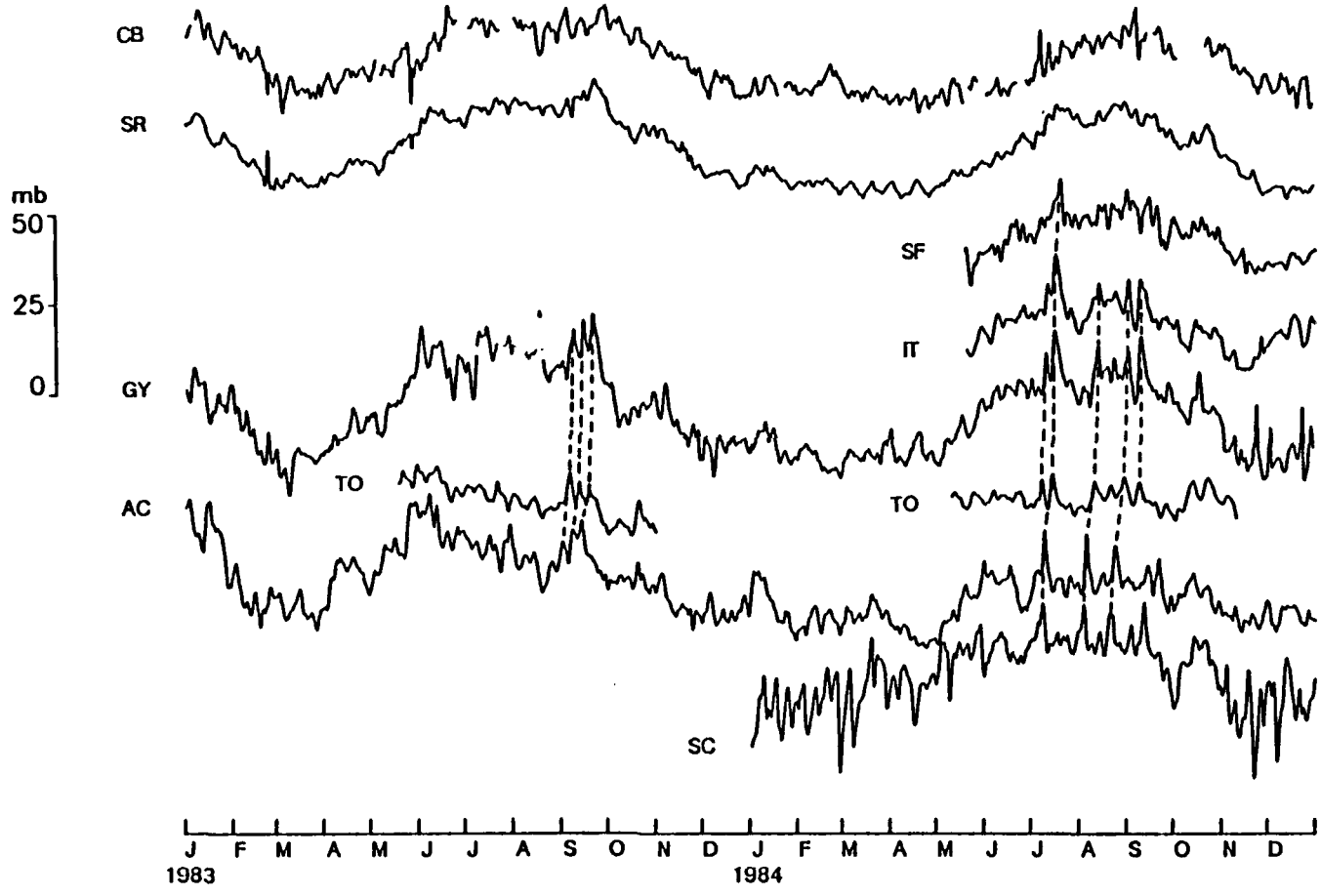


Figure 14. Sea level and pressure along the Mexican Pacific coast and in the Gulf of California during 1983-1984. Energetic propagating events are connected between stations. Guaymas and Santa Rosalia sea level have been adjusted for the inverse barometer effect. Bottom pressure time series are shown for Topolobampo (P1), San Francisquito (P7), and Isla Tiburon (P10). CB = Cabo San Lucas, SR = Santa Rosalia, SF = San Francisquito, IT = Isla Tiburon, GY = Guaymas, TO = Topolobampo, AC = Acapulco, SC = Salina Cruz.

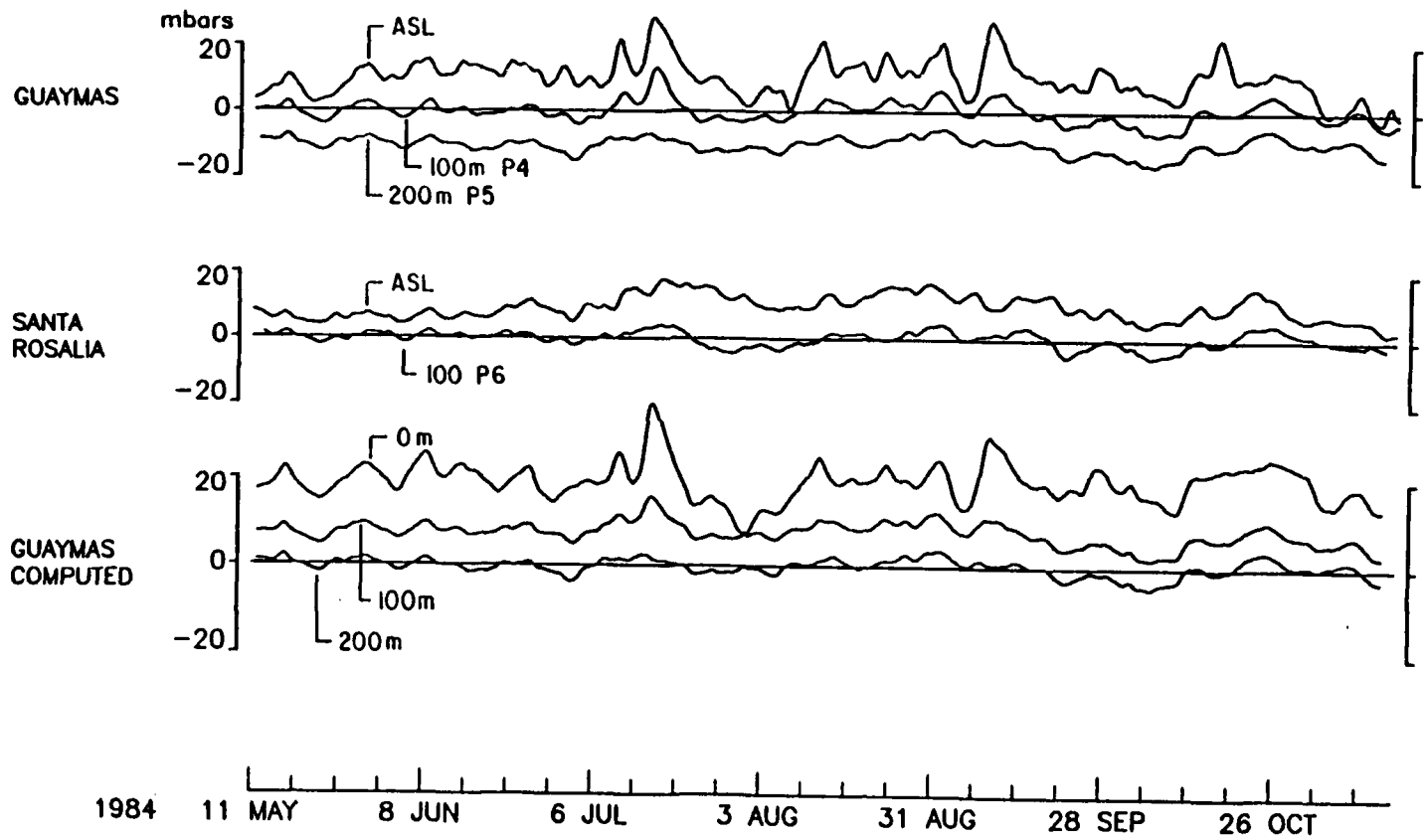


Figure 15. Adjusted sea level and bottom pressure at 100 m (P4) and 200 m (P5) at Guaymas, adjusted sea level and 90-m bottom pressure (P6) at Santa Rosalia, and Guaymas computed pressure at 0 m and 100 m above the 200-m (P5) sensor, using equation 2.

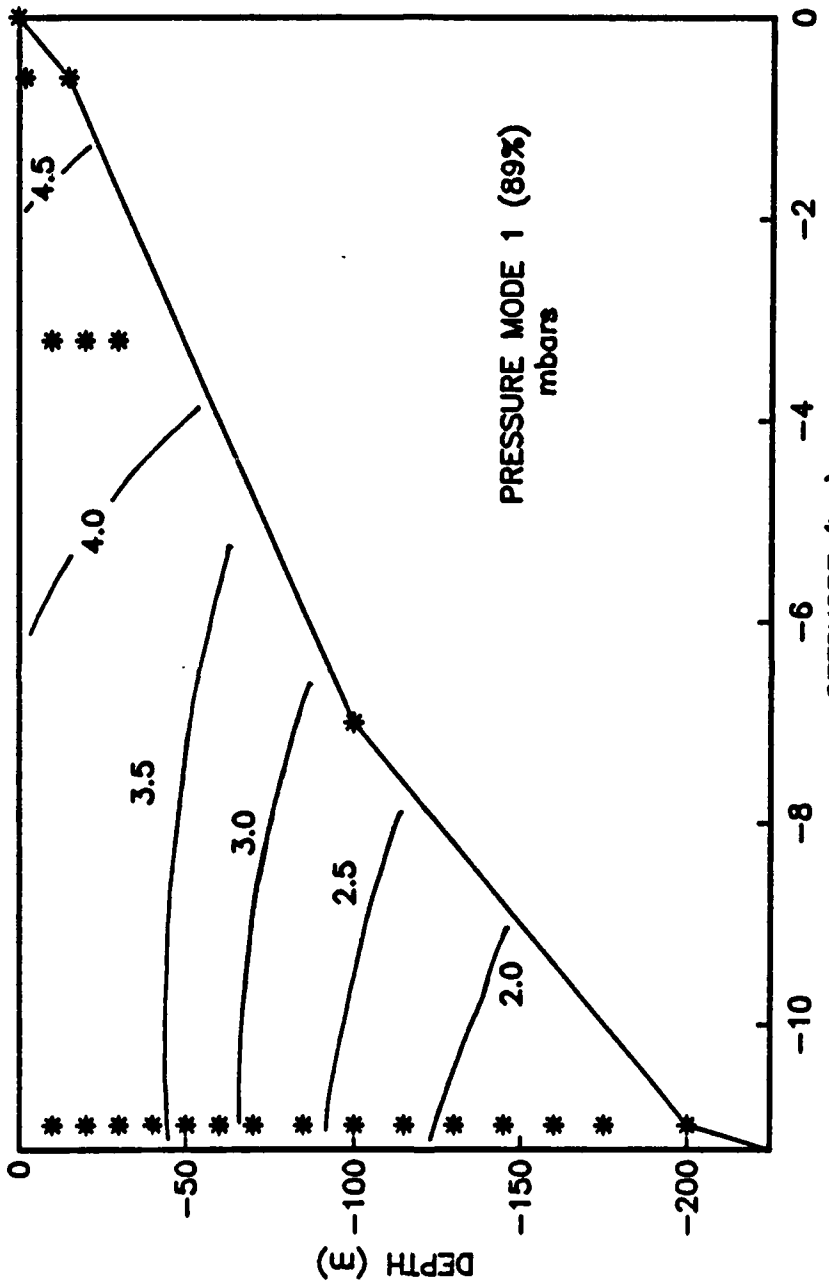


Figure 16. The mode 1 spatial EOF of low frequency pressure fluctuations on the Guaymas shelf. Asterisks indicate location of pressure observations used in forming EOF, including adjusted sea level at the coast, and computed pressure using temperature observations. Surface pressure at M6 is constructed from a weighted average of adjusted sea level at the coast and surface pressure at M8. Values are proportional to the low frequency rms pressure described in this mode.

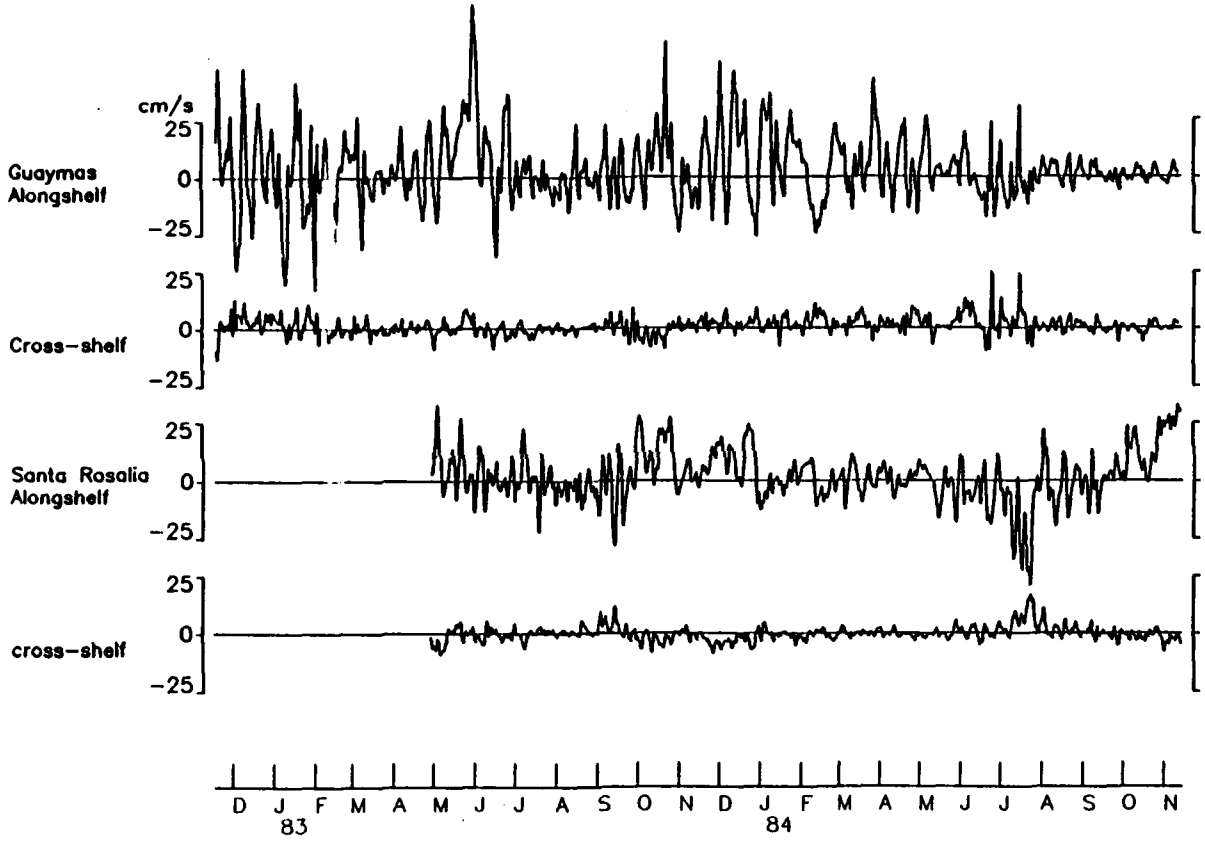


Figure 17. Low frequency currents at Santa Rosalia ($M11_{10\ m}$) and Guaymas ($M7_{10\ m}$ from 11/82-4/83, $M7_{75\ m}$ 5/83-8/83, $M7_{10\ m}$ 9/83-10/83, $M7_{70\ m}$ 11/83-4/84, average between $M6_{20\ m}$ and $M8_{10\ m}$ for 5/84-11/84).

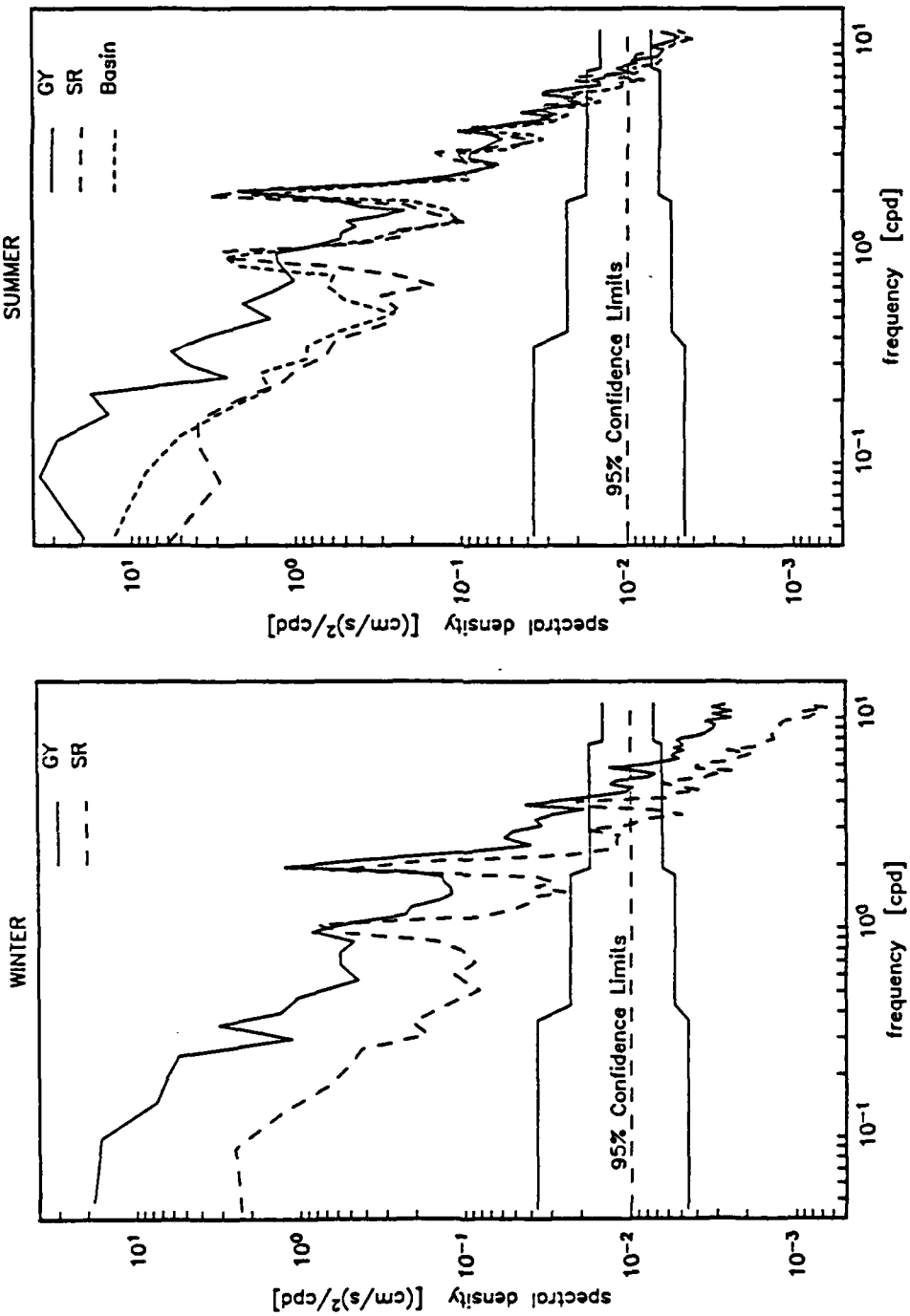


Figure 18. Total kinetic energy spectra for winter and summer currents. Guaymas winter currents are from $M7_{10\ m}$ during 11/82-4/83. Santa Rosalia winter currents are from $M11_{10\ m}$ during 11/83-4/84. Summer currents are $M8_{10\ m}$ at Guaymas, $M9_{50\ m}$ in the basin, and $M11_{10\ m}$ at Santa Rosalia during 5/84-11/84.

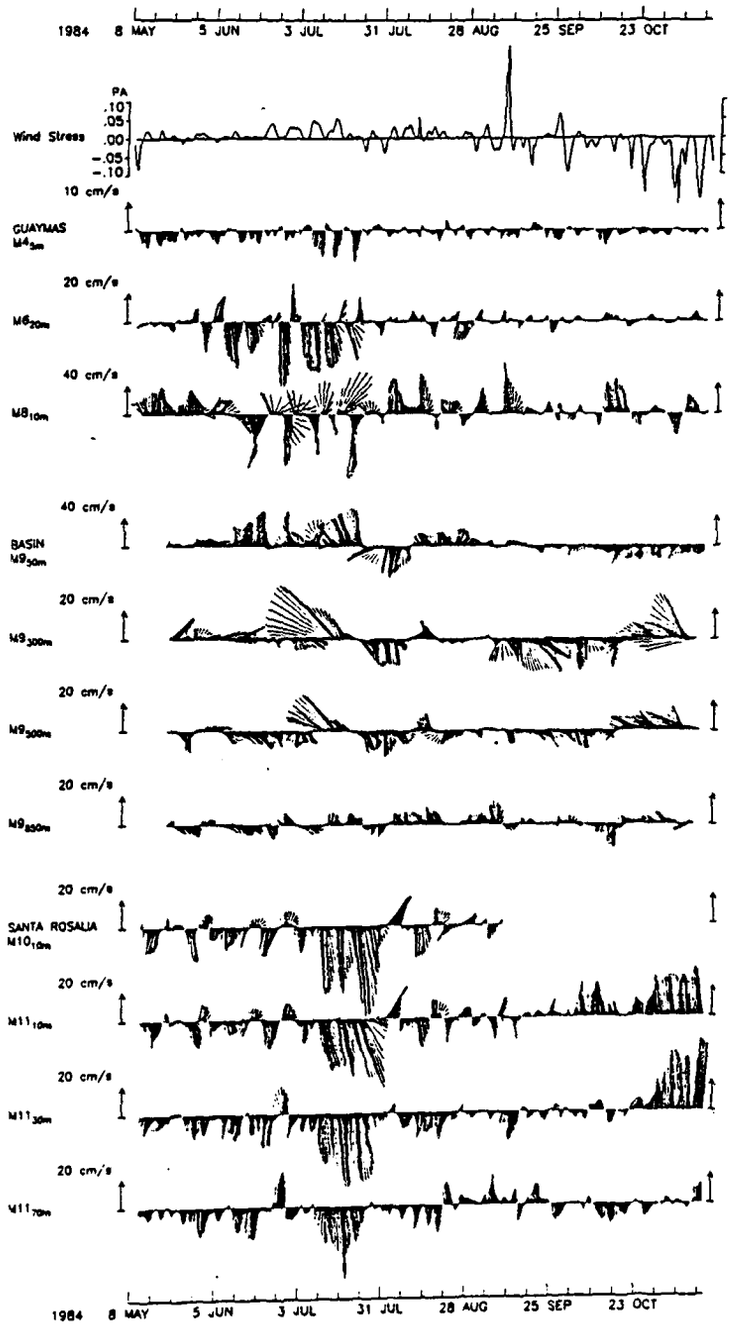


Figure 19.

Low frequency vector time series of currents across the Guaymas-Santa Rosalia transect during the summer-fall 1984 deployment and mode 1 wind stress. A vector pointing up the page corresponds to upgulf flow.

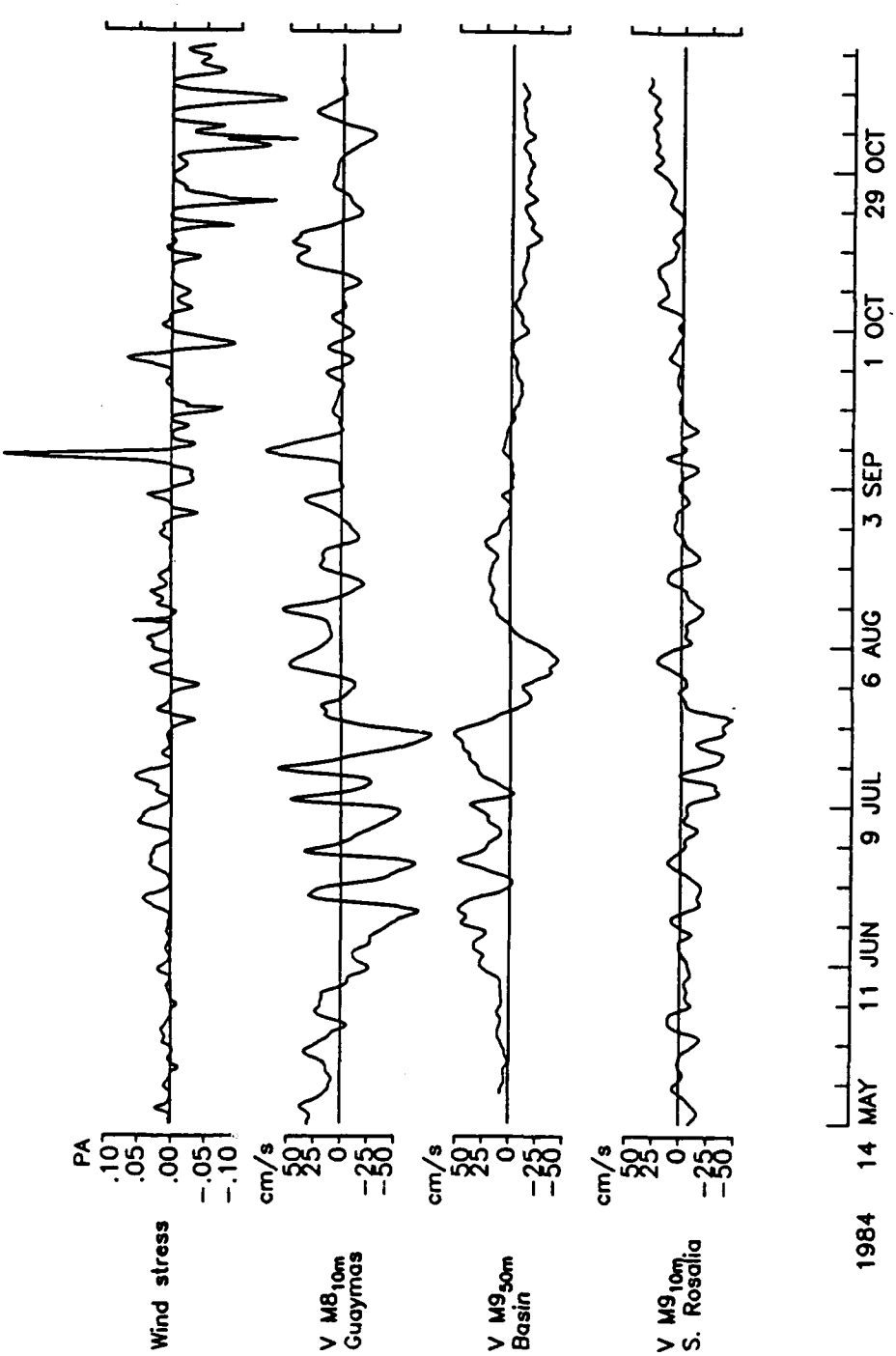


Figure 20. Comparison of alongshelf currents in the basin, on the Guaymas and Santa Rosalia shelves, and mode 1 wind stress during the summer-fall 1984 deployment.

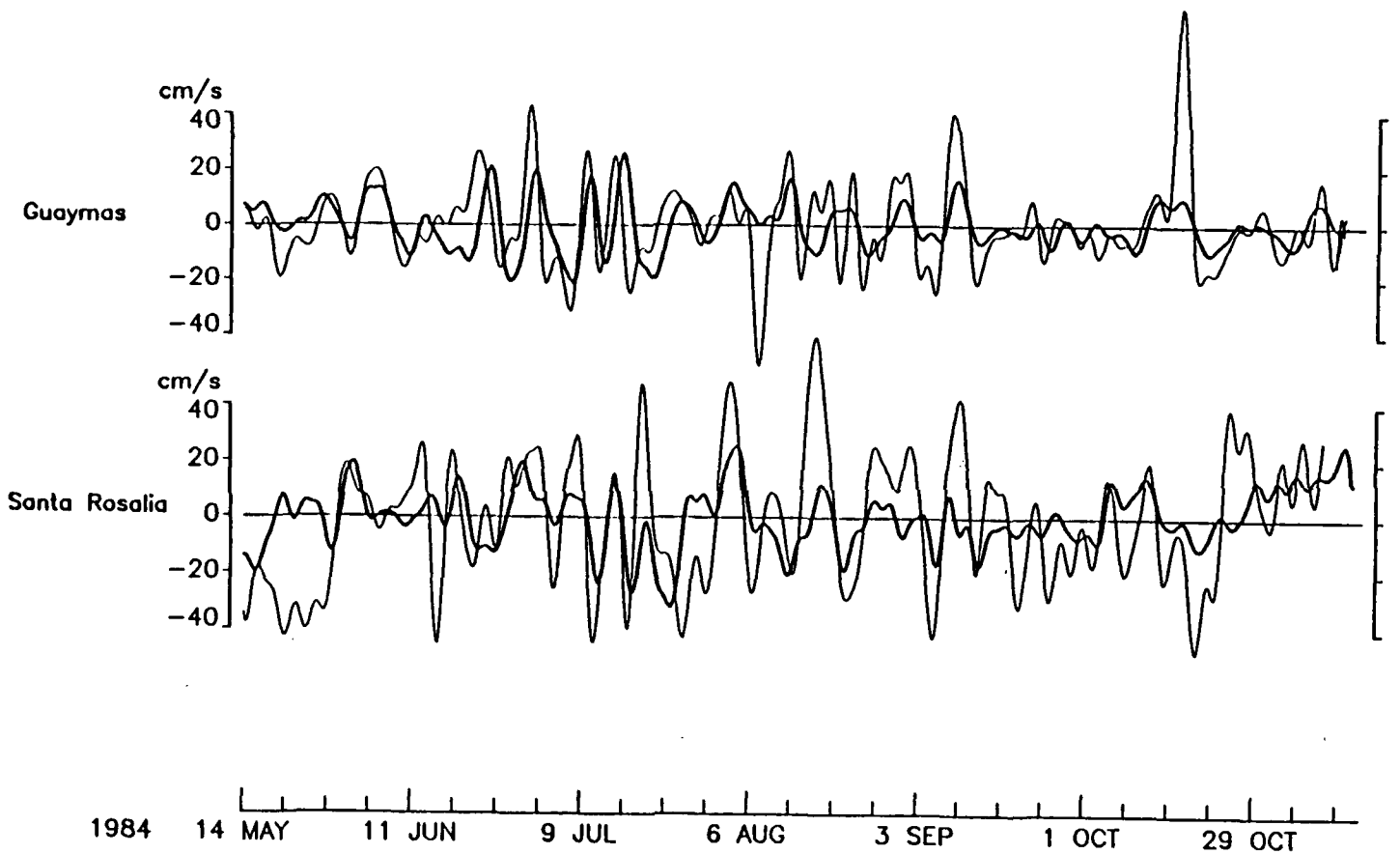


Figure 21. Observed (dark) and geostrophic (light) currents on the Guaymas and Santa Rosalia shelves. Observed current at Guaymas is an average of alongshelf flow at $M4_{5\,m}$, $M6_{20\,m}$, and $M8_{10\,m}$. Observed current at Santa Rosalia is current measured at $M11_{10\,m}$. The geostrophic estimate is formed from the surface pressure gradient between the coast and the shelf break at Guaymas, and the coast and the 100-m isobath at Santa Rosalia. Surface pressure is computed at the Guaymas shelf break from equation 2 using P5 and the thermistor chain observations. Surface pressure at Santa Rosalia is obtained from P6 and temperature measured at VMCMs at M11.

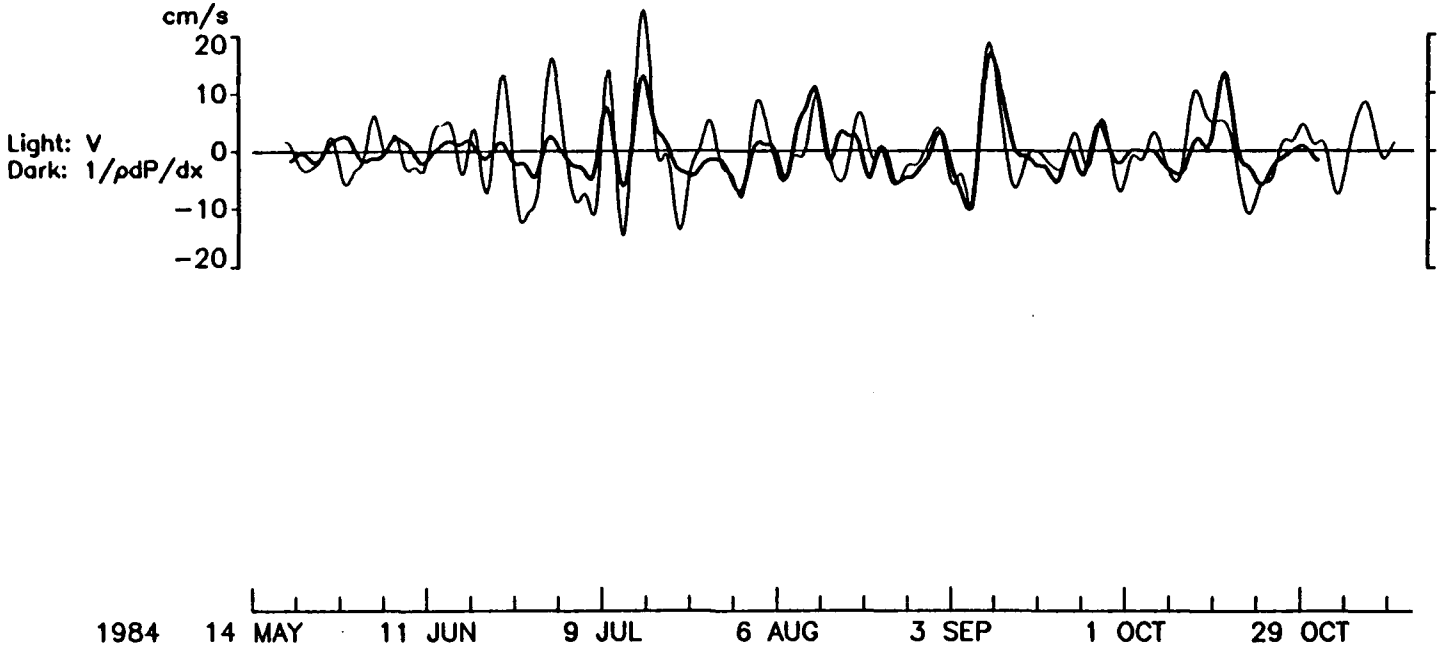


Figure 22. Net along-gulf geostrophic surface current at the Guaymas-Santa Rosalia transect (dark), and average along-gulf current across the transect. Coastal adjusted sea level was used to obtain the geostrophic current. Average current is an equally weighted average of $M8_{10\,m}$, $M9_{50\,m}$, and $M11_{10\,m}$.

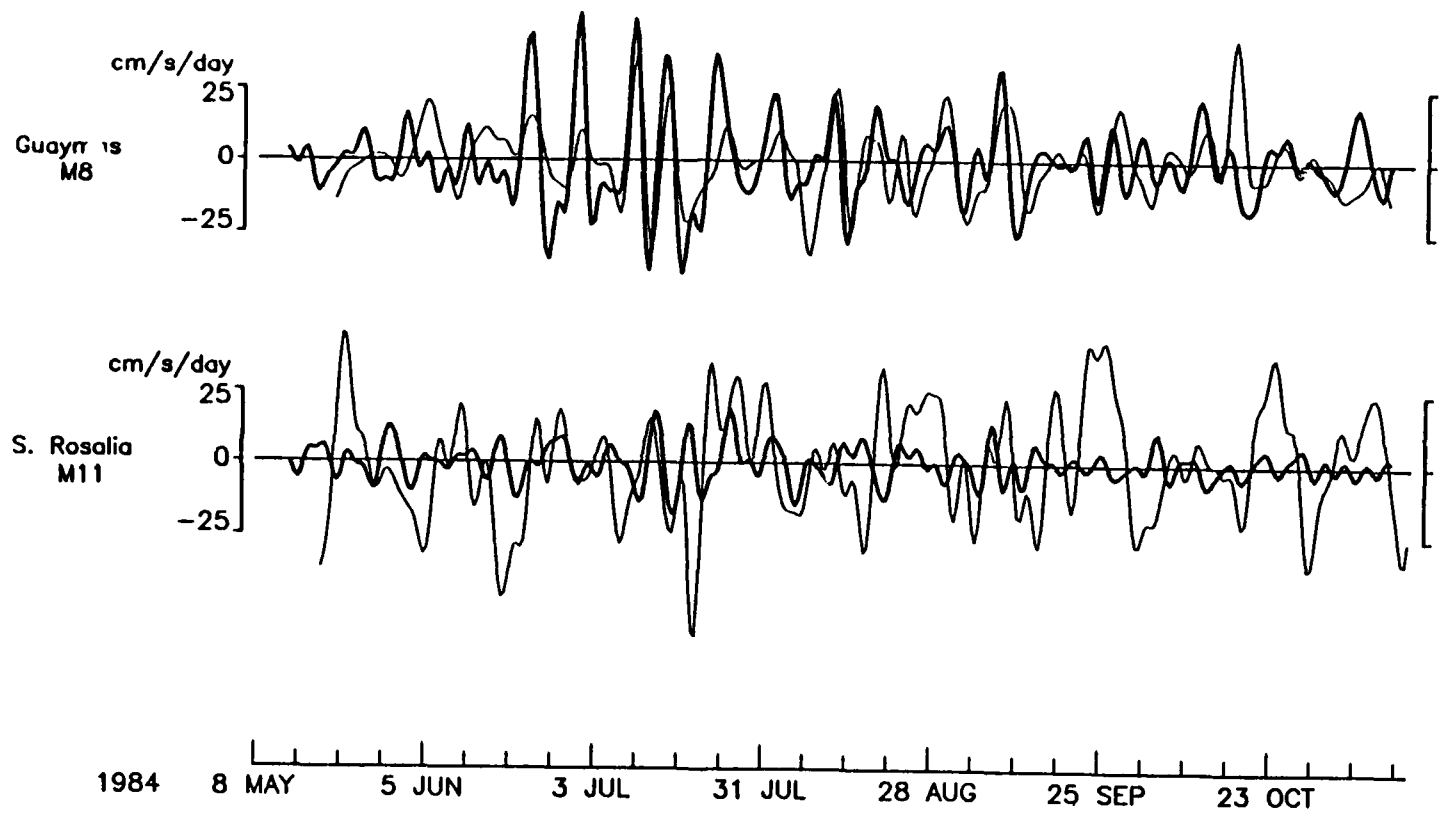


Figure 23. The time derivative of alongshelf currents (dark) at Guaymas ($M8_{10\,m}$) and Santa Rosalia ($M11_{10\,m}$) versus the alongshelf pressure gradient (light). The pressure gradient is obtained from the near surface pressure difference between Guaymas and Isla Tiburon (P10) on the mainland shelf, and Santa Rosalia and San Francisquito (P7) on the Baja California shelf.

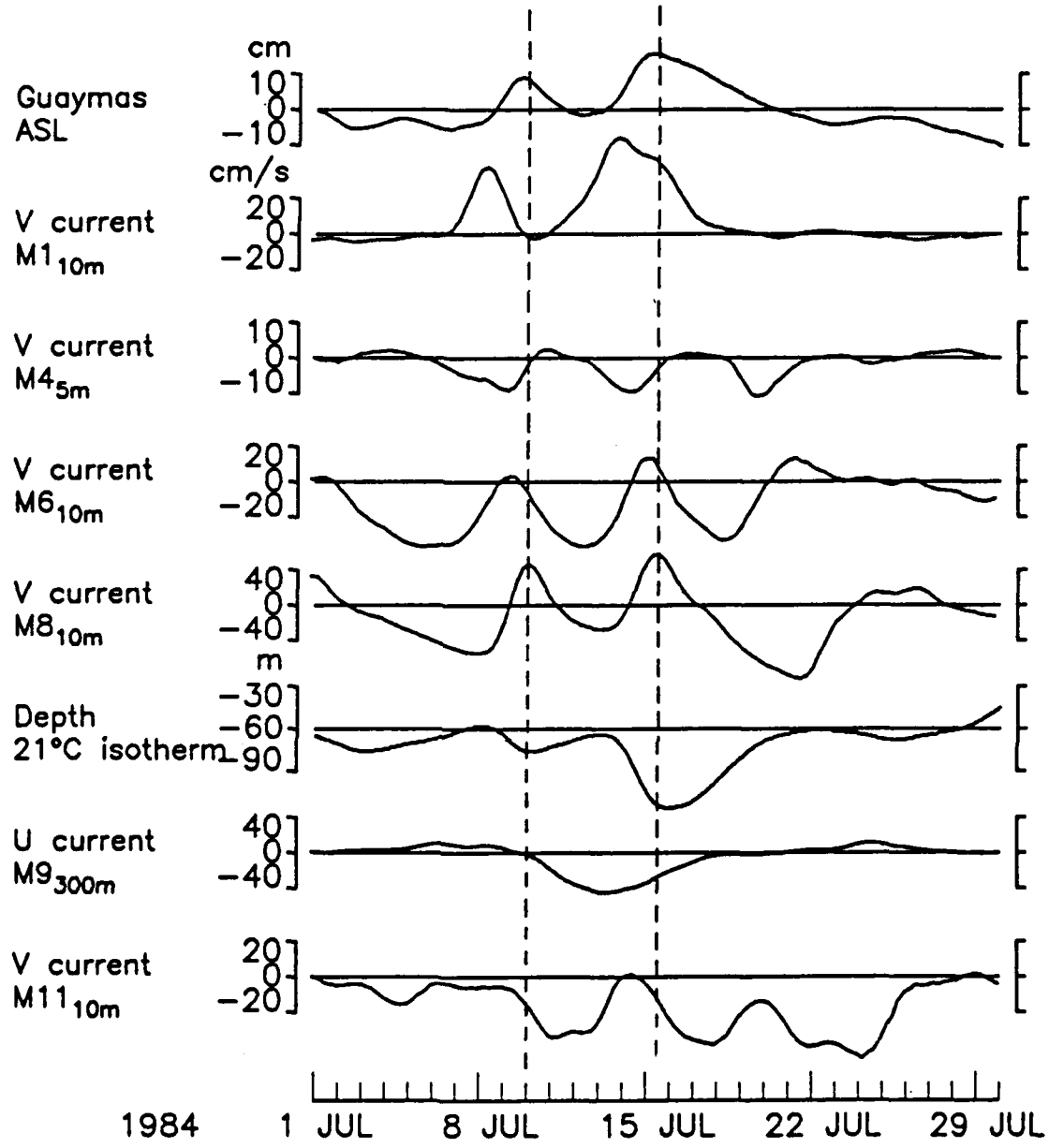


Figure 24.

Current and temperature observations in the Gulf of California during the most energetic propagating event of 1984 as seen in adjusted sea level at Guaymas.

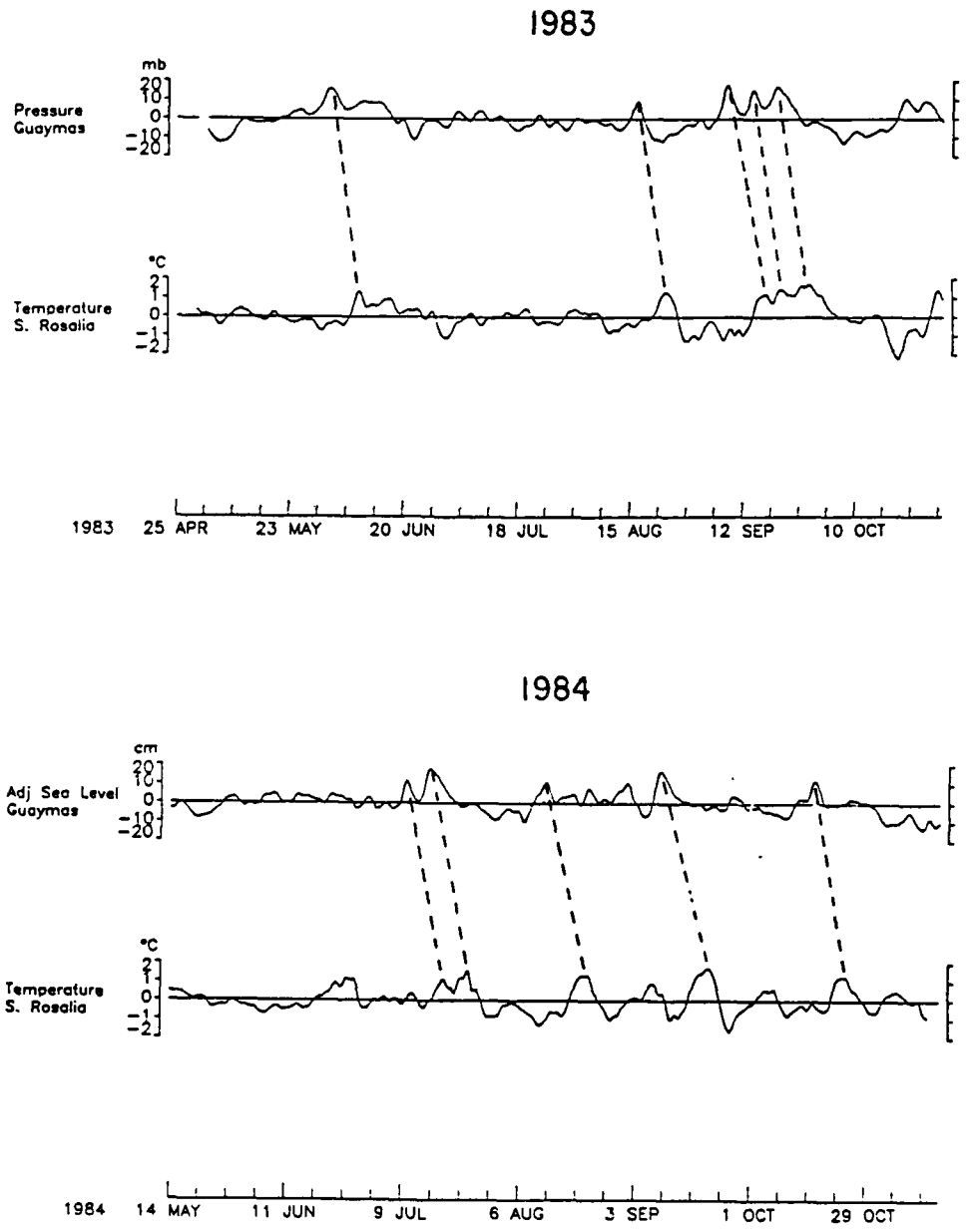


Figure 25.

Comparison of shallow bottom pressure and adjusted sea level at Guaymas with temperature at Santa Rosalia for the summers of 1983 and 1984. Events which appear to correspond in both records are connected.

CHAPTER 2

# A COMPARISON OF PRESSURE, CURRENT, AND DENSITY OBSERVATIONS WITH COASTAL-TRAPPED WAVE THEORY

## 1. INTRODUCTION

Sub-tidal sea level events, with positive elevations of 10-30 cm and 10 day time scales, have been reported propagating poleward along the Mexican coast and into the Gulf of California (Christensen et al., 1983; Enfield and Allen, 1983, henceforth CDG and EA). Based on estimates of phase speed, offshore extent, and mass transport, CDG conclude that these sea level signals are the surface expression of hybrid coastal-trapped waves, more similar to baroclinic Kelvin waves than barotropic shelf waves. EA use cross-spectra, case history and multiple regression analysis to show that these waves are associated with tropical storms and hurricanes that occur during the summer and early fall off the Pacific coast of Mexico. They find good agreement between the observed propagation and free coastal-trapped wave phase speeds north of 20°N, while faster propagation south of 20°N is consistent with the speeds of the traveling storms. These waves are somehow dissipated in the Gulf of California, as they are not detected in tide gauge observations on the Pacific Ocean side of the Baja California peninsula (CDG).

The internal characteristics of these waves have been observed with a moored array in the Gulf of California (Merrifield and Winant, 1988, or thesis chapter 1, henceforth MW). On the mainland coast during an energetic event, currents are strongest at the shelf break and decrease rapidly towards the coast. Consistent with the hypothesis that the events are wavelike, MW find the alongshelf current is in approximate geostrophic balance with the cross-shelf pressure gradient, and the acceleration of the alongshelf current is well correlated with the alongshelf pressure gradient and uncorrelated with local winds. Over the mainland shelf, a sea level rise of 10 cm corresponds to a 20-m downward displacement of isotherms below the mixed layer. On the Baja California shelf, subthermocline temperature fluctuations are signficantly correlated with sea level at Guaymas at an 8 to 9 day lag suggesting that some form of wave energy propagates around the head of the gulf and returns down the peninsula. Sea level and current observations, however, do not indicate equatorward wave propagation on this side of the gulf.

In this chapter, we attempt to determine if this propagating variability is consistent with a forced coastal-trapped wave model (Clarke and Van Gorder, 1986). Due to the lack of reliable

wind observations along this portion of the Mexican coast, a complete hindcast comparison is not possible. Instead, the nature of the more energetic storm-related events described above are investigated by extrapolating storm winds to the coast. An empirically derived propagating signal, obtained from observed coastal pressure and sea level, is extracted from the moored observations and compared to the model. These gulf observations provide a test of the coastal-trapped wave model under several unique conditions: summer stratification is very strong (buoyancy frequency = 250 cpd), wave events tend to be isolated occurrences that can be tracked over several thousand kilometers, and there is little evidence of local wind forcing in the gulf. The paper is organized as follows. A brief description of the observations and the coastal wind estimate during storms is given in section 2, a discussion of the coastal-trapped wave model and the free wave parameters for this region is contained in section 3, the empirical propagating signal is derived and compared to model hindcasts in section 4, and a discussion and summary follow in section 5.

## 2. OBSERVATIONS

Moored observations of currents, temperature, and bottom pressure have been collected in the Gulf of California during a joint field study by Centro de Investigación Científica y de Educación Superior de Ensenada (CICESE) and the Scripps Institution of Oceanography (SIO) in 1983-84 (Fig. 1). A cross-gulf transect between Guaymas on the mainland coast and Santa Rosalia on the Baja California peninsula is the primary study site. Current observations are made with vector measuring current meters (VMCMs), while temperature is measured at each VMCM and pressure sensor and with thermistor chains in 200 m of water on the Guaymas and Santa Rosalia shelves. Winds and atmospheric pressure are measured with Portable Automated Mesonet (PAMII) weather stations positioned at six island and coastal sites. In addition, sea level is obtained from tide gauges maintained by CICESE and the National Autonomous University of Mexico (UNAM), and atmospheric pressure south of the gulf is obtained from the World Meteorological Organization. A complete description of the gulf observations is contained in MW.

Reliable coastal wind measurements in the region south of the Guaymas-Santa Rosalia transect are not available during this experiment. Winds measured at airports near the coast contain numerous gaps and spurious points and are not considered to be representative of winds over water. Moreover, storm events are typically missing from these wind observations. Large scale geostrophic winds, obtained from the Fleet Meteorological Center, do not have the spatial resolution needed to detect hurricane winds and are of dubious value at the low latitudes in this study.

Thus, in order to study the coastal-trapped wave model response during energetic tropical storm events, storm track and maximum wind speed data, obtained from the National Climatic Data Center, are used to estimate winds at the coast. During a tropical storm or hurricane, an estimate of storm position and wind speed is made every six hours from satellite data (Dvorak, 1973), with occasional ship and aircraft verification. Given the approximate storm center and maximum wind speed, we extrapolate tangential winds to the coast using typical radial wind speed profiles for hurricanes and tropical storms (Fig. 2) given by Riehl (1954). Different radial profiles for tropical storm force winds are used before and after a hurricane under the assumption that a storm in formation has a larger spatial extent than a decaying storm. In this case, we use the hurricane radius of maximum wind speeds after the disturbance has been downgraded to a tropical storm. If the storm does not reach hurricane intensity, however, the tropical storm profile is used continuously. Storm centers that are greater than 500 km from the coast and tropical depressions are not included in the analysis. Wind stress is then computed using the expression of Large and Pond (1981). A synthetic time series, which only accounts for storm related alongshore winds, is then used to force the coastal wave model.

## 3. THE COASTAL-TRAPPED WAVE MODEL

The dynamical model used in the present study is based on the forced barotropic shelf wave formulation of Gill and Schumann (1974), extended to include stratification (Gill and Clarke, 1974), cross-shelf topography (Clarke, 1977), and bottom friction (Brink and Allen, 1978; Brink, 1982; Clarke and Van Gorder, 1986). Following Clarke and Van Gorder (1986), the linear, long wave, wind-driven response at the coast can be expressed as a vorticity-type equation for pressure $P$,

$$\frac{P_{xx}}{f^2} + \frac{P_{zz}}{N(z)^2} = 0 , \tag{1}$$

where $f$ is the coriolis parameter, $N(z)$ is the Brunt-Vaisala frequency, and $x$ and $z$ are the cross-shelf (positive in the offshore direction) and vertical coordinates. The boundary conditions are no flow through the bottom, a rigid lid at the surface, zero depth-averaged cross-shelf flow, u, at a depth equal to three times the Ekman depth (see Mitchum and Clarke, 1986), and $u_x = 0$ at an offshore distance L which is typically equal to twice the shelf/slope width. Equation 1 is solved at a given alongshelf location by expanding $P$ in terms of the complete set of free wave modes $F_j(x, z)$,

$$P(x,y,z,t) = \sum_{j=1}^{\infty} F_j(x,z)\,\phi_j(y,t)\,, \tag{2}$$

with each $\phi_j$ satisfying a forced, first order wave equation,

$$c_j^{-1}\phi_{jt} + \phi_{jy} + \sum_{i=1}^{\infty} a_{ij}\phi_j = b_j \tau^y(y,t)\,, \tag{3}$$

where $\tau^y$ is the alongshelf wind stress, $c_j$ is the free wave phase speed, $b_j$ is the wind coupling coefficient, and $a_{ij}$ are the frictional parameters. Friction has the effect of coupling the modal solutions in (3), as well as providing dissipation. The competing effects of generation by alongshelf winds and frictional dissipation are thus integrated as the wave propagates poleward. In practice, $P$ is obtained by dividing the coastline into approximately uniform sections (Fig. 3), and for each section, specifying a representative bathymetry and stratification and computing the free wave parameters $F_j(x,z)$, $c_j$, $a_{ij}$, and $b_j$ from a program listed in Brink and Chapman (1985). A coastal wall is placed at a depth of 10 m to approximate the coastal boundary condition of Mitchum and Clarke (1986a). $\phi_j$ is then computed at a given alongshelf location from (3) using a program provided by Dr. Allan Clarke. The solution for $\phi_j(y,t)$ requires the specification of $\phi_j(0,t)$ at the start of the grid. The $\phi_j(0,t)$ used in this study are described in the following section. Alongshelf current and density are then obtained directly from P using,

$$V = \frac{P_x}{\rho_o f} = \frac{1}{\rho_o f}\sum_{j=1}^{\infty} F_{jx}\,\phi_j \quad , \tag{4}$$

$$\rho = \frac{1}{g}P_z = \frac{1}{g}\sum_{j=1}^{\infty} F_{jz}\phi_j\,. \tag{5}$$

This model has had the most success in hindcasting coastal sea level and alongshelf currents (Battisti and Hickey, 1984; Mitchum and Clarke, 1986b; Chapman, 1987; Church et al., 1986), although current speeds are usually underpredicted. Density and cross-shelf current hindcasts, however, are generally poor (e.g., Chapman). Chapman (1987) has tested the sensitivity of the model in hindcasting observations made during the CODE experiment off northern California. He finds the model is most sensitive to the choice of wind forcing with measured coastal winds yielding better hindcasts than the larger scale geostrophic winds.

To compute the free wave parameters, bathymetry charts (reference) are used to obtain representative cross-shelf depth profiles for each section. The Brink and Chapman program requires the specification of a flat bottom beyond the shelf slope for numerical stability. A constant depth of 4000 m is used for sections 1 through 5 while 3500 m is used for sections 6 and 7 as the ocean floor rises near the mouth of the gulf. In sections 8 through 12, the basin shaped bathymetry profile of the Gulf of California is used instead of a flat bottom. The boundary conditions are no flow through the offshore solid boundary, and $u_x = 0$ at $x = L$, where $L$ is the width of the gulf. The rugged bathymetry of the island region of the northern gulf is simplified to a smooth, shallow basin of approximately 200-m depth. Test runs confirm that the modes used in this study are stable to small changes in the gulf bathymetry profile. A further restriction of the model is a straight coastline. This is a reasonable assumption along most of the Mexican coast except in the northern gulf where the coastline orientation changes by 180°. In this study, the Gulf of California will simply be "unfolded" with the coastline assumed straight from the mainland to the Baja California shelves. Summer stratification profiles for sections 1 through 7 are obtained from historic EASTROPAC and CALCOFI hydrographic data. The stratification for sections 8 and 9 is an average profile obtained from the thermistor chain on the Guaymas shelf during the 1984 summer, sections 10 and 11 is an average of hydrographic observations made during this experiment (Bray, 1987), and section 12 is obtained from the thermistor and mooring temperature observations on the Santa Rosalia shelf. An average of historic hydrographic data is used to obtain a single profile of stratification below 200-m depth for all locations. This profile is specified as a decaying exponential with a length scale of 500 m. Near-bottom velocities are not available to empirically determine the bottom friction parameter $r$ ($a_{ij}$ is proportional to $r$, see Clarke and Van Gorder, 1986). A constant value of 0.05 cm/s, used in previous wave studies (e.g., Chapman, 1987; Church et al., 1986), is chosen for all sections.

The free wave parameters computed along the Mexican coast are pictured in Fig. 4 for the first four modes. Mode 1 free wave phase speeds are in agreement with previous values for this region computed by EA, except near Salina Cruz. The close agreement between our mode 2 and EA's mode 1 suggests that they may have missed the lowest mode in their analysis. Alongshore variation in the parameters reflects changes in shelf width. Wide shelf regions, such as near Salina Cruz and Mazatlan, have higher free wave phase speeds while narrow shelf regions, such as between Puerto Angel and Manzanillo, have weaker wind coupling coefficients. Frictional decay length scales, measured as the inverse of $a_{jj}$, are shortest in wide shelf regions and in the Gulf of California, except at the narrow shelf near Santa Rosalia. The free wave parameters are reasonably stable to changes in input bathymetry and stratification that reflect the

uncertainty in specifying a single profile for a given section. Mode 1 parameters typically do not vary by more than 10% while mode 4 parameters, particularly the $a_{ij}$, can change by 50% or more in some cases. Mode 4 is the highest mode considered in this study. As noted by EA, it is important to specify the Baja California peninsula for the Gulf of California sections rather than assuming a deep ocean offshore. The presence of the Baja California peninsula increases phase speeds by approximately 10-15%.

The free wave offshore structures for pressure, alongshelf current, and density at section 9 are shown in Fig. 5. The profiles reflect the hybrid nature of free waves in this region with a more barotropic structure over the shelf, and baroclinic structure over the slope. The offshore decay scales, as noted by EA, are typically less than 1/2 the width of the gulf. Using a flat bottom offshore condition does not significantly alter the wave structures over the mainland shelf and slope.

## 4. FORCED WAVE RESULTS

Since we are interested in storm generated events rather than a complete hindcast of gulf shelf observations, it is desirable to statistically isolate a propagating signal in the moored data, to compare with the model results. CDG and EA are able to detect poleward propagation in coastal sea level records from Acapulco to the Gulf of California in both the time and frequency domains. We prefer to isolate the propagating signal in the time domain, however, since wave events are non-dispersive, short-term, isolated features that are wide-banded in frequency (0.02-0.37 cpd from EA). One seemingly appropriate time domain statistical technique is complex empirical orthogonal function (CEOF) analysis (Barnett, 1983). CEOFs have been used to identify propagating variability in large data sets (e.g., White 1987) which cannot be simply accomplished with a standard EOF analysis (Lorenz, 1956). Tests of CEOF analysis on synthetic time series that approximate the propagating signals of this study indicate, however, that the method may not be appropriate for wide-banded, non-dispersive processes (see chapter 3). Instead, we proceed by using standard EOFs on time shifted series. Coastal adusted sea level and pressure observations from Acapulco to Isla Tiburon are band-passed to include only frequencies with poleward phase propagation identified by EA, and shifted in time to obtain maximum correlation with adjusted sea level at Guaymas (Fig. 6). An EOF of these shifted time series has a lowest mode which describes 77% of the variability with nearly equal spatial amplitude at each of the four locations. When mode 1 is removed from each time series, residual propagating features are not observed (Fig 6). Thus, we assume that the propagating signal is represented by this single

mode. The propagation speeds derived from the time lags shown in Fig. 6, are consistent with the previous estimates of EA obtained from sea level cross-spectra (MW).

Next, a multivariate regression analysis is performed on the gulf moored observations to estimate propagating and locally forced variability. Each estimate consists of two inputs: local forcing represented by wind stress measured at W5 (equivalent to the dominant wind EOF mode described in MW), and the remotely forced propagating signal described above. The inputs are lagged in time to coincide with maximum correlation with the estimand, and all time series are band-passed filtered (0.03-0.33 cpd). Temperature is converted to density using the relationship given in MW. Density at Guaymas has slightly higher correlations with the wave signal at small, non-zero time lags. In this study the zero-lagged response is investigated.

For all observations in the gulf, the local wind mode does not describe a significant portion of the variability. This is true for lags of up to 2 days between wind stress and the variable being estimated. MW attribute this lack of local wind forcing to the combination of weak winds and high stratification found in the gulf region. In contrast, the propagating signal accounts for much of the coastal pressure variability along the coast from Salina Cruz to Isla Tiburon (Table 1). The amplitude and percentage of variance explained by the propagating signal is weaker at Salina Cruz than at mainland coastal stations to the north, consistent with wave forcing occurring north of Salina Cruz (EA). The offshore pressure structure associated with the propagating signal decays offshore as can be seen, for example, at Guaymas. The propagating amplitude at Topolobampo is lower than that at neighboring stations due to the offshore location (100-m isobath) of the sensor. The propagating signal is also detected in pressure observations on the Baja California shelf, but with low amplitude. The signal on this side of the gulf lags the mainland coast signal by 1.3-1.8 days at Santa Rosalia-Guaymas, and 2.4 days at San Francisquito-Isla Tiburon.

In the Gulf of California, density and alongshelf current measurements also have a detectable propagating component. Density fluctuations associated with the propagating signal are significant below the upper mixed layer at Guaymas and Topolobampo and explain approximately 40 to 60% of the variability (Table 1). Density fluctuations at and below 70-m depth at Santa Rosalia are also correlated with the propagating signal at an approximate 9 day lag relative to Guaymas, as noted in MW. The propagating signal explains a significant, although low percentage, of the alongshelf current variability on the mainland coast. MW report that the flow field is more complex than the pressure and density fields with considerable variability not directly accounted for by either local winds or propagating events. Thus individual current time series will be directly compared with model hindcasts.

Since observed propagation speeds are most similar to mode 1 free wave phase speeds (EA, CDG), the empirically derived propagating signal is first compared with mode 1 model results, followed by an examination of the effects of including higher modes. The comparison between observed and mode 1 coastal pressure is shown in Fig. 7. In this initial run, $\phi_1(0,t)$ is set to zero under the hypothesis that most of the wave variability is generated north of Salina Cruz. The model does reasonably well in reproducing the largest 1984 events from Topolobampo to Isla Tiburon which are associated with hurricanes Fausto and Genevieve in July (Fig. 8). Two of the three smaller events in late July and August associated with weaker tropical storms are also reproduced by the model, although the amplitudes are underestimated by approximately 30-50%. The model does predict an event in early June that is not apparent in the observations. Maximum correlations between the EOF propagating signal and the mode 1 coastal pressure hindcasts indicate that observed arrival time on the mainland shelf is 36 hours earlier than the model estimate at Toplobampo, 24 hours at Guaymas, and 18 hours at Isla Tiburon. Correlations between the EOF signal and the mode 1 hindcast are approximately 0.6 in the Gulf of California.

The model indicates that wave generation should occur primarily between Manzanillo and Mazatlan where storms are strongest and closest to shore (Fig. 8). The corresponding events in observed sea level, however, appear much further south. For example, the strong July events are present only in the model's mode 1 coastal pressure north of Manzanillo in contrast to the observations which seem to show the events as far south as Salina Cruz (see also EA for similar events in 1971, 1973-1974). Storm tracks do not show either Fausto or Genevieve far enough south to generate the event at Salina Cruz using our extrapolation technique. The sea level events associated with weaker tropical storms in late July and August also appear further south than the model indicates. The model fit is not improved by using Salina Cruz adjusted sea level to specify $\phi_1(0,t)$. For the value of bottom friction used in this study, the signal input at Salina Cruz decays by 90% before reaching Acapulco, while the observations show little decay over this distance. It is not, however, simply a matter of adjusting the friction parameter as the free wave speeds are too slow for the event seen at Salina Cruz to reach Acapulco in the observed time span. The propagation speed between Salina Cruz and Acapulco during the large July events is almost 8 m/s, nearly three times as large as the mode 1 phase speed. This observed speed, however, is still far too slow for a barotropic Kelvin wave which has a speed on the order of 200 m/s. This discrepancy in the location of wave generation is most likely due to the inherent limitations of estimating the coastal wind field. The radial profiles of tangential winds are for well-developed storms. During the early formation stages of these storms, which often occur in the

vicinity or south of Salina Cruz, the wind field is certainly far less structured and may not be adequately represented by our simple coastal wind extrapolation. We could not find, however, a simple variation of the radial storm profile that is more consistent with all the observed events. Nonetheless, the temporal changes of propagating events in observed sea level between Acapulco and the Gulf of California (Fig. 7) do seem to support the model result that some forcing must occur north of Acapulco. In addition, the model comparisons north of Acapulco verify that the typical winds around storms in this region are sufficient to generate the observed sea level amplitudes. The event of roughly 15 cm in July is reproduced by the model when forced by coastal winds of 20-30 m/s near Manzanillo and Mazatlan. When PAMII winds with rms speeds of 5 m/s are used to force the model in the gulf, the associated response is on the order of 1 cm for sea level and 1 cm/s in current speed again confirming the weak local wind forcing in the gulf.

The model's mode 1 pressure and density cross-shelf structures at Guaymas are qualitatively similar with profiles obtained from the multivariate analysis (Fig. 9). In addition to the measured 100-m and 200-m bottom pressure and adjusted coastal sea level, pressure is computed at various depths above the 200-m pressure sensor using density, obtained from the thermistor chain, and the hydrostatic equation (described in MW). The mode 1 and observed pressure and density fields are normalized to correspond to a 10 mbar pressure rise, or 10 cm sea level rise, at the coast. The two pressure fields have largest amplitudes at the coast, decaying offshore and with depth. The observed pressure field, however, as a stronger baroclinic component and decays approximately twice as fast offshore. The mode 1 and observed cross-shelf density fields are also qualitatively similar in structure with largest fluctuations in the thermocline region between 40-m and 70-m depth with amplitudes stronger near the shelf break than at the coast (Fig. 10). The model's mode 1 amplitudes, however, are almost 3 times weaker than those observed. As model pressure and density are in hydrostatic balance, the barotropic structure of the mode 1 pressure field is a direct result of the model's weak density response over the shelf.

On the Santa Rosalia shelf, the density, alongshelf current, and pressure fluctuations are found to be related to the propagating signal (Table 2), but at different lags. The propagating signal in pressure is lagged roughly 1.5 days relative to Guaymas pressure, while density, at 70-m and 100-m depth at the 100-m isobath, is lagged by 8.5 days. The mode 1 travel time around the head of the gulf is roughly 8.2 days with the next highest mode taking 15.5 days, indicating that wave energy exhibits mode 1 propagation even over the very complicated bathymetry of the northern gulf. The model's mode 1, however, has the strongest density fluctuations in the thermocline region above 40-m depth in contrast to the observations which only show a detectable propagating response below 70 m. The model's mode 1 also underestimates the amplitude of the

deep density fluctuation by two orders of magnitude. For mode 1 to reproduce the observed density amplitude would require an unrealistic 50-cm rise in coastal sea level. The time lag of the Santa Rosalia pressure/current fluctuations relative to Guaymas is much too short for this response to be associated with the equatorward signal observed in density. The pressure/current signal at Santa Rosalia would appear to be the offshore edge of the wave as it travels poleward along the mainland shelf. The decay scale across the gulf (150 km), however, does not agree with the offshore decay seen on the Guaymas shelf (30 km) or with the model's mode 1 pressure (50 km). In addition, the time lag between Guaymas and Santa Rosalia pressure cannot be accounted for by the first wave mode. That the Santa Rosalia pressure/current signal is not simply an extention of the wave across the gulf is also supported by the insignificant correlation between Santa Rosalia alongshelf currents and Guaymas sea level during the 1983 summer deployment. In constrast, Santa Rosalia density, which we do directly associate with the wave events, is correlated in both summers. MW suggest that the current signal at Santa Rosalia may be associated with eddy-like features setup by the larger wave events rather than a component of the wave structure.

Alongshore current observations on the mainland shelf agree with the model's mode 1 vertical structure, but not in cross-shelf structure. During the energetic July wave events, alongshelf currents at Topolobampo are in good agreement with the magnitude and direction of the model's mode 1 response and confirm that these currents are essentially barotropic over the shelf (Fig. 11). The comparison of the weaker currents in August, however, is poorer but may be due to the masking of wave variability by other processes. This appears to be the case at Guaymas (Fig. 12) where considerably more variability occurs which is not associated with storm events. The July wave event is assumed strong enough, however, to allow a direct examination of currents during this time period. Currents measured in total water depths of 200 m, 50 m, and 15 m show a clear diminishing of current speed towards the coast, in contrast to mode 1 currents which increase towards the coast. Observed currents at M4 (15-m depth) have peak speeds of 10 m/s compared to model predictions of over 50 m/s. In addition the direction of 15-m currents appears to be counter to observed offshore currents and model currents. There is also a slight phase lag between peak current occurrences across the shelf during the July propagating events, M6 leads M8 by 18 hours, that is not explained by mode 1. Although the exact details of the complicated Guaymas flow field may be beyond the scope of this wave model, the model's increase in current amplitude towards the coast is certainly unrealistic.

While mode 1 is successful in accounting for most of the propagating events seen in coastal sea level in the gulf, the cross-shelf structures of alongshelf current, density, and pressure

suggest the presence of higher modes. Specifically, the model's alongshelf current field should decrease rather than increase towards the coast, and the amplitude of density fluctuations are underpredicted by a factor of three, thus underpredicting the baroclinic component to the pressure field over the shelf. Several model runs are made to investigate the effect of including higher modes in the model hindcast.

The first set of model runs use all four modes shown in Fig. 5, without frictional coupling between modes ($a_{ij} = 0$ for $i \neq j$). The energy in modes 3 and 4 is essentially dissipated before reaching the Gulf of California for the chosen magnitude of the frictional parameter. Mode 2, with a slower propagation speed, arrives in the gulf approximately 5 days after mode 1. This result is inconsistent, however, with the inability to detect higher propagating signals in coastal sea level observations (Fig. 6). A similar result is found in the fully coupled case. Thus, we assume that higher modes ($j > 1$) do not freely propagate into the gulf, but are excited by the dominant mode 1 through the frictional coupling as it travels along the coast. In the next set of model runs, higher modes are excited by mode 1 only at section 9 where the observations are made. For 2 coupled modes at Guaymas, the velocity field is improved somewhat with a less rapid increase in current amplitude towards the coast. Density fluctuations, however, are now even weaker over the shelf. Modes 3 and 4 are only weakly coupled with mode 1 at Guaymas and do not alter the cross-shelf structures obtained from the first two modes.

These problems can be addressed by increasing the frictional parameter which would damp out modes higher than mode 1 from freely propagating into the gulf, as indicated by the observations, and increase mode coupling which might explain the discrepancies between mode 1 and the observations. This increase in friction, however, would also dissipate energy in mode 1, which is contrary to the minimal decay in wave amplitude between Guaymas and Isla Tiburon (Table 1), and would result in even less available energy to increase the amplitude of density fluctuations.

## 5. DISCUSSION AND SUMMARY

Propagating sea level events in the Gulf of California are similar to mode 1 coastal-trapped waves. The hindcast of mode 1 coastal pressure using a simple estimate of storm winds at the coast, is successful in reproducing the amplitude and approximate propagation speed of energetic wave events north of Mazatlan. Wave generation, however, is predicted to occur primarily between Manzanillo and Mazatlan during 1984, while observations indicate generation occurring at least as far south as Salina Cruz for some events. This discrepancy is most likely

due to our limited knowledge of the coastal wind field rather than an inherent problem with the model. At the Guaymas shelf, the observed pressure field is trapped to the coast in the same manner as mode 1, although the observed field is more baroclinic over the shelf and has a shorter offshore decay scale. The observed and mode 1 density fields at Guaymas are also similar in structure, although observed amplitudes are nearly three times larger than predicted by mode 1. Alongshelf currents are barotropic during energetic wave events at the midshelf, in accordance with mode 1. Currents are observed to decay in amplitude towards the coast, however, in contrast to mode 1 current profiles which have highest amplitudes at the coast. Higher modes reduce the increase in current speed towards the coast, but at the expense of less realistic pressure and density profiles over the shelf. Moreover, alongshelf current observations, made primarily in depths shallower than 20 m, are probably in frictional regions unsuitable for the coastal-trapped wave model dynamics. Thus the use of higher modes to hindcast currents outside the model domain is not justifiable. The inclusion of modes higher than mode 4 are unlikely to significantly improve the hindcast results, while increasing the frictional parameter to increase mode coupling, would also increase the dissipation of the wave events in contrast to the observations.

We have demonstrated that coastal winds during a hurricane or tropical storm in the eastern north Pacific are sufficient to excite observed wave amplitudes. How far south the generation occurs is, however, unresolved as it is uncertain what the nature of the signal is at Salina Cruz where storms are generally weak. CDG and EA report low correlations or coherences between sea level at Salina Cruz and more northern stations for the summers of 1971 and 1973-1974, which supports their argument that forcing occurs north of Salina Cruz. While propagating events are weak or absent at Salina Cruz in the 1971 summer, several energetic events do seem to appear as far south as San Jose (shown in Fig. 3) in 1973-1974 (see EA Figs. 2 and 4). A better description of the wind field along the Mexican coast is needed, but particularly south of Salina Cruz, in order to unequivocably link all propagating events to tropical storms and hurricanes.

In addition, the results from this study suggest that the coastal-trapped wave model does not accurately estimate the amplitude of the density response. Chapman (1987) and Brink (1982) also report poor hindcasts of density, but contend that mixed layer and other non-wave related phenomena contaminate the wave signal in density. In this study, we are able to empirically identify a propagating signal in density independently of the model and find that lower, more dominant modes are not able to explain the observed response. The model dynamics assume that density fluctuations are due solely to the vertical advection of the mean stratification. This assumption is consistent with the description of the temperature field in the gulf presented by MW. The mean stratification does vary over the 1984 instrument deployment in contradiction to

a model assumption, but the magnitude is not significant enough to explain the model's underestimate of density. The problem seems to involve the model's underestimate of the vertical velocity. If so, the addition of more realistic surface and bottom boundary layers may improve the performance of the model.

Acknowledgments

The Gulf of California observations used in this study were collected under the direction of C. Winant, A. Badan-Dangon, N. Bray, M. Hendershott, and R. Guza. A. Clarke and D. Chapman provided the numerical codes on coastal-trapped waves. Hydrographic data south of the gulf region was provided by A. Mantyla and S. Tsuchiya, and sea level observations by G. Gutierrez. I am indebted to N. Christensen, Jr., R. Guza, and C. Winant for valuable comments and suggestions. J. Becker suggested numerous improvements to the manuscript. This work was funded by the Office of Naval Research (N00014-85-C-0104, N00014-87-K-0005).

# REFERENCES


Barnett, T. P., Interaction of the Monsoon and Pacific Trade Wind System at interannual time scales. Part 1: The equatorial zone, *Mon. Wea. Rev., 111*, 756-773, 1983.

Battisti, D. S., and B. M. Hickey, Application of remote wind-forced coastal-trapped wave theory to the Oregon and Washington coast, *J. Phys. Oceanogr., 14*, 887-903, 1984.

Bray, N. A., M. C. Hendershott, J. M. Robles, and A. C. Carrasco, Pichicuco 6: Gulf of California CTD data report, *SIO Ref. 86-4*, 254 pp., 1986.

Brink, K. H., A comparison of long coastal-trapped wave theory with observations off Peru, *J. Phys. Oceanogr., 12*, 897-913, 1982.

Brink, K. H., and J. S. Allen, On the effect of bottom friction on barotropic motion over the continental shelf, *J. Phys. Oceanogr., 8*, 919-922., 1978.

Brink, K. H., and D. C. Chapman, Programs for computing properties of coastal-trapped waves and wind-driven motions over the continental shelf and slope, *Woods Hole Oceano. Inst. Tech. Rept. 85-17*, 99 pp., April 1985.

Chapman, D. C., Application of wind-forced, long coastal-trapped wave theory along the California coast, *J. Geophys. Res., 92*, 1798-1816, 1987.

Christensen, N., Jr., R. de la Paz, and G. Gutiérrez, A study of sub-inertial waves off the west coast of Mexico, *Deep-Sea Res., 30*, 835-850, 1983.

Church, J. A., N. J. White, A. J. Clarke, H. J. Freeland, and R. L. Smith, Coastal trapped waves on the East Australian continental shelf. Part II: Model verfication, *J. Phys. Oceanogr., 16*, 1945-1957, 1986.

Clarke, A. J., Observational and numerical evidence for wind-forced coastal-trapped long waves, *J. Phys. Oceanogr., 7*, 231-247, 1977.

Clarke, A. J., and S. Van Gorder, A method for estimating wind-driven frictional, time-dependent, stratified shelf and slope water flow, *J. Phys. Oceanogr., 16*, 1011-1026, 1986.

Dvorak, V. F., A technique for the analysis and forecasting of tropical cyclone intensities from satellite pictures, *NOAA Tech. Memo. NESS 45*, 19 pp., 1973.

Enfield, D. B., and J. S. Allen, The generatiion and propagation of sea level variability along the Pacific coast of Mexico, *J. Phys. Oceangr., 13*, 1012-1033, 1983.

Gill, A. E., and A. J. Clarke, Wind-induced upwelling, coastal currents and sea level changes, *Deep-Sea Res., 21*, 325-345, 1974.

Gill, A. E., and E. H. Schumann, The generation of long shelf waves by the wind, *J. Phys. Oceanogr., 4*. 83-90, 1974.

Gunther, E. B., and R. L. Cross, Annual Summary: Eastern North Pacific tropical cyclones of 1984, *Mon. Wea. Rev., 113*, 1393-1410, 1985.

Horel, J. D., Complex principal component analysis: Theory and examples, *Climate Appl. Meteor., 23*, 1660-1673, 1984.

Large, W. G., and S. Pond, Open ocean momentum flux measurements in moderate to strong winds, *J. Phys. Oceanogr., 11*, 324-336, 1981.

Lorenz, E., Empirical orthogonal function and statistical weather prediction, *Rep. No. 1, Statistical Forecasting Program*, Dept. of Meteorology, MIT, 44 pp., 1956.

Merrifield, M. A., and C. D. Winant, Shelf circulation in the Gulf of California: A description of the variability, submitted to *J. Geophys. Res.*, 1988.

Mitchum, G. T., and A. J. Clarke, The frictional nearshore response to forcing by synoptic scale winds, *J. Phys. Oceanogr., 16*, 934-946, 1986*a*.

Mitchum, G. T., and A. J. Clarke, Evaluation of frictional, wind forced long wave theory on the West Florida Shelf, *J. Phys. Oceanogr., 16*, 1027-1035, 1986*b*.

Rhiel, H., *Tropical Meteorology*, McGraw-Hill, 281-357, 1954.

White, W. B., and S. Tabata, Interannual westward-propagating baroclinic long-wave activity on line P in the eastern midlatitude North Pacific, *J. Phys. Oceanogr., 17*, 385-396, 1987.

TABLE 1. Results from the multivariate regression of the empirically determined propagating signal and alongshelf wind stress on moored observations in the Gulf. The alongshelf wind stress does not have a significant component in the observations and is not listed.

| Instrument Location | $\alpha$ | Lag (days) | % Variance |
|---|---|---|---|
| PRESSURE | | | |
| Salina Cruz (SC) | 0.70 ± 0.11 | -8.5 | 31.7* |
| Acapulco (AC) | 0.97 ± 0.25 | -6.4 | 61.9* |
| Topolobampo 100 m (TO) | 0.63 ± 0.04 | -1.2 | 78.9* |
| Guaymas Harbor (GY) | 1.20 ± 0.04 | 0.0 | 85.4* |
| Guaymas 100 m (P4) | 0.59 ± 0.02 | 0.0 | 67.7* |
| Guaymas 200 m (P5) | 0.25 ± 0.06 | 0.0 | 25.9* |
| Isla Tiburon 7 m (IT) | 1.03 ± 0.02 | 0.9 | 83.3* |
| S. Francisquito 7 m (SF) | 0.38 ± 0.04 | 3.3 | 19.8* |
| S. Rosalia Harbor (SR) | 0.29 ± 0.02 | 1.3 | 36.6* |
| S. Rosalia 100 m (P6) | 0.27 ± 0.08 | 1.8 | 20.5* |
| DENSITY | | | |
| M1 70/100 m | -0.37 ± 0.06 | -1.1 | 24.4* |
| M4 2/15 m | 0.05 ± 0.01 | 0.0 | 3.6 |
| 14/15 m | -0.06 ± 0.04 | 0.0 | 1.7 |
| M6 10/50 m | 0.02 ± 0.02 | 0.0 | 0.4 |
| 20/50 m | -0.11 ± 0.04 | 0.0 | 4.6 |
| 30/50 m | -0.38 ± 0.08 | 0.0 | 18.7* |
| M7 100/100 m | -0.54 ± 0.02 | 0.0 | 53.7* |
| M8 10/200 m | -0.03 ± 0.06 | 0.0 | 0.7 |
| 20/200 m | -0.20 ± 0.04 | 0.0 | 8.8* |
| 30/200 m | -0.48 ± 0.10 | 0.0 | 19.2* |
| 40/200 m | -0.74 ± 0.13 | 0.0 | 30.5* |
| 50/200 m | -0.91 ± 0.11 | 0.0 | 45.0* |
| 60/200 m | -0.92 ± 0.06 | 0.0 | 58.7* |
| 70/200 m | -0.84 ± 0.04 | 0.0 | 62.5* |
| 85/200 m | -0.65 ± 0.08 | 0.0 | 58.2* |
| 115/200 m | -0.40 ± 0.02 | 0.0 | 56.9* |
| 130/200 m | -0.30 ± 0.02 | 0.0 | 53.8* |
| 145/200 m | -0.24 ± 0.02 | 0.0 | 51.3* |
| 160/200 m | -0.21 ± 0.01 | 0.0 | 49.0* |
| 175/200 m | -0.18 ± 0.01 | 0.0 | 49.8* |
| 200/200 m | -0.11 ± 0.02 | 0.0 | 47.4* |
| M9 50/1000 m | 0.10 ± 0.02 | 0.0 | 2.2 |
| M11 10/100 m | 0.05 ± 0.08 | 0.0 | 0.8 |
| 30/100 m | 0.07 ± 0.15 | 0.0 | 0.9 |
| 70/100 m | -0.24 ± 0.04 | 9.6 | 31.3* |
| 100/100 m | -0.25 ± 0.02 | 8.5 | 38.3* |
| ALONGSHELF CURRENT | | | |
| M1 70/100 m | 0.90 ± 0.23 | -1.6 | 8.3* |
| M4 5/15 m | 0.15 ± 0.02 | -1.8 | 8.4* |
| M6 20/50 m | -0.95 ± 0.12 | 2.1 | 12.0* |
| M8 10/200 m | 2.71 ± 0.54 | -0.25 | 16.2* |
| M9 50/1000 m | 1.06 ± 0.42 | 2.1 | 7.9 |
| M11 10/100 m | -1.16 ± 0.25 | 1.7 | 16.6* |
| 30/100 m | -1.24 ± 0.17 | 1.5 | 25.0* |
| 70/100 m | -1.15 ± 0.12 | 1.5 | 21.6* |

* above 95% significance level

The regression coefficient, $\alpha$ ($g/cm^3/mb$ for density, $cm/s/mb$ for current), is relative to the magnitude of the propagating signal at Guaymas. Time series are shifted in time (lag) to obtain maximum correlation with the propagating signal. Pressure observations which do not include a depth refer to adjusted coastal sea level.

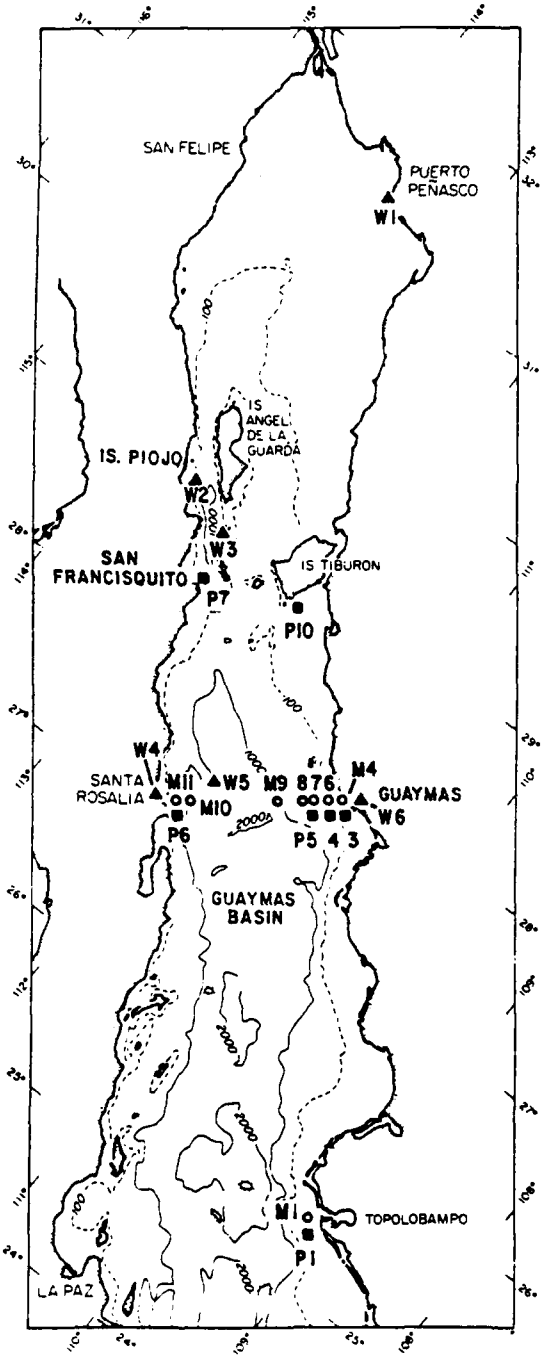


Figure 1.

The Gulf of California showing mooring (M), bottom pressure (P), and PAMII meteorological station (W) locations.

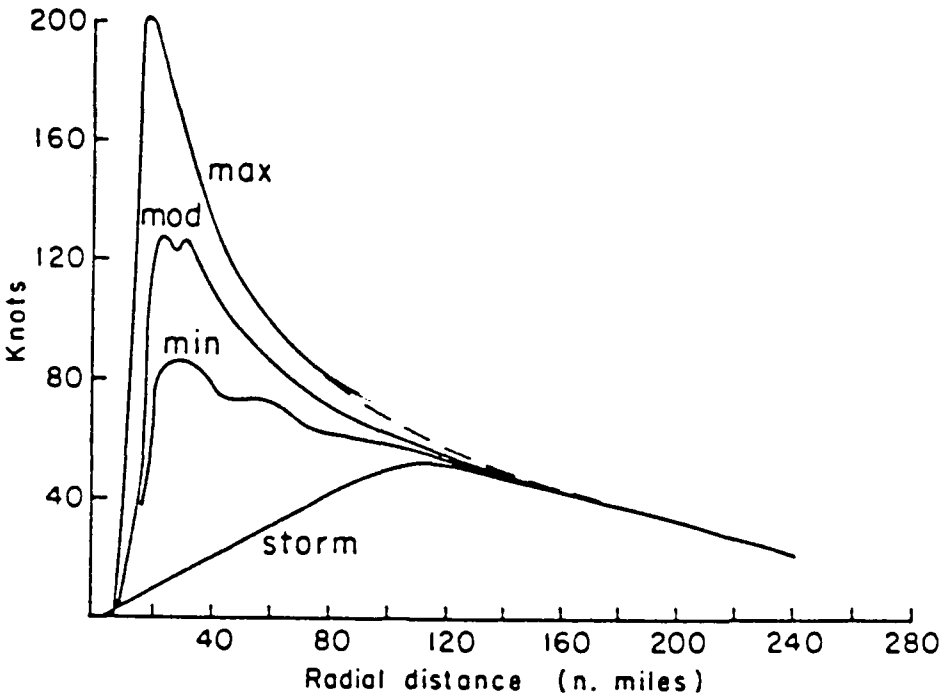


TROPICAL STORM:

(35 knots < w < 60 knots)

$w(r) = w_{max} - 0.15(r - r_{max})$

$r_{max} = 100$ n.m.

HURRICANE:

(w > 60 knots)

$w(r) = w_{max}\exp[-(r-r_{max})/A]$

$r_{max} = 30$ n.m.

$A = 630\exp[-(w_{max} - 80)/50]$

Figure 2.

The extrapolation of tropical storm and hurricane winds to the coasts, based on the radial wind speed profiles of Riehl, 1954. The exponential decay scale for hurricane winds is a function of wind speed. The wind field is taken to decay linearly for tropical storms. w=wind speed, $w_{max}$=maximum wind speed, r=radial distance from storm center, $r_{max}$=radius of maximum wind speed.

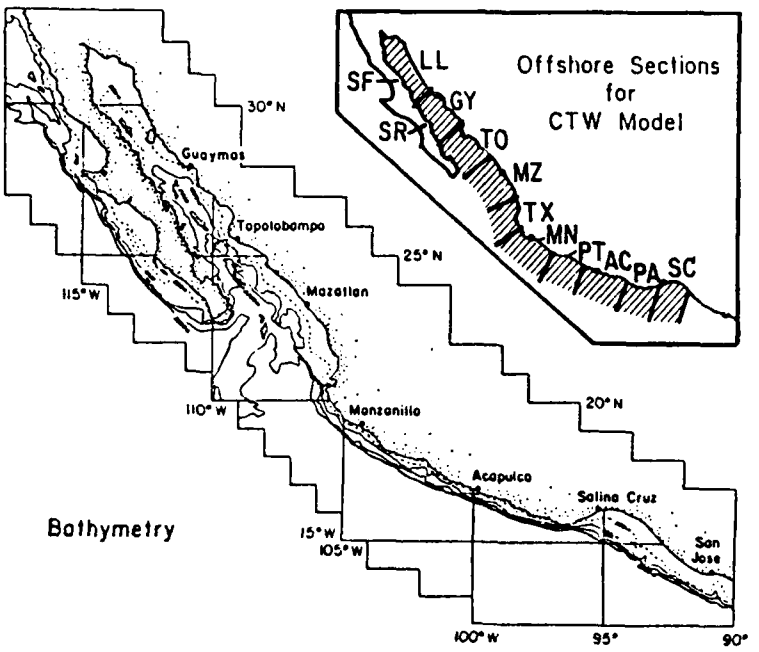


Figure 3.

The bathymetry of the Pacific coast of Mexico showing the 200-m (dashed) and 1000-, 2000-, and 3000-m isobaths (solid). Inset is a map showing the 12 sections for the coastal-trapped wave model. Original figure from Enfield and Allen (1983).

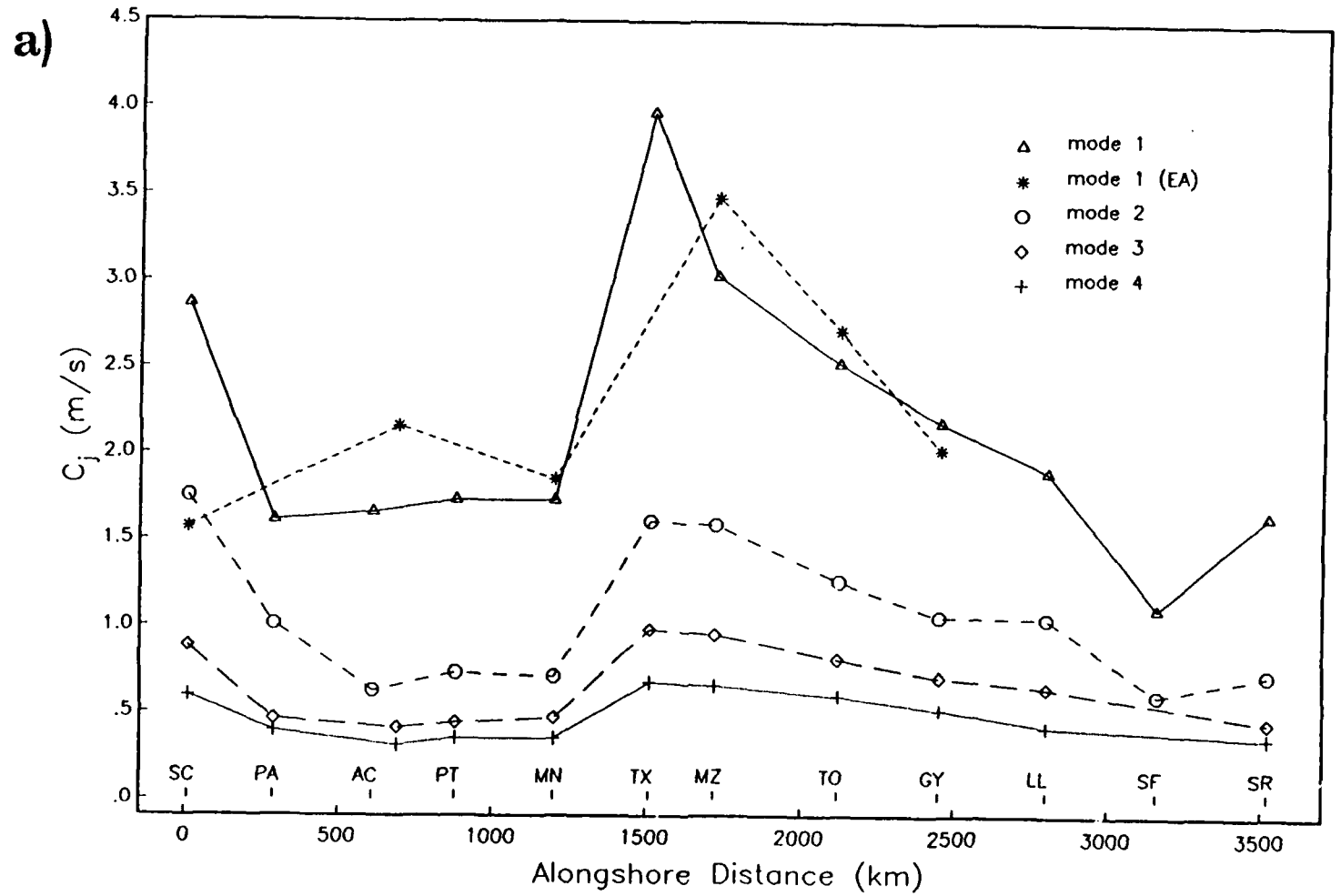


Figure 4. The phase speed (a), wind coupling coefficient (b), and frictional decay length scale (c) along the Pacific coast of Mexico for the first four free coastal-trapped wave modes. The mode 1 phase speed calculated by Enfield and Allen (1983) is included for comparison. The decay length is equal to the inverse of the friction coefficient, $a_{jj}$. Section labels (see Fig. 3) are plotted along the x axis.

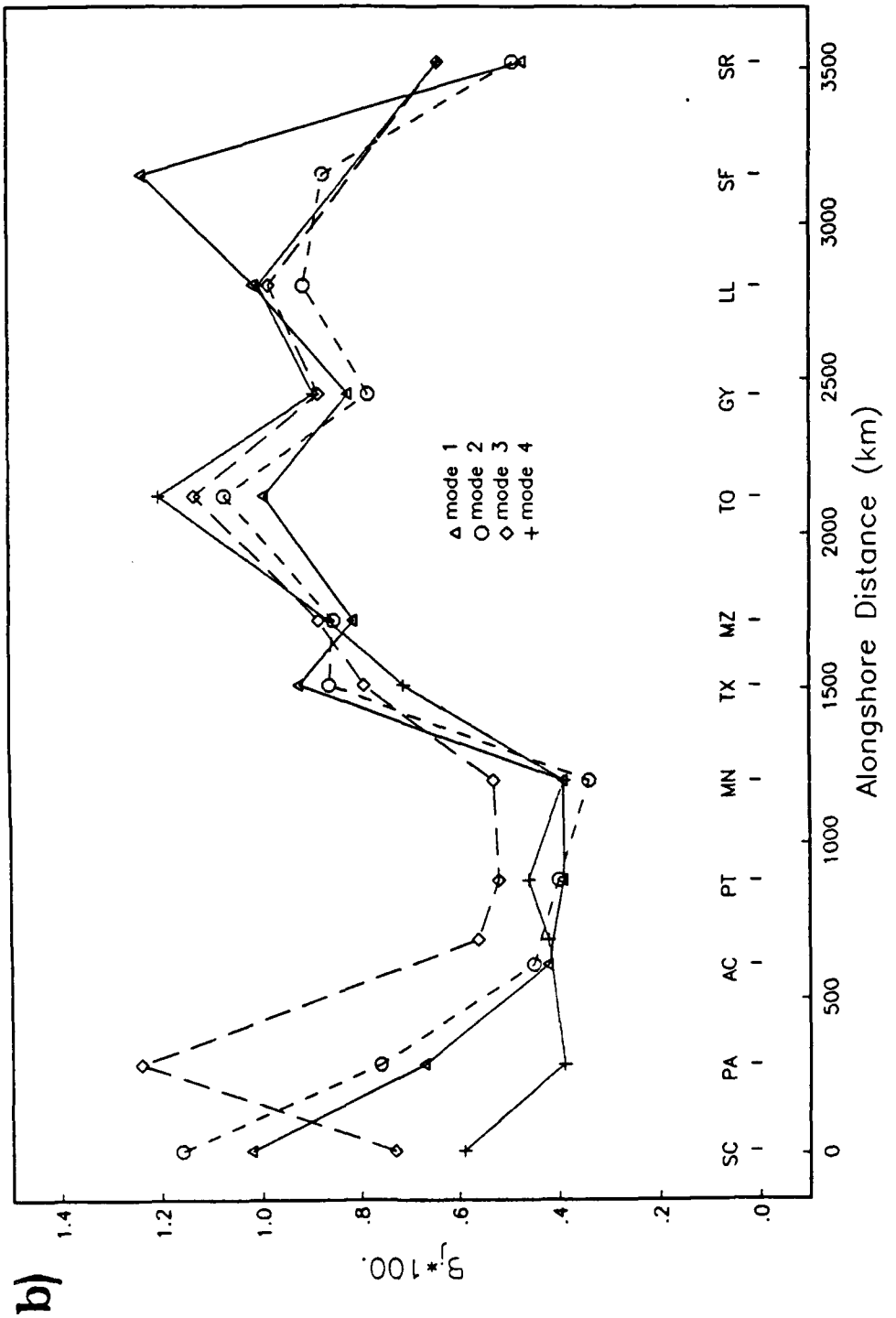


Figure 4. continued

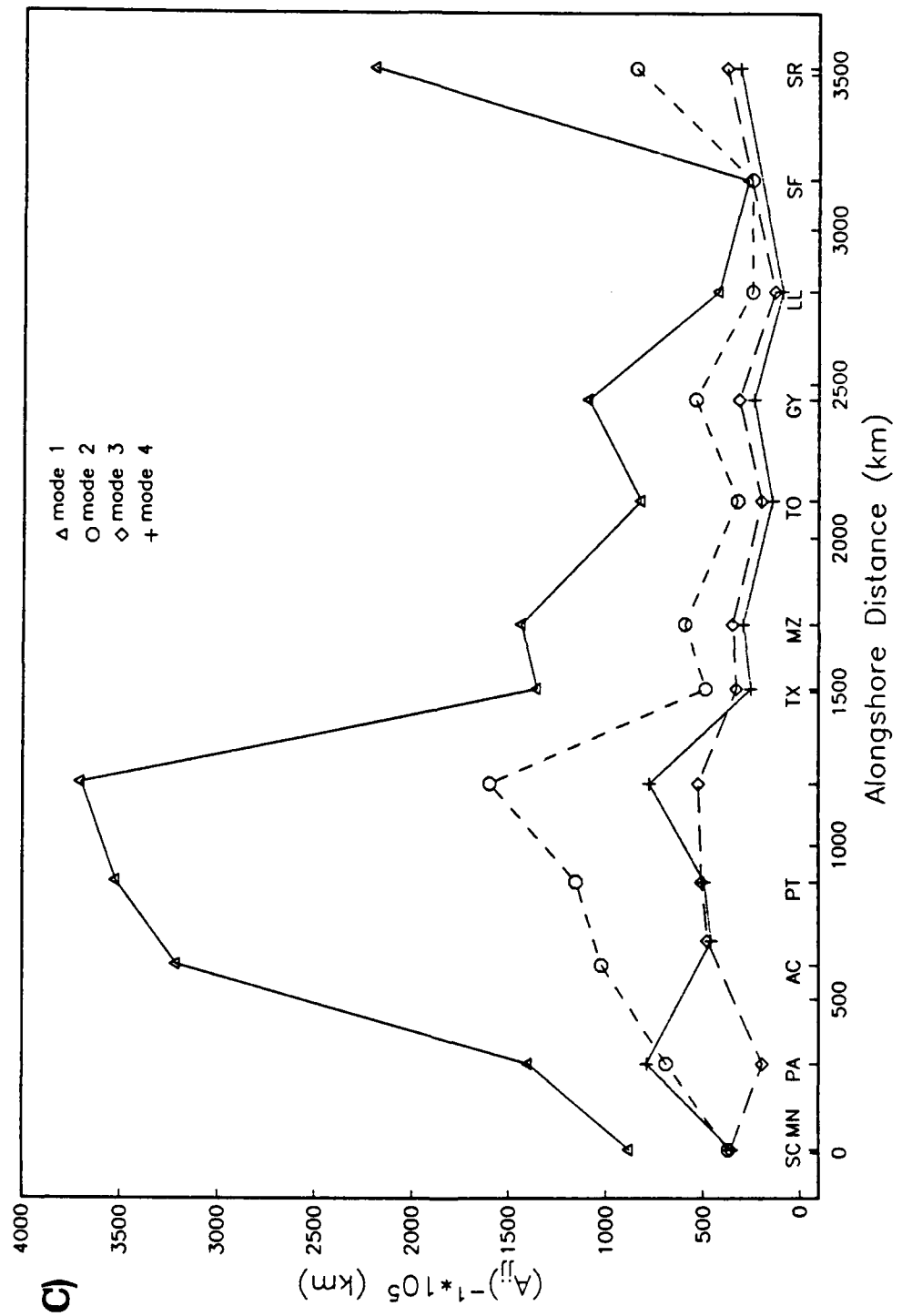


Figure 4. continued

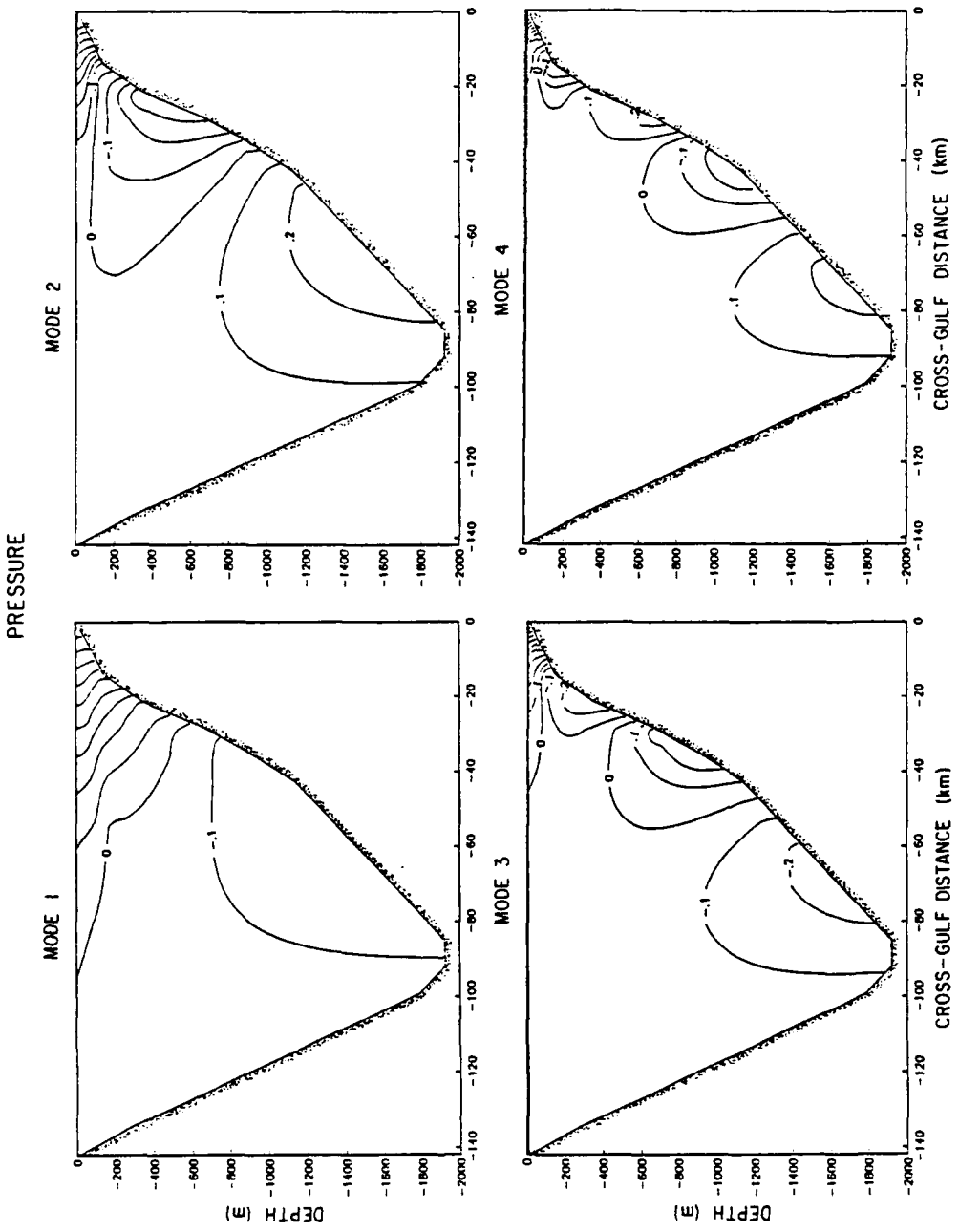


Figure 5. The first four free coastal-trapped wave cross-shelf structures of pressure (a), alongshelf current (b), and density (c). The units are arbitrary.

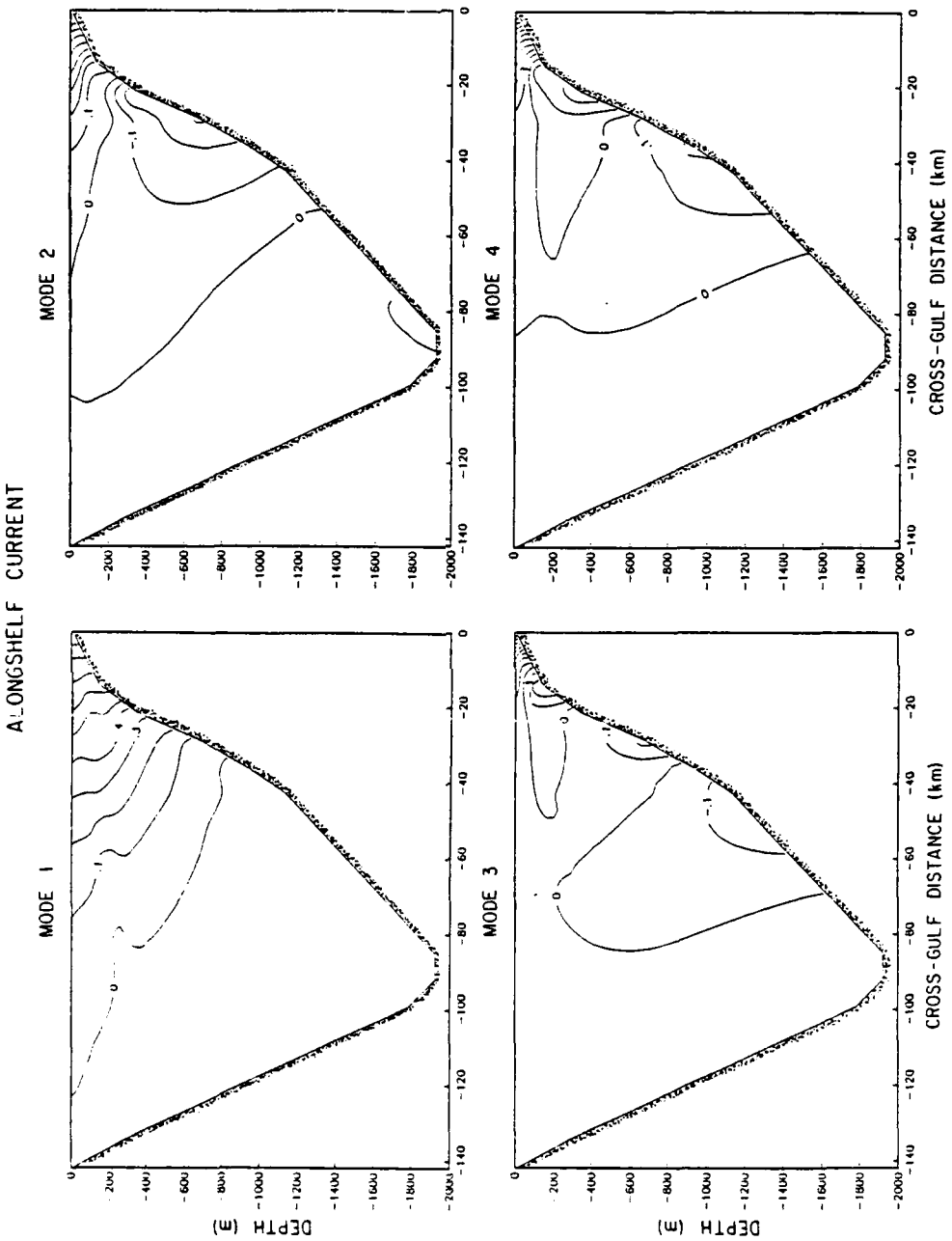


Figure 5. continued

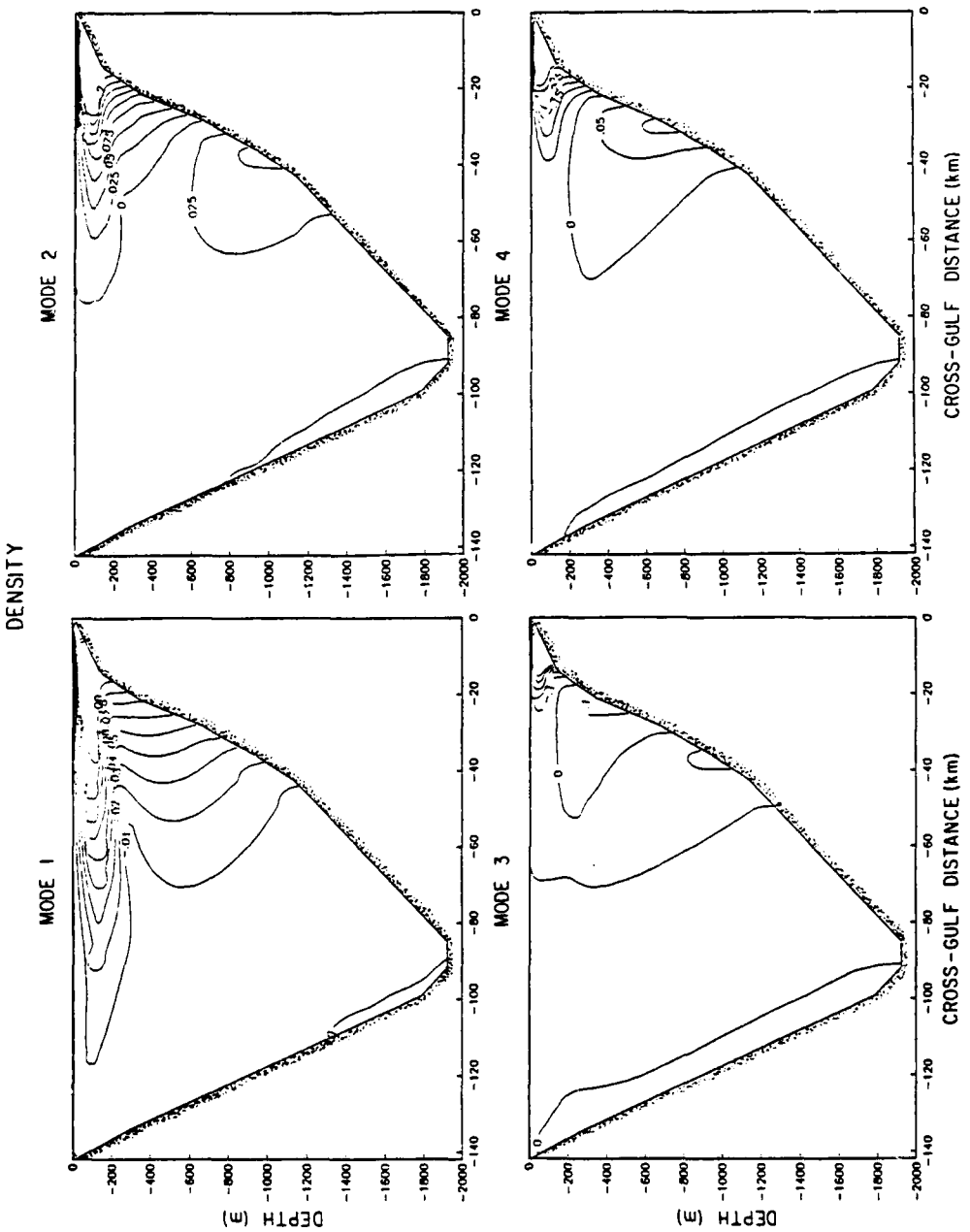


Figure 5. continued

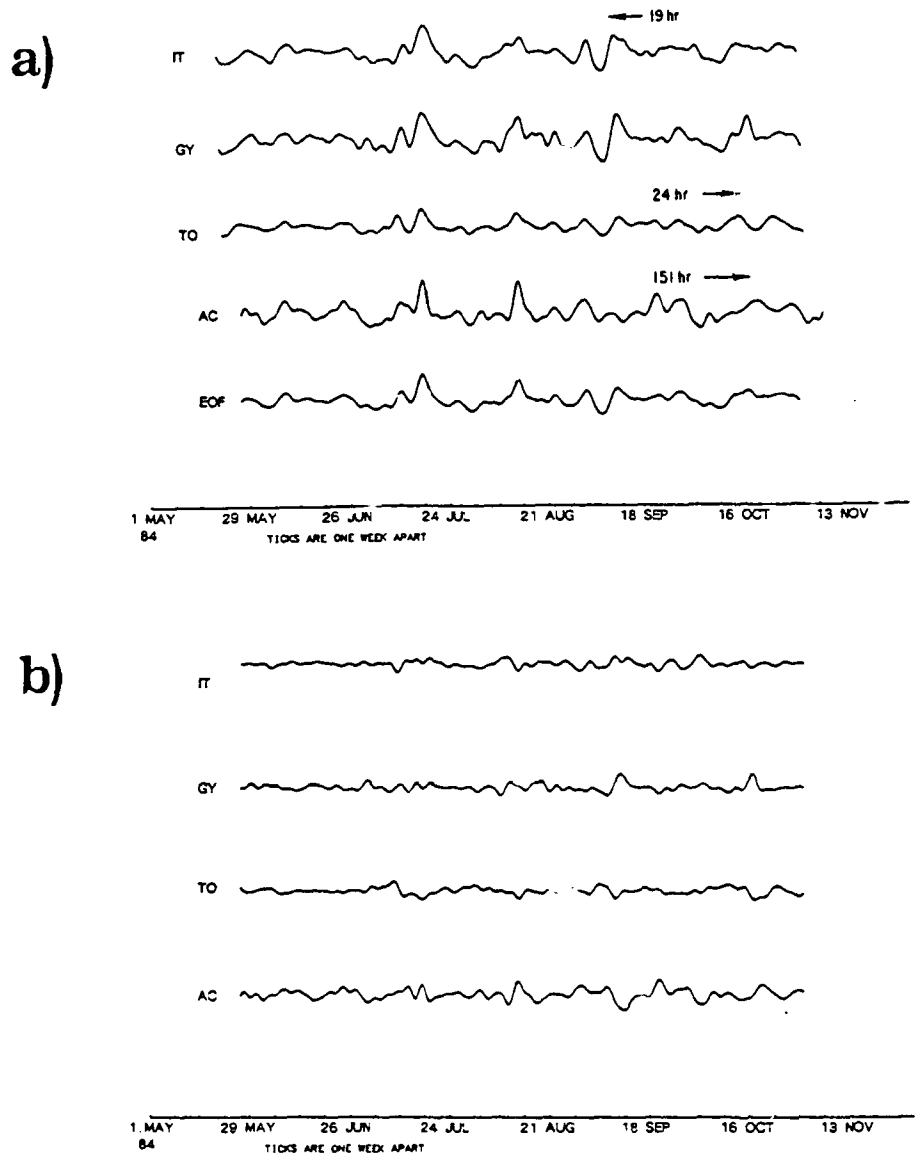


Figure 6.

(a) Coastal bottom pressure at Isla Tiburon (7-m depth), and Topolobampo (100-m), and adjusted sea level at Guaymas and Acapulco with each series time shifted to obtain maximum correlation with the Guaymas time series. The dominant EOF mode of the four time series is plotted last. (b) The same four time series minus mode 1. The residual time series are not significantly correlated and do not exhibit propagating variability.

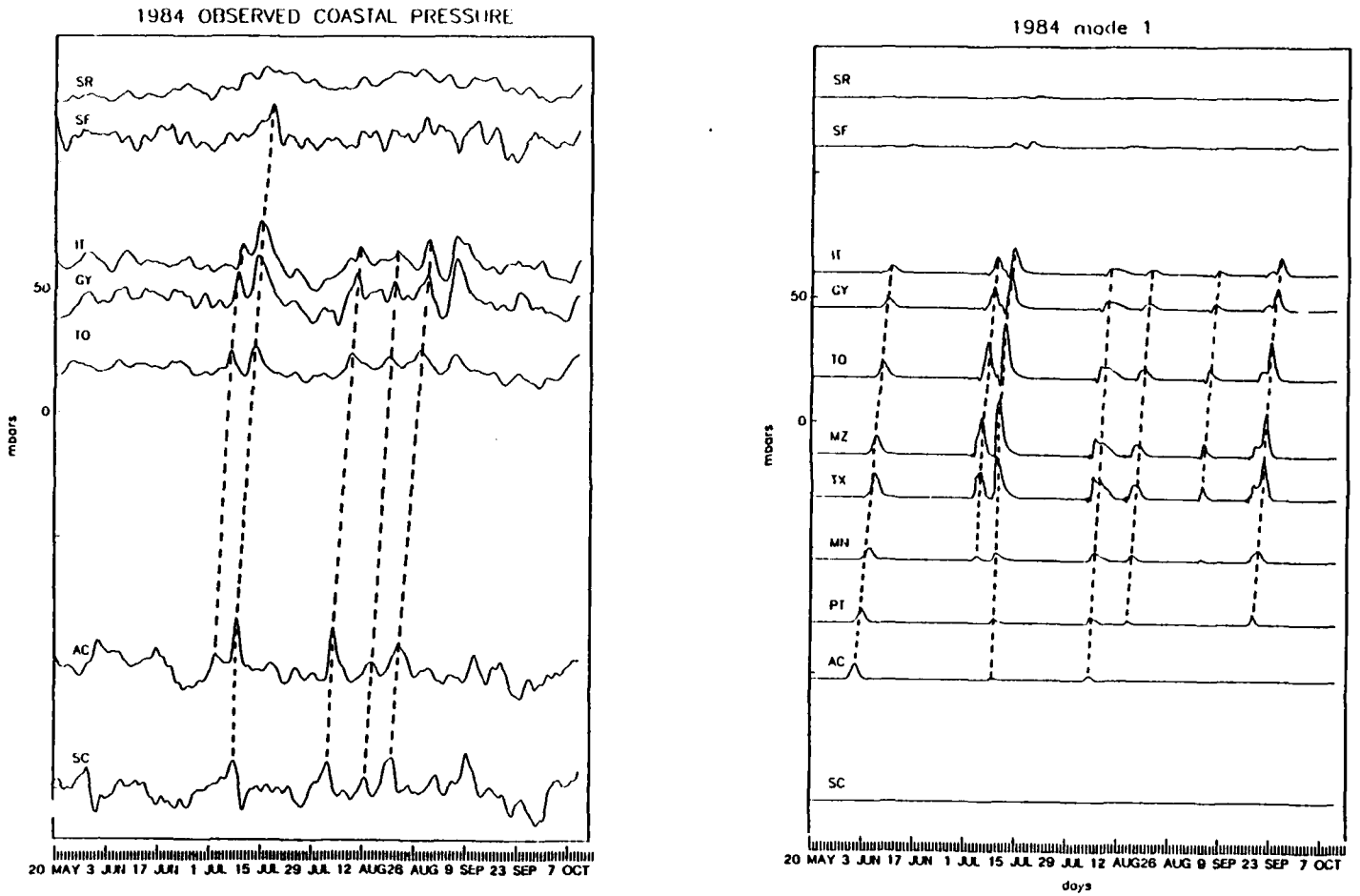


Figure 7. The observed adjusted sea level at Salina Cruz (SC), Acapulco (AC), Guaymas (GY), and Santa Rosalia (SR) and bottom pressure at Topolobampo (TO, 100-m depth), Isla Tiburon (IT, 7-m depth), and San Francisquito (SF, 7-m depth) compared to the coastal-trapped wave model mode 1 hindcast of coastal pressure. The vertical spacing between time series is proportional to the alongshelf distance between the stations. The dashed lines connect propagating events.

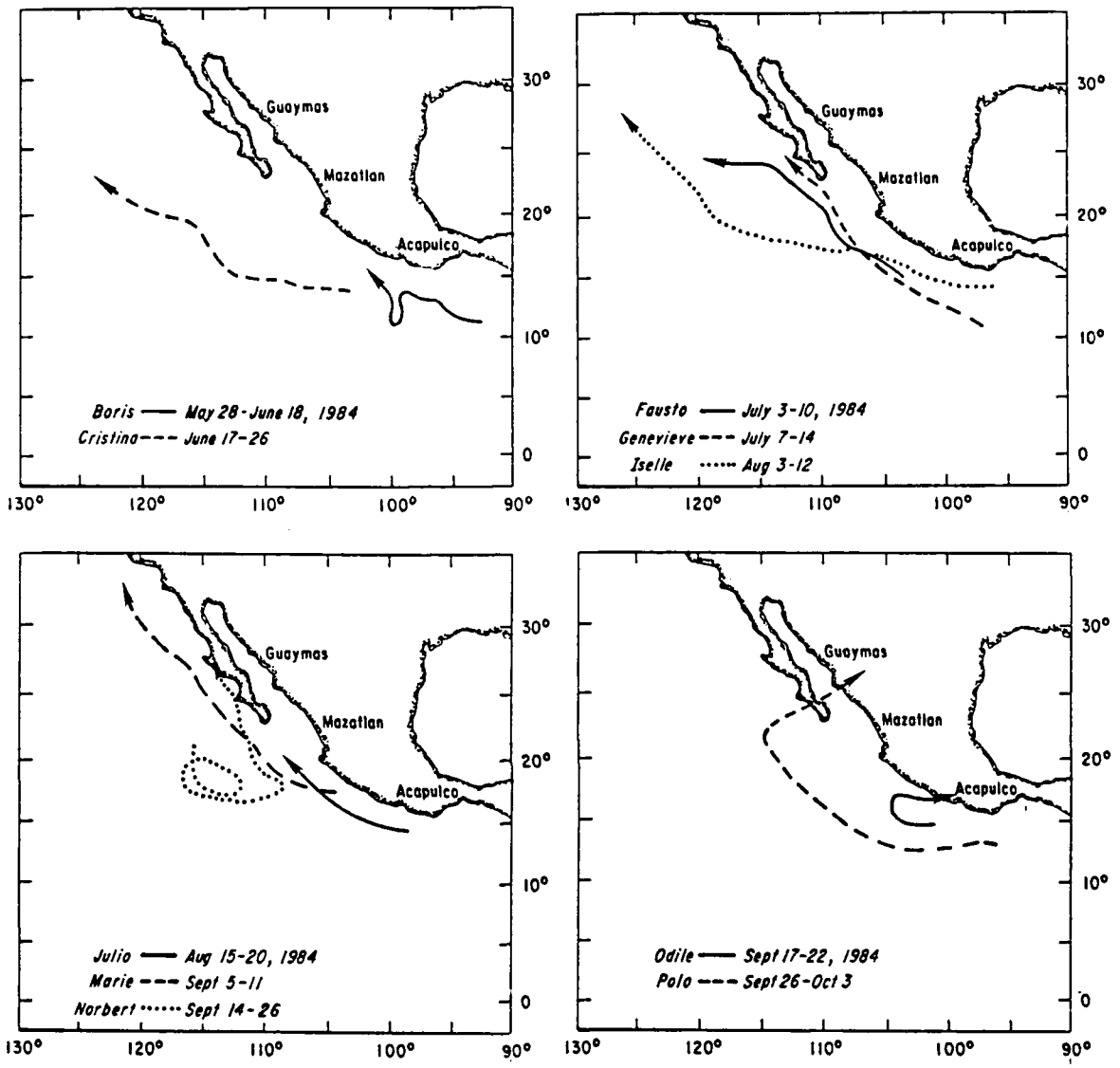


Figure 8.

Tracks of Eastern North Pacific tropical storms for 1984 from Gunther and Cross (1985). All storms reached hurricane intensity along portions of the coast except Julio.

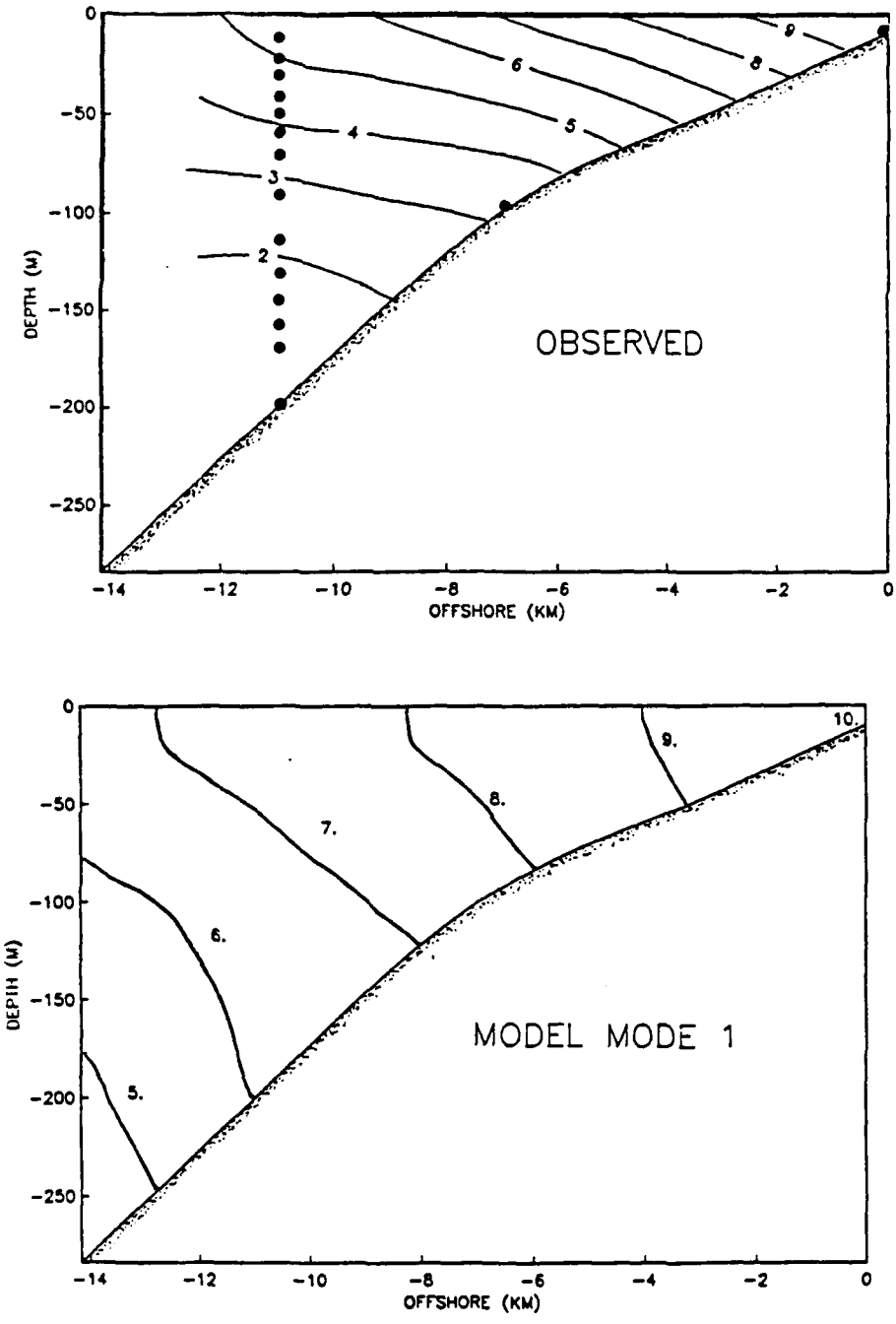


Figure 9.

The Guaymas cross-shelf structure of pressure, in millibars, from the multi-variate regression analysis (observed) and the coastal-trapped wave model mode 1. The pressure fields are normalized to 10 millibars at the coast.

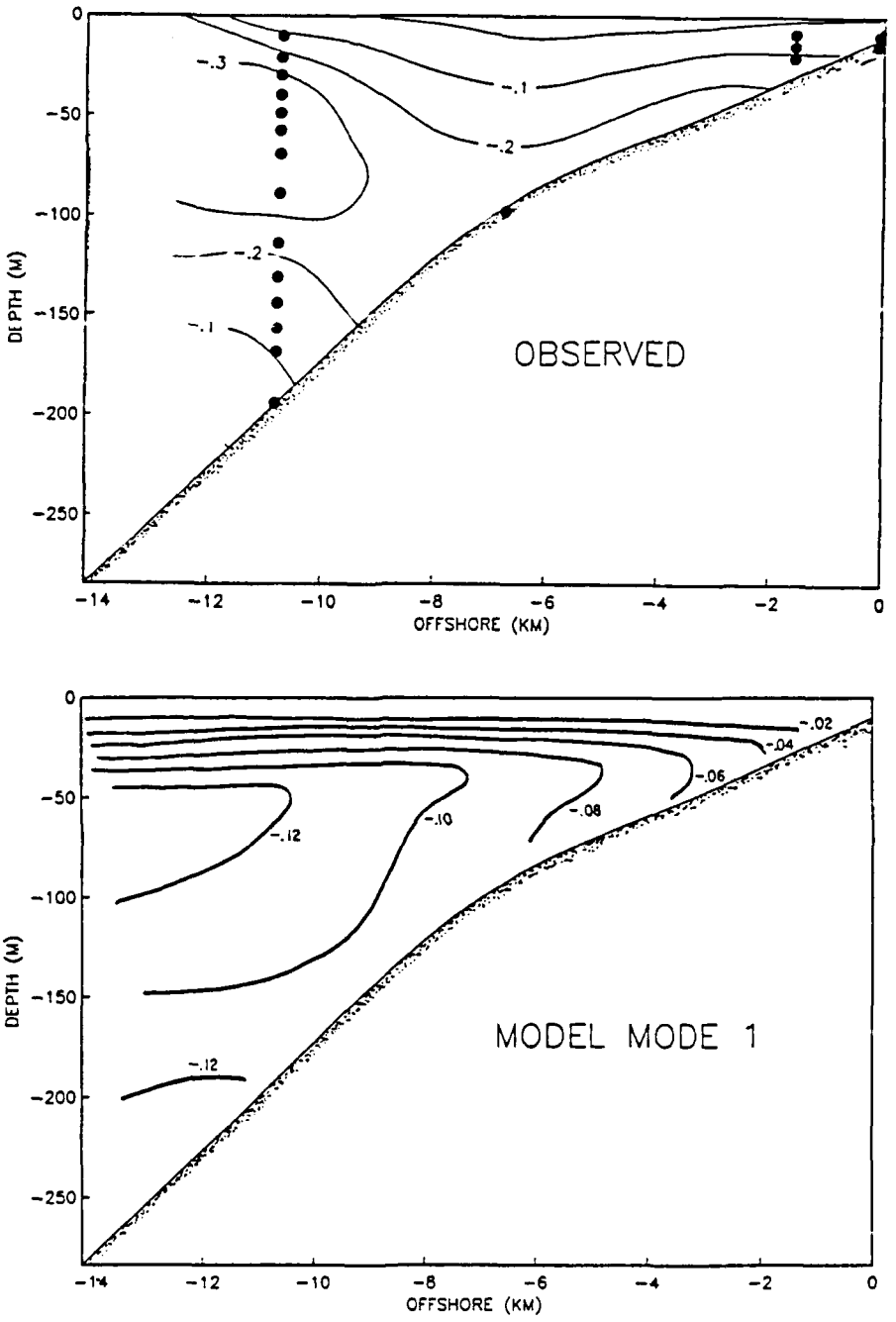


Figure 10.

The Guaymas cross-shelf structure of density, in g/cm$^3$, from the multi-variate regression analysis (observed) and the coastal-trapped wave model mode 1. The density fields are normalized to correspond to a 10 millibar pressure rise at the coast.

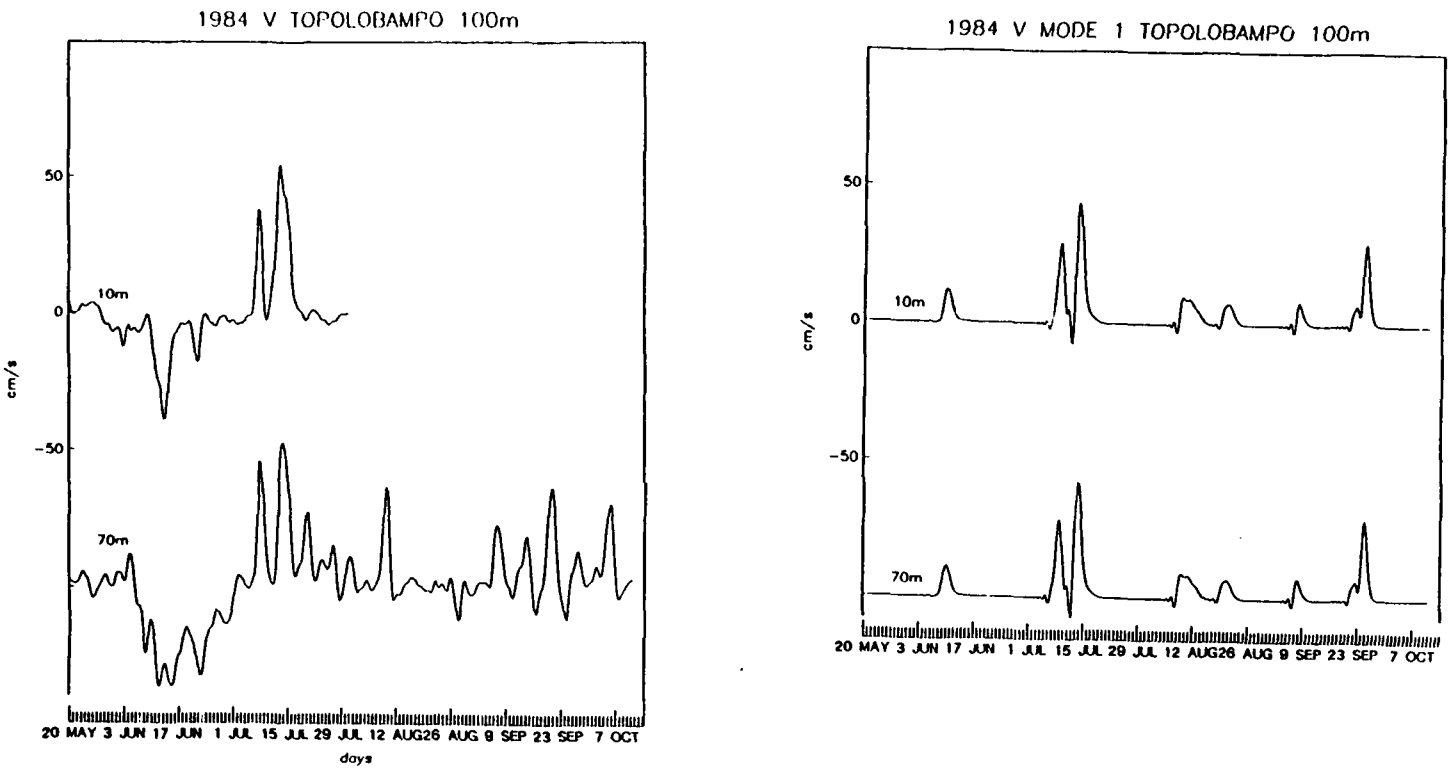


Figure 11. Observed alongshelf currents (V) at Topolobampo (M1, 100-m total depth), compared with the coastal-trapped wave mode 1 alongshelf current hindcast.

CHAPTER 3

# COMPLEX EMPIRICAL ORTHOGONAL FUNCTION ANALYSIS: WIDE VERSUS NARROW BANDED PROCESSES

## 1. INTRODUCTION

Empirical Orthogonal Functions (EOFs, see Lorenz, 1956 for a description) are now a standard technique for describing coherent variability in geophysical data sets. EOFs are designed to give the most efficient description of the observed variability, often reducing large data sets to a few dominant modes. These dominant modes are sometimes useful in representing physical process in the data (e.g., Kundu et al., 1975), although the requirement of orthogonality in both time and space, the use of the covariance (or correlation) matrix at zero lag to describe the variability, and the particular sampling of the observed field require careful consideration before assigning any physical significance to a given mode. In particular, the use of the zero-lagged covariance matrix limits the analysis to the identification of standing wave patterns.

An alternative method for detecting propagating patterns is complex empirical orthogonal function analysis (CEOFs, Rasmusson et al., 1983). This method, carried out in the time domain, has been used to detect large-scale travelling patterns in meteorological (Barnett, 1983) and oceanographic observations (White and Tabata, 1987). Horel (1984) discusses several tests of the method on simulated data. In this chapter, we investigate the suitability of CEOFs for isolating propagating signals associated with coastal-trapped waves along the Mexican Pacific coast. Specifically, we are interested in isolating a single CEOF mode which characterizes the propagation observed in coastal sea level and moored observations in the Gulf of California. After several test cases using simulated data, we conclude that the method is not appropriate for this particular application, and may not be suitable in general for broad-banded processes. A brief description of the method is given in section 2, the model test is described in section 3, and a summary follows in section 4.

## 2. METHOD

CEOFs involve obtaining quadrature information about a scalar field without resorting to a frequency domain analysis. Following Barnett (1983), we represent a scalar field $u_j(t)$, where $j$ signifies spatial position ($j$ = 1,2,..., N) and $t$ is time, in the usual Fourier sense as

$$u_j(t) = \sum_{\omega}[a_j(\omega)\cos(\omega t) + b_j(\omega)\sin(\omega t)] \,. \tag{1}$$

To obtain quadrature information between stations, a complex representation of $u_j(t)$ is invoked,

$$U_j(t) = \sum_{\omega} c_j(\omega)e^{i\omega t} \,, \tag{2}$$

where $c_j(\omega) = a_j(\omega) + ib_j(\omega)$. Then $U_j(t)$ can be written in the form,

$$U_j(t) = \sum_{\omega} \{[a_j(\omega)\cos(\omega t) + b_j(\omega)\sin(\omega t)]$$

$$+ i[b_j(\omega)\cos(\omega t) - a_j(\omega)\sin(\omega t)]\}$$

$$= u_j(t) + i\hat{u}_j(t) \tag{3}$$

The real part of (3) is the original scalar field; the imaginary part is the quadrature function of $u_j(t)$, or the Hilbert transform (Thomas, 1969). As is evident from the Fourier representation, the Hilbert transform phase shifts each spectral component of $u_j(t)$ by 90° in time. In this study, $\hat{u}$ is obtained from the Fourier coefficients.

The covariance matrix of $U_j(t)$ is

$$C_{jk} = \langle U_j^*(t)U_k(t)\rangle_t \tag{4}$$

where $\langle\ldots\rangle_t$ denotes time averaging. It follows from standard spectral analysis theory that

$$C_{jk} = \int_{o}^{\omega_n} \phi_{jk}(\omega)d\omega \tag{5}$$

where $\phi_{jk}$ is the cross spectrum and $\omega_n$ is the Nyquist frequency. Thus, $C_{jk}$ is equivalent to the cross-spectral matrix integrated over all frequencies.

As in a standard EOF analysis, complex eigenvectors, $B_n(x)$, are obtained from $C$. The complex temporal expansions are given by,

$$A_n(t) = \sum_{j=1}^{N} U_j(t) B_n(x) . \tag{6}$$

$U$ can then be represented as,

$$U_j(t) = \sum_{n=1}^{N} A_n(t) B_n{}^*(x) . \tag{7}$$

As an example, CEOFs are obtained for a traveling sinusoid of the form $u(x,t) = a \sin(k_o x - \omega_o t)$. The spatial phase is defined by

$$\theta_n(x) = arctan\,[ImB_n(x) / ReB_n(x)] . \tag{8}$$

In this case, there is only one eigenfunction with $d\theta_1 / dx = k_o$. The spatial amplitude is given by

$$S_n(x) = [B_n(x) B_n{}^*(x)]^{0.5} . \tag{9}$$

In the case of a constant amplitude sinusoid, $S_1(x) = a$. The temporal phase is defined by

$$\phi_n(t) = arctan\,[ImA_n(t) / ReA_n(t)] . \tag{10}$$

Again, all energy is in the first mode with $d\theta_1(t) / dt = \omega_o$. The temporal amplitude is defined by

$$R_n(t) = [A_n(t) A_n{}^*(t)]^{0.5} \tag{11}$$

For a sinosoid whose amplitude does not vary with time, $R_1(t)$ is a constant. It follows that the phase speed is obtained by

$$c_n(x,t) = \omega / k = (d\phi_n(t) / dt) / (d\theta_n(x) / dx) , \tag{12}$$

which in the case of the sinusoid is $c_1(x,t) = \omega_o / k_o$.

## 3. TEST CASE

The coastal-trapped wave test case (Fig. 1) consists of a series of irregularly spaced Gaussian bumps that propagate non-dispersively past a one-dimensional, ten-station array. The time series schematically represent coastal sea level observations during one tropical storm season (6 months), at equally spaced stations over a distance equivalent to the separation between Salina Cruz and Guaymas (2500 km, see chapter 2, Figure 3). Wave events have 10 day period, constant amplitude, and 2.5 m/s phase speed (215 km/day). As in the case of the travelling sinusoid above and in the absence of any background noise, we seek a single mode which characterizes this simple travelling pattern.

CEOFs, however, are unable to isolate all the variability in a single mode. The first mode, describing 72% of the total variance, is used to reconstruct the time series at each station (Fig. 2). The wave field is only partially accounted for by mode 1, with the percentage of variance described at each station decreasing towards the ends of the array (Fig. 3). The average temporal phase is used to obtain a representative $\omega$, and $k$ is obtained from the slope of the spatial phase function. The phase speed of mode 1, computed from equation 12, underestimates the true phase speed by 33%.

The limitations of CEOFs found in this particular test case are due in part to the wide-banded nature of the wave signal. This is illustrated in the following example. The complex eigenvector $B_1(x)$ obtained from the covariance matrix $C$ has an arbitrary phase. The absolute phase is determined when $B_1(x)$ is projected on the data to obtain $A_1(t)$ from equation 6. Consider a spatial phase shift of $B_1(x)$ such that at station $x_5(j=5)$, $\theta_1(x_5) = 0$. Then from equations 3 and 7,

$$U(x_5,t) = u(x_5,t) + i\hat{u}(x_5,t)$$

$$= a_1^r(t) b_1^r(x_5) + i\,[a_1^i(t) b_1^i(x_5)] \qquad (13)$$

where $a_n^r$, $a_n^i$, $b_n^r$, $b_n^i$, denote the real and imaginary components of $A_n$ and $B_n$, and $b_1^i(x_5) = 0$ for this particular phase orientation of $B_1(x)$. Hence, the real part of $A_1(t)$ is proportional to the observed wave signal at station 5, and the imaginary part of $A_1(t)$ is proportional to the Hilbert

transform of the wave signal. The real and imaginary parts of $A_1$ are pictured in Fig. 4. At the remaining stations, where $b_1^i(x_i)$ does not necessarily equal zero, a simple linear superposition of $a_1^r$ and $a_1^i$ cannot reproduce $u_i$ at each station. In the case of the sinusoid, the imaginary part of $A_1$ is simply a negative cosine function. Thus, the real and imaginary components of $A_1$, with the appropriate spatial phase weighting, can recover the signal entirely at any station. It becomes less likely that a superposition of two temporal functions can reproduce a propagating signal as the energy in that signal is spread out more in frequency. This result for wide-banded functions was implied by Horel (1984) for a similar test case. He notes that wide-banded signals are better represented by the CEOF as the phase speed increases. In this limit, the temporal lag between time series is reduced and the simple superposition discussed above is more tenable.

An additional consideration is the ability of CEOFs to reproduce the phase speed, $c$. For a non-dispersive process, $c$ is a constant and $k$ varies linearly with frequency. The CEOF, however, determines a single $(\omega, k)$ pair. The spectrum for the Gaussian bump wave train (Fig. 5) is wide-banded at low frequencies (< 0.2 cpd), making a determination of a single $(\omega, k)$ seem somewhat arbitrary. To some extent, the value of $(\omega, k)$ obtained by the CEOF is an energy-weighted average over the spectral range, which accounts for their ratio approximating the given $c$ in the above test case.

The application of CEOF analysis on band-passed time series should improve both the reproduction of the time series, by making the signal more periodic, and the phase speed, by restricting the choice of $(\omega, k)$ to a narrower frequency band. The treatment of separate frequency bands is easily accomplished by constructing $U$ (equation 2) only over a desired frequency range. In the next example, the same Gaussian wave train is analyzed but in 5 different frequency bands (0.0 - 0.5, 0.5 - 1.0, 1.0 - 1.5, 1.5 - 2.0, 2.0 - 2.5 cpd). The values of mode 1 $(\omega, k)$ obtained for each frequency band (Fig. 6) more accurately reproduce the given phase speed (represented by the straight line). The value of $(\omega, k)$ obtained from the analysis over the entire frequency range is shown for comparison. The time series at each station are reproduced from mode 1 in each band and summed together. The reproduced time series are now more consistent with the original signal (Fig. 7), and explain more of the variance at each station (Fig. 8).

The treatment of narrower frequency bands clearly improves the analysis, as it must since the coherence between stations approaches 1.0 as the bandwidth approaches zero. For real data, however, a narrower bandwidth will degrade the CEOF results as statistical errors arise in the determination of the covariance, or equivalently cross-spectral, matrix. To investigate this effect, statistical noise is added to the cross-spectral matrix, $C$, for the five frequency bands discussed above before applying the CEOF. Following Davis and Regier (1977), we first add a

random amount of instrument noise at each station that is not more than 10% of the propagating variability and is independent between stations. Next, we account for statistical sampling errors by assuming that instrument noise is negligible and that the statistics of the Fourier coefficients used in computing $C$ have approximately joint normal probability distributions. If the process is stationary and the sample statistics are reasonably accurate, the error matrix, $V$, of the cross-spectra is given by

$$V = \langle C_{ij} C_{nm} \rangle \simeq M^{-1} \hat{C}_{im} \hat{C}_{nj} \tag{14}$$

where $M$ is the number of independent spectral components used to compute the observed cross-spectra, and $\hat{C}$ is the true cross-spectra. In practice, $V$ is obtained by substituting the observed cross-spectra for $\hat{C}$ and $M$ is taken to be the number of Fourier coefficients in the band. The errors for $C$ are represented as a linear combination of the eigenvectors of $V$. The coefficients of each eigenvector are obtained by selecting a random number from a Gaussian population with zero mean and variance given by the corresponding eigenvalue (Long and Hasselmann, 1979). CEOFs are then repeated for 100 different noisy cross-spectral matrices with $M$ = 18 for each frequency band. Phase speed is then obtained from the five $(\omega, k)$ pairs. The results confirm that the addition of instrument and statistical noise signficantly alters the CEOF results. The average phase speed is off by 7% with a statistical uncertainty of 16%. In addition, the amount of variance explained at each station is degraded by up to 10% over the band-passed test case with no noise, although still better than the original test case over all frequencies (Fig. 9). The effect of noise degradation (assuming that the process is truly Gaussian) is underestimated, however, in the specification of $M$. The choice of $M$ assumes a white spectra with equal contributions from each spectral component used to obtain the cross-spectra. This is an invalid assumption for the red spectra of this signal; thus $V$ should be even larger. Prewhitening, although not considered in this study, can make $M$ equal to the number of spectral components.

## 4. SUMMARY

Test runs on synthetic data indicate that complex empirical orthogonal function analysis is unable to accurately detect wide-banded propagating signals similar to the coastal-trapped waves observed off the Pacific coast of Mexico. In the absence of noise and any band-pass filtering, the CEOF recovers a propagating mode that is 30% off in phase speed and that explains a decreasing amount of the variability towards the ends of the sensor array. The results are

significantly improved by analyzing narrower frequency ranges. A trade-off arises, however, between the CEOF's inability to handle wide-banded signals, and statistical noise degrading the results when the bands become too narrow. For the case of 18 degrees of freedom, which is typical of the degrees of freedom available in a band-by-band analysis of the actual observations, the method returns a 16% uncertainty in the phase speed and explains on the order of 10% less of the variability at certain stations. Given the shortcomings of the method illustrated by this very idealized test case, we abandon CEOFs as a means of detecting the observed coastal-trapped wave signal off Mexico.

# REFERENCES

Barnett, T. P., Interaction of the Monsoon and Pacific Trade Wind System at interannual time scales. Part 1: The equatorial zone, *Mon. Wea. Rev., 111*, 756-773, 1983.

Davis, R. E., and L. A. Regier, Methods of estimating directional wave spectra from multi-element arrays, *J. Mar. Res., 35*, 453-477, 1977.

Horel, J. D., Complex principal component analysis: Theory and examples, *Climate Appl. Meteor., 23*, 1660-1673, 1984.

Kundu, P. K., J. S. Allen, and R. L. Smith, Modal decomposition of the velocity field near the Oregon coast, *J. Phys. Oceanogr., 5*, 683-704, 1975.

Long, R. B., and K. Hasselmann, A variational technique for extracting directional spectra from multi-component wave data, *J. Phys. Oceanogr., 9*, 373-477, 1979.

Lorenz, E., Empirical orthogonal function and statistical weather prediction, *Rep. No. 1, Statistical Forecasting Program*, Dept. of Meteorology, MIT, 44 pp., 1956.

Rasmusson, E. M., P. A. Arkin, W. Y. Chen, and J. B. Jalickee, Bienniel variations in surface temperature over the United States as revealed by singular decomposition, *Mon. Wea. Rev., 109*, 181-192, 1981.

Thomas, J. B., *An Introduction to Statistical Communication Theory*, Wiley, 663 pp., 1969.

White, W. B., and S. Tabata, Interannual westward-propagating baroclinic long-wave activity on line P in the eastern midlatitude North Pacific, *J. Phys. Oceanogr., 17*, 385-396, 1987.

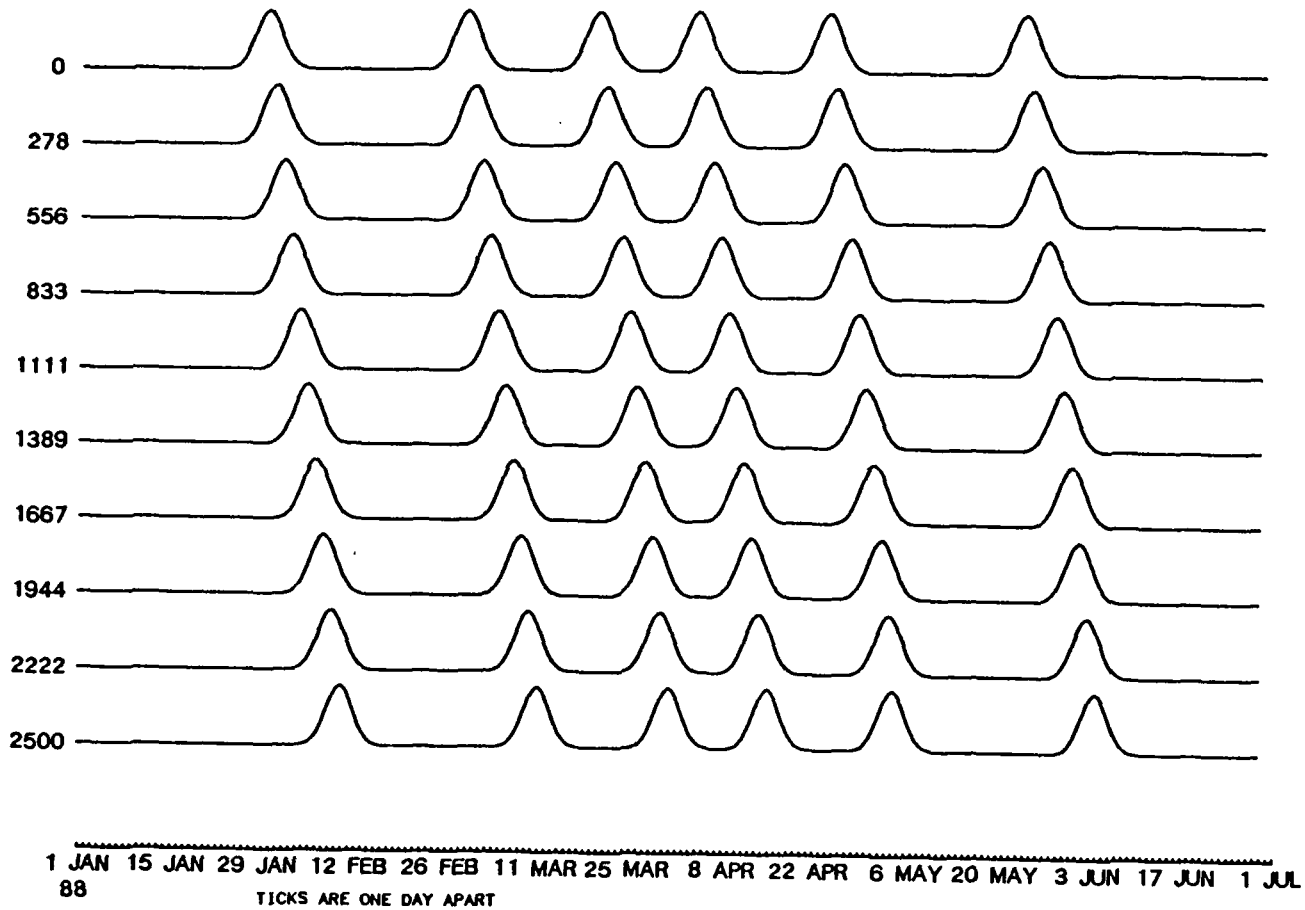


Figure 1. Synthetic time series of 6 propagating Gaussian bumps. Events have constant phase speed of 2.5 m/s, periods of 10 days, and travel past a 2500-km, evenly space, sensor array. The 6 month long time series are schematically representative of coastal-trapped waves propagating poleward along the Pacific coast of Mexico during the summer/fall storm season.

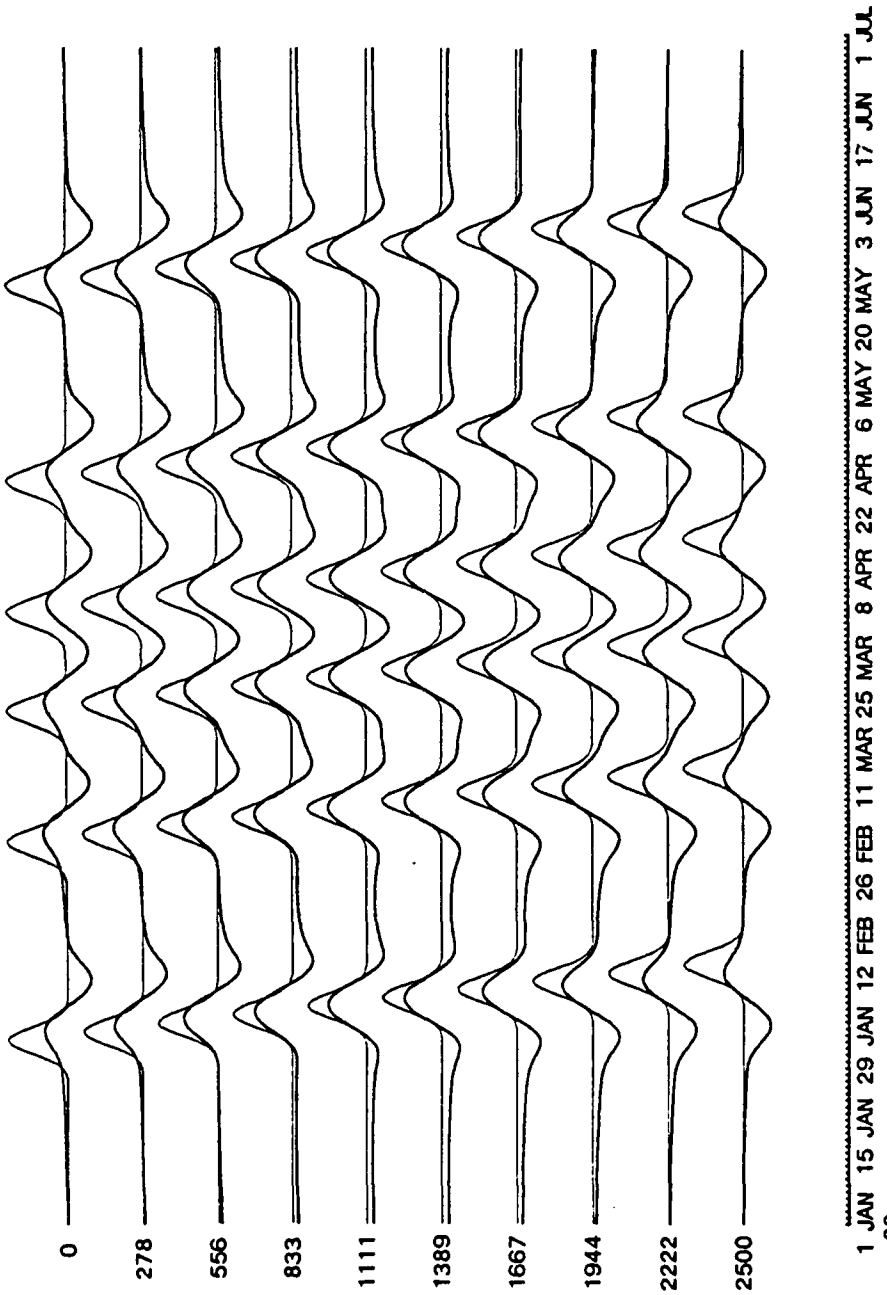


Figure 2. The CEOF mode 1 reconstructed time series (dark) and the original time series (light).

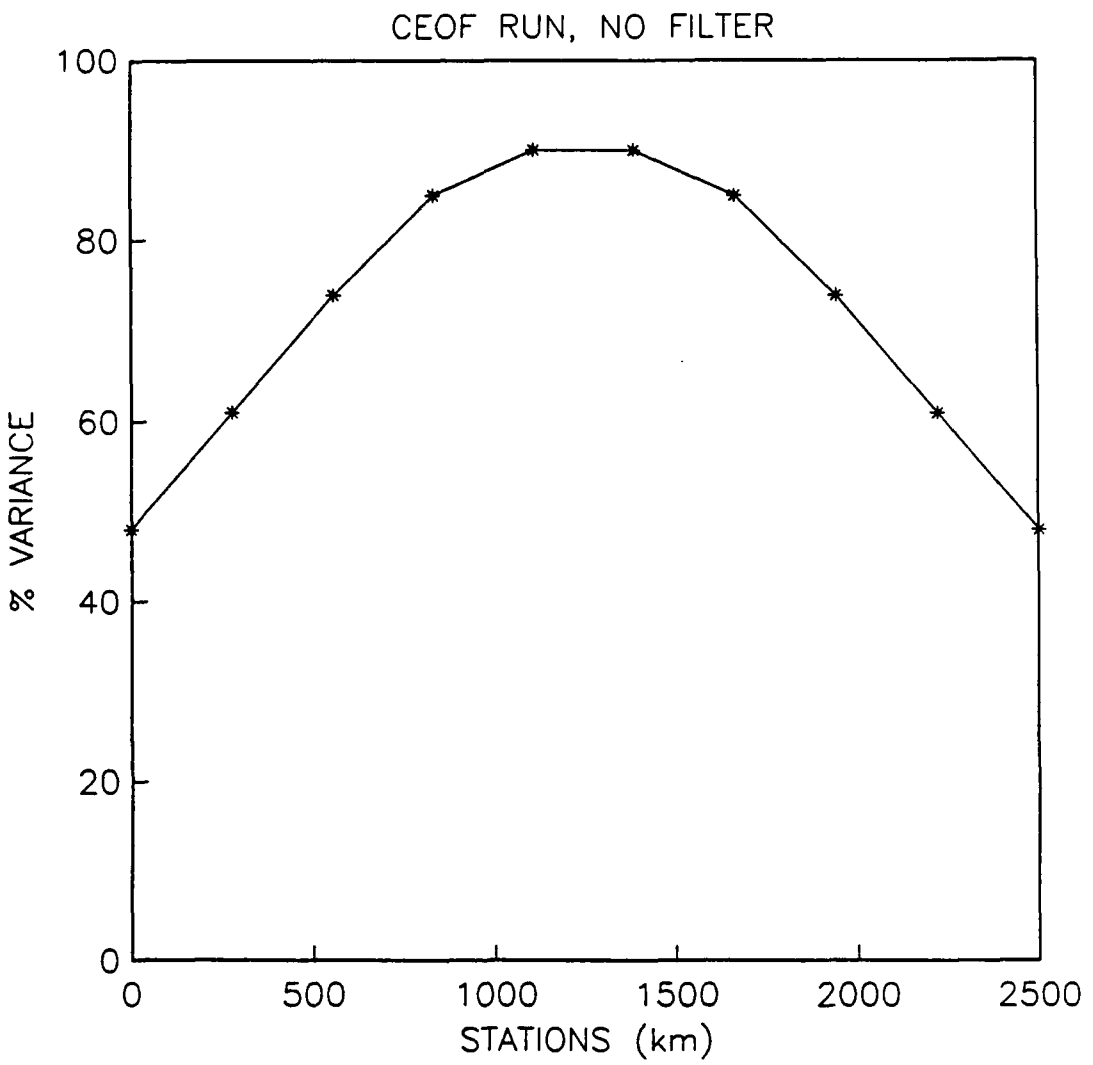


Figure 3.

The percentage of variance explained by the CEOF mode 1 at each station.

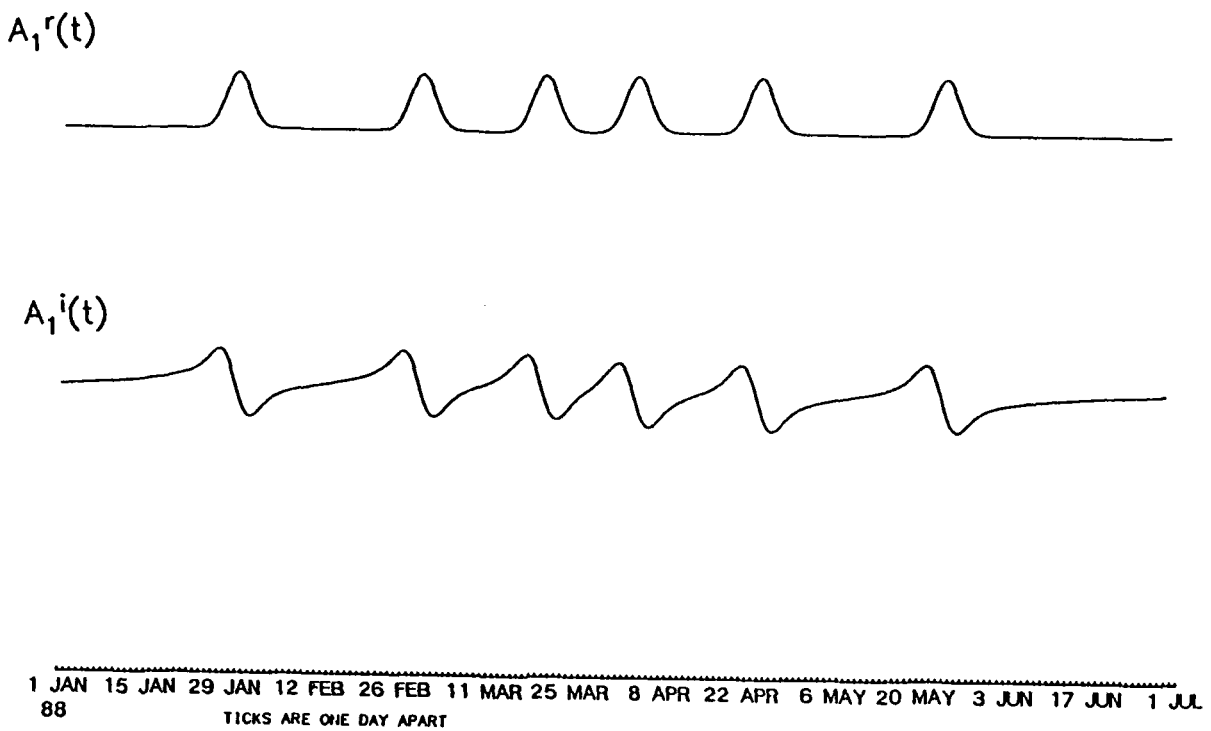


Figure 4. The real and imaginary parts of $A_1(t)$.

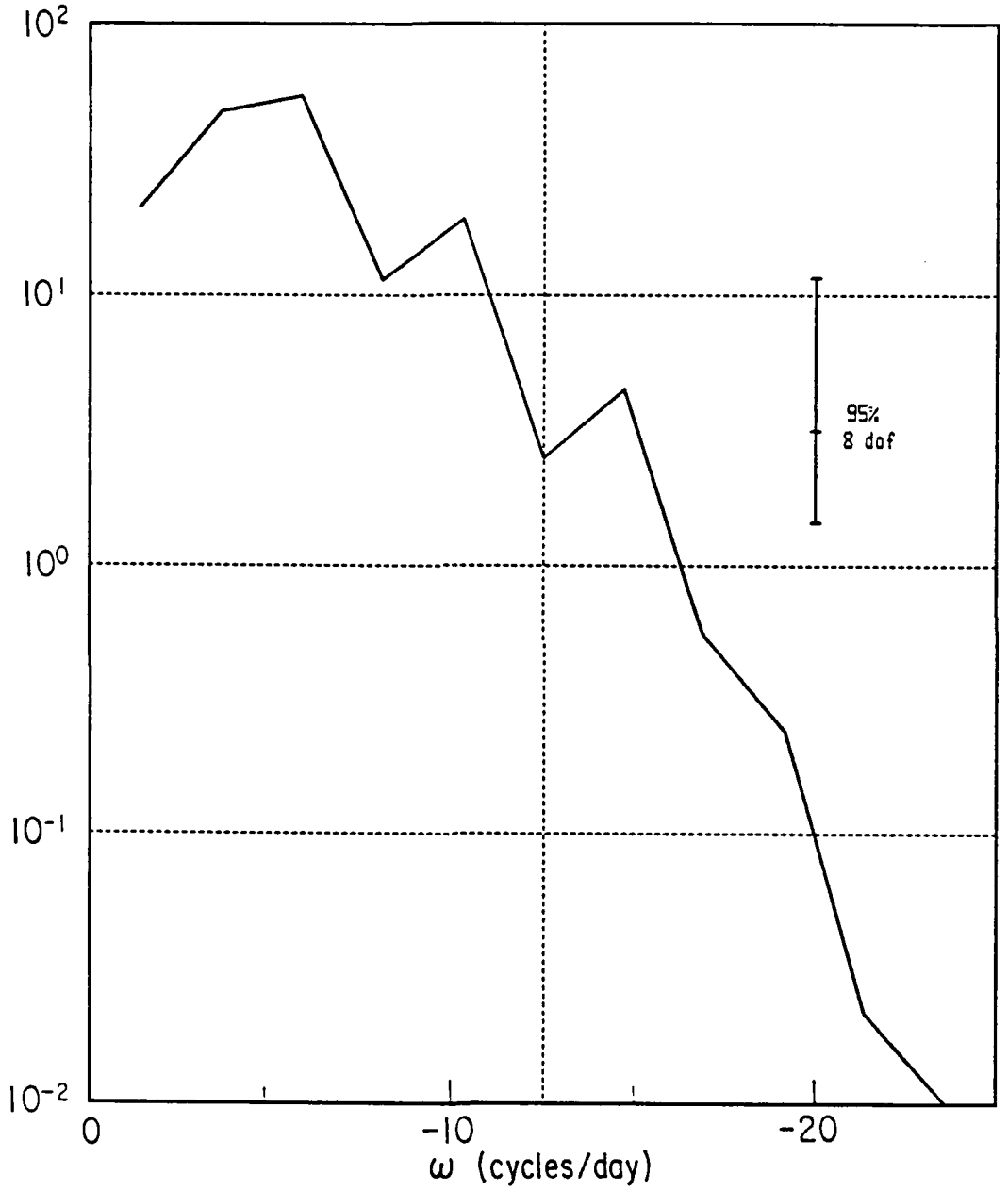


Fig. 5. Power spectra of the events shown in Fig. 1.

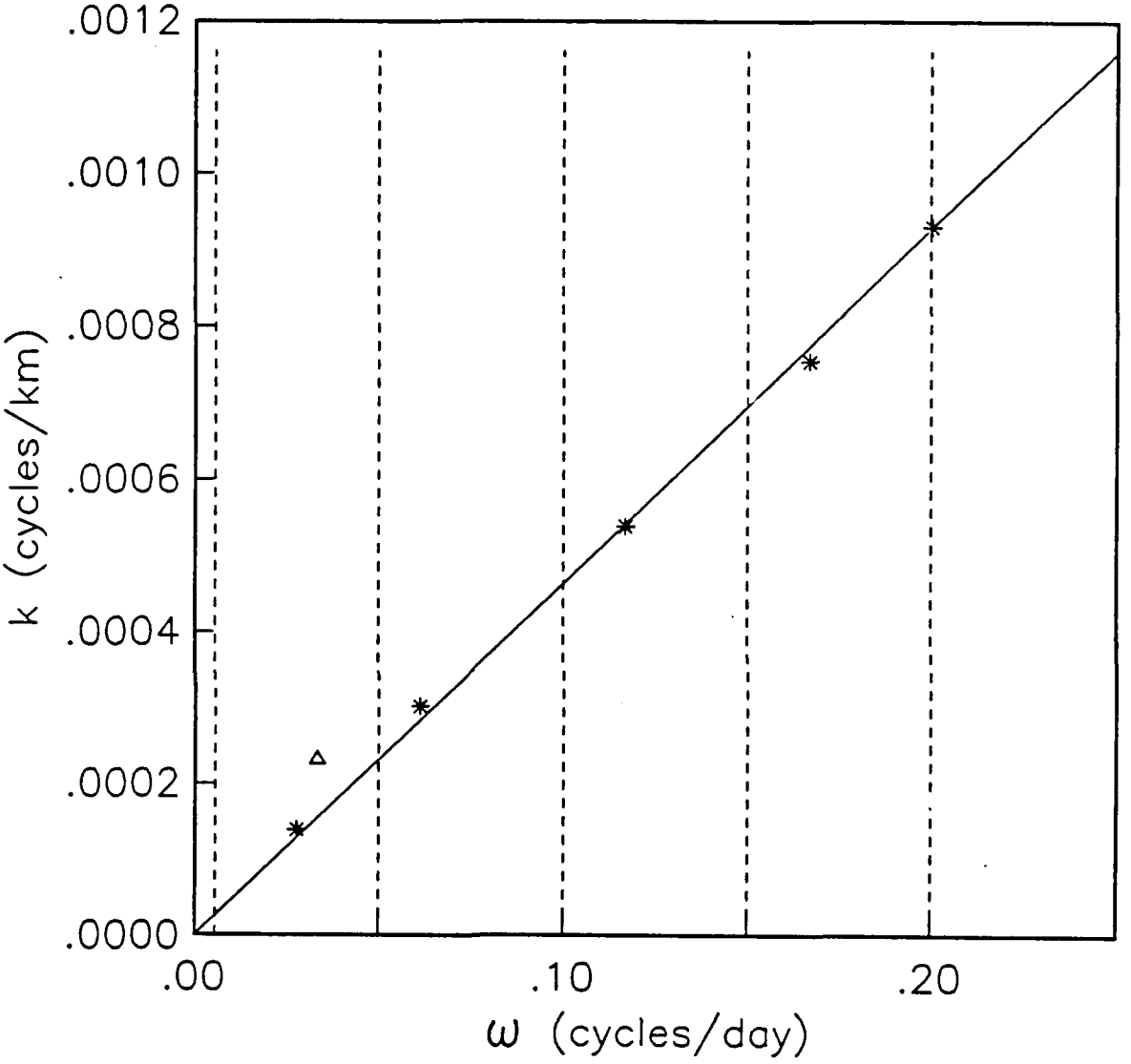


Figure 6.

CEOF derived $(\omega,k)$, denoted by asterisks, for 5 frequency bands, delineated by dashed lines. Slope of the solid line represents the true phase speed. The triangle represents the $(\omega,k)$ for the CEOF over all frequencies.

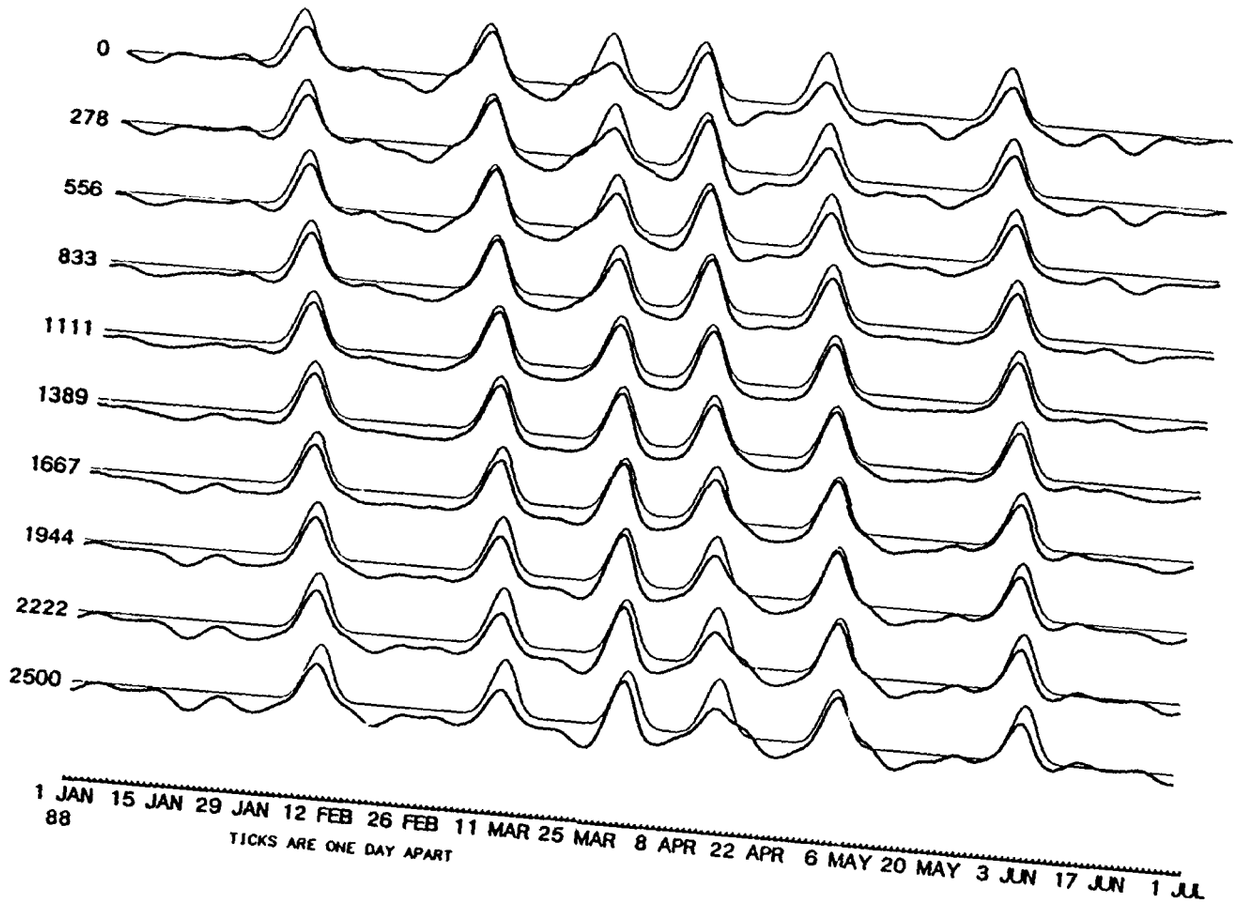


Figure 7. The reconstructed time series obtained by summing the mode 1 contributions from the five frequency bands shown in Fig. 6.

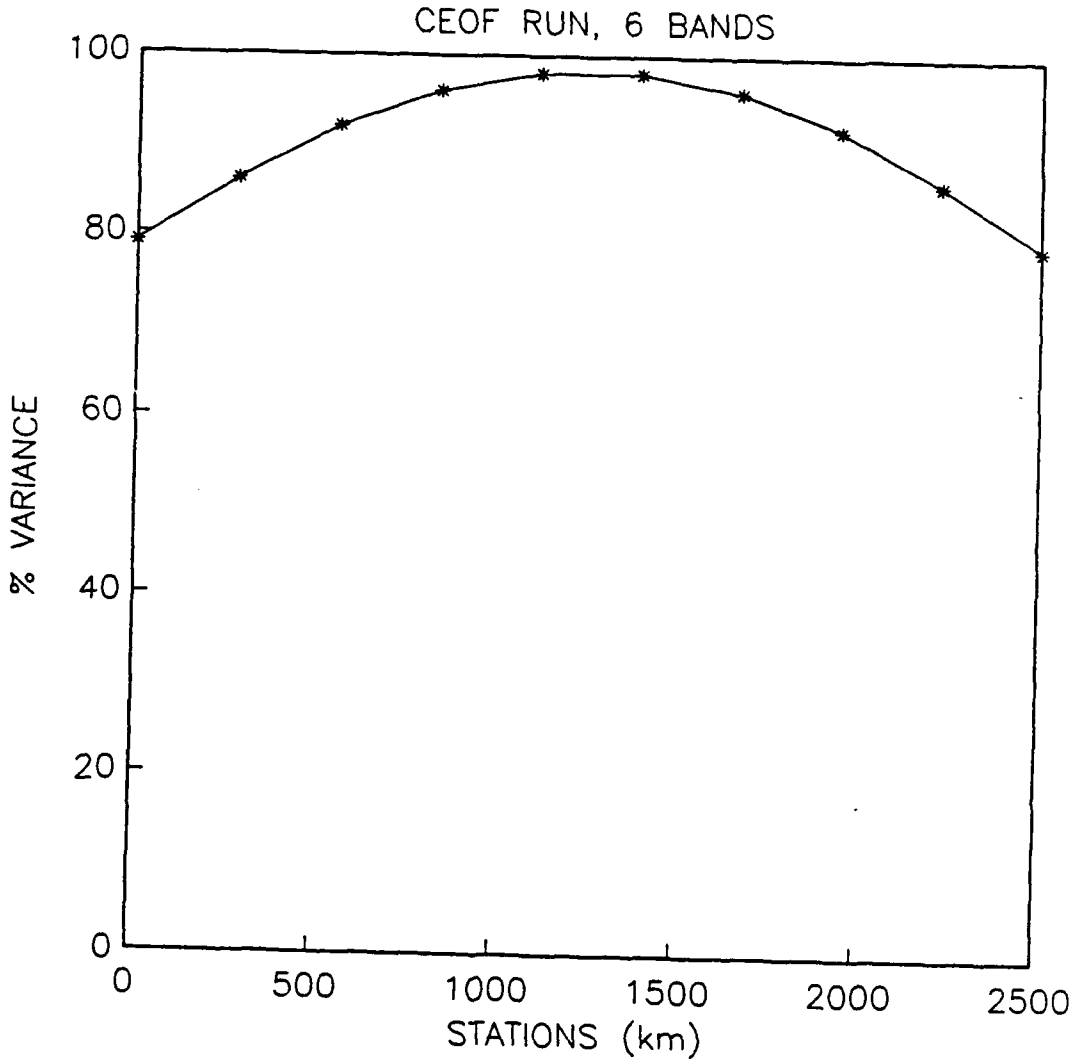


Figure 8.

The percentage of variance explained by the combined mode 1 for the five frequency bands shown in Fig. 6.

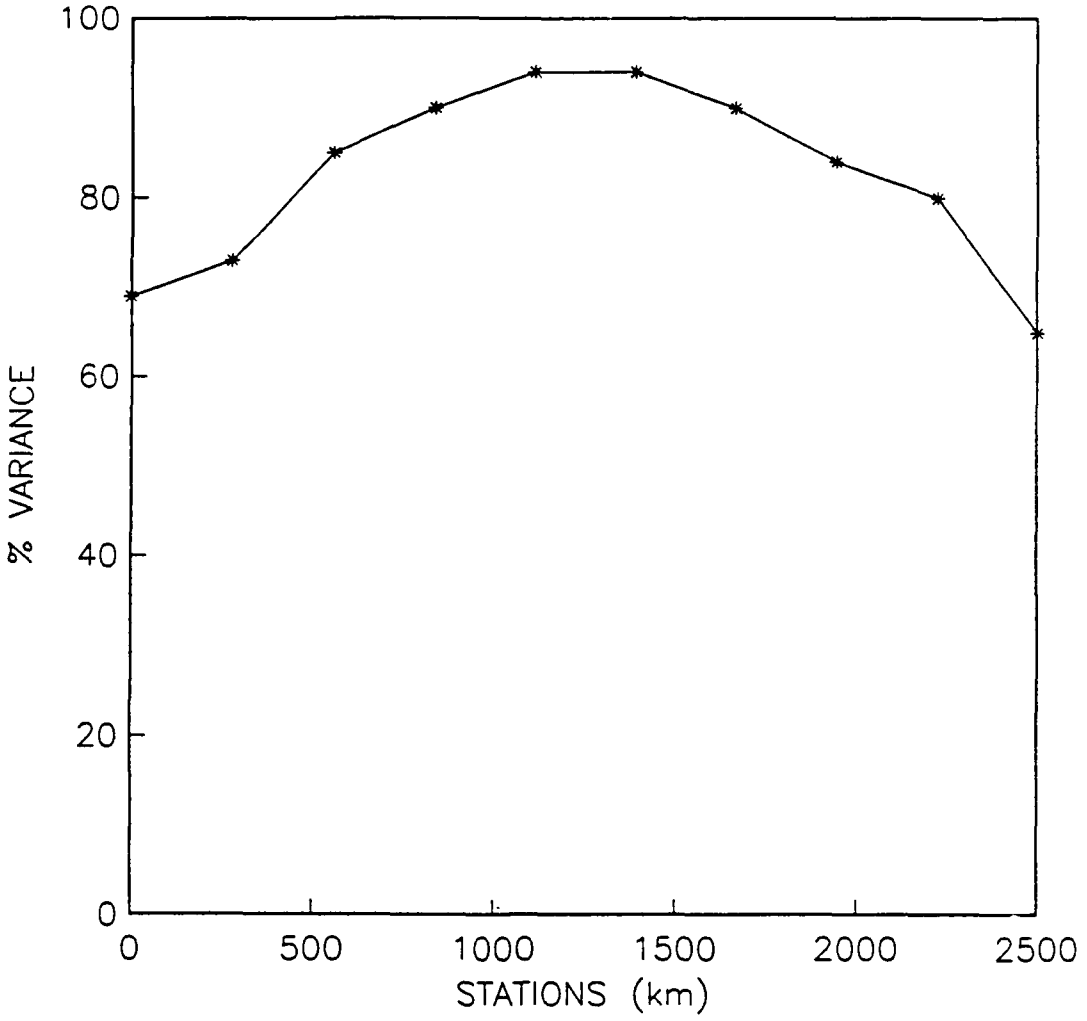


Figure 9.

The percentage of variance explained by the combined mode 1 for the five frequency bands shown in Fig. 6 with statistical and instrument noise added to the cross-spectral matrices.